PATIENT-SPECIFIC FDG DOSIMETRY FOR ADULT MALES, ADULT FEMALES, AND VERY LOW BIRTH WEIGHT INFANTS

By

ERIN NIVEN, M.Sc.

A Thesis

Submitted to the School of Graduate Studies

in Partial Fulfillment of the Requirements

for the Degree

Doctorate of Science

McMaster University

PATIENT-SPECIFIC FDG DOSIMETRY FOR ADULT MALES, ADULT FEMALES, AND VERY LOW BIRTH WEIGHT INFANTS

DOCTORATE OF SCIENCE (2003)
(Medical Physics)

McMaster University
Hamilton, Ontario

TITLE: Dosimetry of FDG

AUTHOR: Erin Niven, M.Sc. (McMaster University)

SUPERVISOR: Dr. Claude Nahmias

NUMBER OF PAGES: xv, 217

Abstract

Fluorodeoxyglucose is the most commonly used radiopharmaceutical in Positron Emission Tomography, with applications in neurology, cardiology, and oncology. Despite its routine use worldwide, the radiation absorbed dose estimates from FDG have been based primarily on data obtained from two dogs studied in 1977 and 11 adults (most likely males) studied in 1982. In addition, the dose estimates calculated for FDG have been centered on the adult male, with little or no mention of variations in the dose estimates due to sex, age, height, weight, nationality, diet, or pathological condition.

Through an extensive investigation into the Medical Internal Radiation Dose schema for calculating absorbed doses, I have developed a simple patient-specific equation; this equation incorporates the parameters necessary for alterations to the mathematical values of the human model to produce an estimate more representative of the individual under consideration. I have used this method to determine the range of absorbed doses to FDG from the collection of a large quantity of biological data obtained in adult males, adult females, and very low birth weight infants. Therefore, a more accurate quantification of the dose to humans from FDG has been completed. My results show that per unit administered activity, the absorbed dose from FDG is higher for infants compared to adults, and the dose for adult women is higher than for adult men. Given an injected activity of approximately 3.7 MBq kg^{-1}, the doses for adult men, adult

women, and full-term newborns would be on the order of 5.5, 7.1, and 2.8 mSv, respectively. These absorbed doses are comparable to the doses received from other nuclear medicine procedures.

Acknowledgements

Through this passage I have learned much about internal dosimetry; more importantly, the journey itself has given me the opportunity to learn more about myself and the world around me. My experience at McMaster has definitely been rewarding. There are many people who encouraged and supported me through this journey, and I wish to recognize them here.

First, with all my gratitude, I want to thank my supervisor, Claude Nahmias. His expertise, insight, and direction were always offered when I needed them, whether I was aware of the need or not. Bill Prestwich and Doug Wyman, my Ph.D. Committee members, helped keep me on track with their knowledge and advice. Of course I wouldn't be here today were it not for the technical skills and endurance of the nurse who ran the PET scanner, Margo Thompson.

I am also grateful to the wonderful team at the Cardiac PET Centre in Ottawa for their aide in providing me with valuable data. Rob deKemp, Rob Beanlands, Terry Ruddy, May Aung, and the rest of the team are all talented and caring individuals, both at work and at play.

I will always have my monkeys, I mean friends, from the MIND Lab in my heart. Nek Manji, Marie-Claude Asselin, Anna Garnett, Geoff Hall, and Shingo Yuki – you all have given me wonderful memories with stories to last a lifetime.

I want to thank my family and closest friends for seeing me through this. Some days were darker than others, but you gave me all the light I needed. Finally, I want to send a special thanks to Matthew Wigston, Agnes Niven, and Dave Ritter, who showed me courage and gave meaning to this research.

Factum Est

Table of Contents

List of Tables

List of Figures

Acronyms

AF	absorbed fraction
CT	computed tomography
DER	Dose Estimate Report
ED	effective dose
EDE	effective dose equivalent
FDG	^{18}F-fluorodeoxyglucose; 2-deoxy-2-[^{18}F]fluoro-D-glucose
FWHM	full-width half-maximum
ICRP	International Commission on Radiological Protection
MIRD	Medical Internal Radiation Dose
MRI	magnetic resonance imaging
NCRP	National Council on Radiation Protection and Measurements; National Committee on Radiation Protection
PET	positron emission tomography
RBE	relative biological effectiveness
RIDIC	Radiation Internal Dose Information Center
ROI	region of interest
SAF	specific absorbed fraction
SNM	Society of Nuclear Medicine
SPECT	single photon emission computed tomography
VLBW	very low birth weight

Chapter 1: PET and FDG

1.1 Positron Emission Tomography

Positron emission tomography (PET) is a unique imaging technology that can quantify metabolic processes within the human body. PET has emerged in the last few decades as a powerful diagnostic and research tool with applications in oncology (Hawkins et al. 1991), neurology and psychiatry (Leenders et al. 1984; Raichle 1989), cardiology (Ruddy et al. 1999), gastroenterology (Skehan et al. 1999), and pharmacology (Jones 1996). Unlike x-ray computed tomography (CT) or magnetic resonance imaging (MRI) which provide anatomic information, PET's contribution as an imaging modality is its insight into the function of the human body (Hounsfield 1980; Brownell et al. 1982; Wagner 1985). This is achieved by allowing the body to incorporate a biological molecule labeled with a short-lived positron-emitting radioisotope. This biological molecule is then traced as it proceeds through its physiologic processes via the coincident photons emitted by the decaying radioisotope. This non-invasive technique provides digital cross-sectional images of the radiopharmaceutical that may be related to its biological distribution within a subject.

Figure 1.1: A transaxial PET image, obtained 60 minutes after intravenous administration of FDG, acquired at the level of the central gray nuclei. The face of the subject is towards the top of the image; the subject's right is on the reader's left. The color scheme is such that the reds and the oranges represent areas of high metabolic activity while the greens and the blues represent areas of low activity.

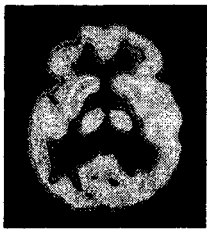

As with any diagnostic test or therapeutic procedure, the benefits of administering a radiopharmaceutical for a nuclear medicine study must be weighed against the risks of its use. One of the important risks considered for a nuclear medicine procedure is the use of a radionuclide and the possible radiation damage that may occur to the body from its administration. This risk is quantified as the radiation absorbed dose; the dose to an individual is determined based on the properties of the radionuclide and its distribution in the organs of the individual's body. Therefore the dose, and hence the risk from undergoing a nuclear medicine procedure, will be different for each person. With over 32 million diagnostic nuclear medicine procedures occurring annually worldwide (UNSCEAR 2000), an accurate quantification of the dose for each procedure has far-reaching value.

1.1.1 History

The use of positron-emitting radionuclides in biological research began shortly after the invention of the cyclotron in 1930 (Mitchell 1946; Ter-Pogossian 1992). The concept of imaging patients who were administered positron-labeled pharmaceuticals was first suggested by Wrenn and others (1951), and the first attempt at recording the three-dimensional distribution of a positron emitter was described by Brownell and Sweet (1953). The first circular section scanner was developed at the Brookhaven National Laboratories in the 1960's by Robertson and others (1973). Advances in computed tomography reconstruction techniques made during the 1970's (Brooks and Di Chiro 1976) along with the introduction of new radiation detector materials (Melcher 2000) facilitated the development of PET into a clinical and research tool (Miraldi 2002).

Although the first device built to measure exclusively positron-emitting radionuclides was developed in the 1950's (Brownell and Sweet 1953), the first of the devices to be used routinely in PET were built by Ter-Pogossian and others in the mid 1970's. This device, named Positron-Emission Transaxial Tomograph (PETT), consisted of six sets of four NaI(Tl) scintillation detectors placed in a hexagonal array around a scanning bed (Ter-Pogossian et al. 1975). Opposing pairs of detectors collected data in the form of coincidence events as the rotating platform moved around the subject. The data were reconstructed with a Fourier-based algorithm written in FORTRAN code. With a sampling resolution of 1.2 cm full-width half-maximum (FWHM) and data collection time of 12 minutes per slice, experiments performed with ^{64}Cu demonstrated

the scanner's capability of providing images with better contrast and resolution than the current single photon scintillation cameras. The continuing work of this group lead to the development of PETT III (Hoffman et al. 1976), which became the prototype for the first commercially available positron emission scanner, the ECAT (Phelps et al. 1978a; Graham and Bigler 1984).

1.1.2 Future

Since its commercial introduction, advances in computer hardware, mathematical algorithms, detectors, and radiopharmaceuticals have improved PET scanning. Today's PET scanners have spatial resolutions on the order of 5 mm and can complete a whole-body scan within 20-40 minutes. The latest innovation in medical imaging involves hybrid cameras; CT and PET scanner technology have been melded to produce fused anatomical and physiological images (Beyer et al. 2000; Townsend and Cherry 2001). The number of PET centers has increased dramatically, from approximately 50 to approximately 300 in just two years (Coleman 2000). With improved technology, a growing inventory of PET radiopharmaceuticals, and increased public appreciation, the future of clinical and research PET is established and certain to expand.

1.2 Fluorodeoxyglucose

The most frequently encountered radioisotopes in PET imaging are ^{11}C, ^{13}N, ^{15}O, and ^{18}F. The fact that carbon, nitrogen, and oxygen are basic constituents of biological molecules and that hydrogen can generally be replaced with fluorine makes these

positron emitting radioisotopes ideal for producing PET radiopharmaceuticals (Stocklin 1998). Examples of PET radiopharmaceuticals routinely used in clinical and research studies are listed in Table 1.1.

Table 1.1: Examples of PET radiopharmaceuticals and their uses.

Radioisotope	Pharmaceutical	Use
^{11}C ($t_{1/2}$ = 20.48 min)	Glucose	Metabolism
	Carbon monoxide	Blood volume
	Acetate	Metabolism
^{13}N ($t_{1/2}$ = 9.97 min)	Ammonia	Blood flow
^{15}O ($t_{1/2}$ = 2.04 min)	Oxygen	Metabolism
	Carbon monoxide	Blood volume
	Carbon dioxide	Blood flow
	Water	Blood flow
^{18}F ($t_{1/2}$ = 109.74 min)	Fluorodeoxyglucose	Metabolism
	Fluoro-dopa	Neurotransmitter metabolism

Although hundreds of positron-labeled radiopharmaceuticals have been developed, none has had as outstanding success as ^{18}F-fluorodeoxyglucose (FDG). FDG is the most commonly used radiopharmaceutical in clinical PET studies today (Kilbourn 1996; Stocklin 1998) and it is being utilized in a wide range of medical fields. The availability and widespread use of this radiopharmaceutical is due in part to the relatively long half-life of ^{18}F. FDG can be produced at a cyclotron and transported to satellite facilities, increasing the accessibility of PET.

1.2.1 Production

The chemical synthesis developed by Hamacher and others is automated in a reaction that produces ^{18}F-FDG in high yields (Kilbourn 1996). The replacement of a hydroxyl group on the second atom with a hydrogen atom yields 2-deoxy-D-glucose; with a fluorine atom yields 2-deoxy-2-fluoro-D-glucose.

Figure 1.2: Chemical form of 2-deoxy-2-[^{18}F]fluoro-D-glucose (FDG).

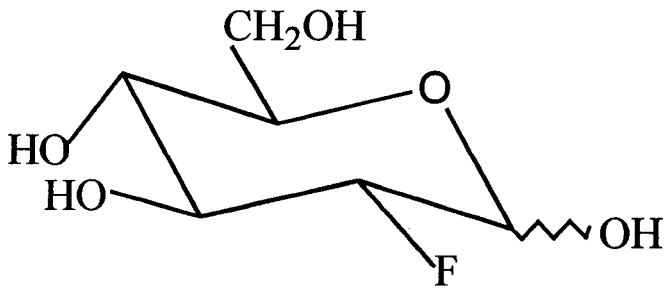

1.2.2 Biodistribution

Early work on deoxyglucose and FDG has been described by Sokoloff and others (1977), Reivich and others (1977; 1979; 1981), Gallagher and others (1977; 1978), Phelps and others (1978b; 1979), and Huang and others (1980). Sokoloff and others (1977) were the first to develop a method for the measurement of the rates of glucose consumption in the brain in vivo using ^{14}C-deoxyglucose and autoradiography. Phelps and others (1979) extended this method for the measurement of local cerebral metabolic rates in humans using FDG and PET. Reivich and others (1982) adapted the Sokoloff method for application in humans using ^{11}C-deoxyglucose and PET.

The biochemical pathway of fluorodeoxyglucose mimics that of glucose until the phosphorylation of fluorodeoxyglucose to fluorodeoxyglucose-6-phosphate (FDG-6-PO_4) in the glycolytic pathway. At this point FDG cannot be further metabolized because the next step in the pathway involves the missing hydroxyl group; it cannot be isomerized to fructose-6-phosphate or glucose-1-phosphate. Because FDG-6-PO_4 has low membrane permeability and a slow rate of dephosphorylation, it is essentially trapped in situ. Thus, FDG is a unique tracer for glucose metabolism because its retention is directly related to the flux of glucose through the glycolytic pathway, the (glucose) energy demands of the tissues.

Figure 1.3: Metabolic pathway of glucose compared to FDG.

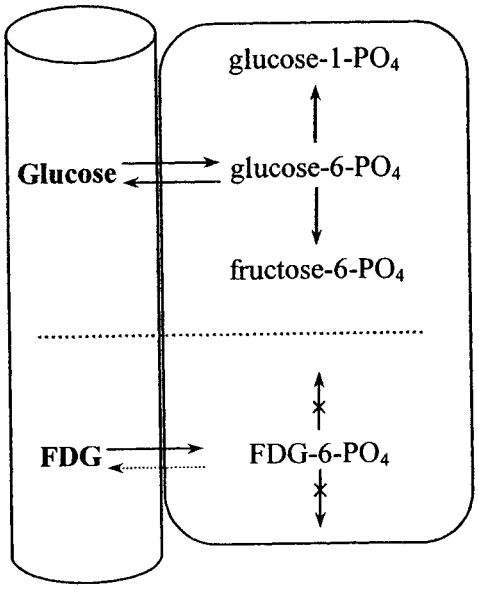

1.2.3 Applications

FDG PET has extensive clinical and research utility. Its original applications were in studying cerebral glucose metabolic rate and regional myocardial glucose metabolism. Today, applications in neurology and cardiology are significant for diagnosis and research of various brain and heart diseases. However, the largest clinical use of FDG worldwide today is in oncology (Scott 2001). Glucose consumption in cancer cells is amplified, providing high signal to background images of FDG. Whole-body PET scans are routinely performed in order to detect primary tumors and metastases; abnormal tumor metabolism can be detected before anatomic changes are visible (Phelps 2000). FDG PET is versatile due to its ability to detect, diagnose, and grade tumors, as well as predict and assess treatment response (Phelps 2000).

Table 1.2: Principal applications of FDG PET.

Medical field	Application
Oncology	Tumor evaluation
	Tumor staging
Neurology/Psychiatry	Alzheimer's
	Epilepsy
Cardiology	Myocardial viability

Although there are a myriad of applications of FDG in adults, use in children and infants has centered primarily on investigations of cerebral function. Regional cerebral glucose metabolism in newborns and infants has been extensively investigated as it relates to behavioral, neurophysiological, and anatomical development (Doyle et al.

1983; Chugani and Phelps 1986; Thorp et al. 1988; Suhonen-Polvi et al. 1993; Suhonen-Polvi 1995; Suhonen-Polvi et al. 1995; Kinnala et al. 1996; Kinnala et al. 1997). Pediatric oncology is a principal field in clinical and research studies with FDG PET, but other applications are being developed. Acute lung injury in neonates has been investigated (Kirpalani et al. 1997), as well as inflammatory bowel disease (Skehan et al. 1999).

1.3 Conclusion

FDG has been established as the primary radiopharmaceutical for PET scanning, and will continue to provide advances in diagnostic imaging and research. As the cost of PET scanning decreases, its availability will increase. With an overall increase in nuclear medicine procedures being performed and the significant progress in radiopharmaceutical production and PET instrumentation (UNSCEAR 2000), it is hoped that PET will be the next plateau for nuclear medicine (Early 1995).

1.4 Thesis statement

Considering the widespread use of FDG in PET scanning, the radiation absorbed dose estimates calculated for FDG have been surprisingly scant. There have been a few dose estimates published for the North American adult male and the Japanese adult male, but there has been little or no mention of variations in the average dose due to sex, age, height, weight, nationality, diet, or pathological condition. One reason for this is the lack of biokinetic data obtained in women, children, and infants, a limitation that is

symptomatic for most nuclear medicine radiopharmaceuticals. In addition, the primary method used to calculate internal doses lacks the detail needed to adjust the dose calculation for variations in organ masses of the individual under consideration.

The first step in my research has been, therefore, to address and resolve the issue of non-standard use of patient-specific dosimetry; I have proposed a simple patient-specific dose equation for use in internal dose calculations. I have then proceeded with an investigation into some of the differences in absorbed doses that exist between men and women undergoing clinical FDG-PET scans for typical diagnostic procedures. While this research was underway, the opportunity to study premature infants provided additional biokinetic data never before collected or analyzed. With no previously published results specifically on the uptake or dose of FDG in women or very low birth weight infants, the data presented in this thesis may be used as the basis for further research into the dosimetry of FDG.

Chapter 2: Internal Dosimetry

2.1 Introduction

Human beings can benefit greatly from the use of radiation in medical, industrial, research, and power generating applications. The realization of these benefits must be weighed against the hazards involved in their procurement and use. The primary radiation protection hazard involves the exposure of individuals to radiation (Turner 1995). Whether external or internal, it is presumed that there is some risk associated with radiation exposure; this is measured as radiation absorbed dose and manifested as deleterious biological effects. The radiation absorbed dose may then be limited to a level regarded as acceptable to the individuals or populations for the assumed risk. The objective of radiation protection is thus to allow the attainment of the benefits of ionizing radiation while minimizing the risks to individuals or populations (Kiefer et al. 1969).

Internal dosimetry is the field of Health Physics dedicated to measuring and recording the absorbed doses from radionuclides deposited within the body. It is essentially " ... the scientific methodology used to measure, calculate, estimate, assay, predict and otherwise quantify the radiative energy absorbed by the ionization and excitation of atoms in human tissues as a result of the emission of energetic radiation by internally deposited radionuclides" (Raabe 1994). Absorbed dose estimates are required

for occupational exposures in radiation protection as well as environmental exposures in radiation epidemiology (Zanzonico 2000). Internal dosimetry is also essential in assessing the risks involved in medical studies, including diagnostic imaging, therapy, or noninvasive physiological and metabolic studies (Loevinger et al. 1991).

2.2 History of internal dosimetry

A brief history of internal dosimetry is presented here. This may be used as a guide for the text presented in this chapter as future material may not necessarily be presented chronologically. Unless otherwise noted, the reference for the material presented in this section is Schlafke-Stelson and others (1995).

Although natural radioactivity was discovered in 1896 by Henri Becquerel, its use did not hold much interest in the medical community, mainly because of its low specific activity. Marie Curie separated radium from uranium ore in 1898, yielding a radionuclide with high specific activity that was encapsulated and used for therapy. The first tracer studies in humans began in the 1920's and expanded, along with therapy, in the 1930's with the introduction of artificial radioactivity. The production of artificial radionuclides was lead by accelerators and cyclotrons and later progressed with reactors. This resulted in the introduction of new tracers and therapeutic agents, which generated the need for internal dose estimates.

Original dose estimates centered on radium and radon implants (capsules, needles, and seeds) which were used to produce exposures that would kill tumor cells while limiting damage to surrounding tissue. Leonidas Marinelli presented the first paper on the internal dosimetry of artificial radionuclides in 1941 at the Annual Meeting of the American Radium Society. The first equations used in dose estimates considered only the dose from beta emissions because this dose was known to be several times higher than that from gamma emissions. In 1948, Marinelli and others addressed this problem and proposed a method for calculating the dose from gamma emissions that was similar to that for beta emissions. However, as noted by Marinelli in 1942, "The main difficulties encountered in isotope dosimetry are of biological nature ..." (Marinelli 1942).

During World War II there was a gap in published papers. Before the war, the United States Advisory Committee on X Rays and Radium Protection had provided recommendations on the safe use of x-rays and radium. This group was reorganized after the war as the National Committee on Radiation Protection and Measurements (NCRP) and later renamed the National Council on Radiation Protection and Measurements. An important meeting of the NCRP and the re-established International Committee on Radiation Protection (ICRP) occurred in 1949 to define corresponding radiation protection practices. At this meeting the need for a "standard man" was recognized and it was agreed that anatomical and physiological data representing an average human for internal dose estimates must be established. Work on Standard Man persisted for over a

decade; further work amassing these data continued under the now recognizable name of Reference Man.

During the 1950's there was an exponential growth in the use of radionuclides in humans. This was due to the establishment of medical research programs by the Atomic Energy Commission in the United States. During this time, Robert Loevinger and others wrote several papers summarizing internal dosimetry calculations and theories for medical and health physicists. The "gold standard' on dosimetry was the book *Radiation Dosimetry* published in 1956, edited by Hine and Brownell. The chapter written by Loevinger, Holt, and Hine titled "Internally Administered Radioisotopes" provided a clearly written summary of the methods currently used for internal dose calculations.

The introduction of computers fueled improvements in internal dose calculations in the 1960's through the Monte Carlo technique. This method followed the path of a gamma ray by statistical means and recorded its history of interactions until its energy was completely absorbed or it escaped the body. Using this technique, source shapes and volumes other than the traditional spheres and cylinders were modeled. In 1964 and 1965 William Ellett and others published tables of Monte Carlo data as absorbed fractions (AFs) – the fraction of emitted gamma ray energy that is absorbed by the geometrical structures of a mathematical model.

Great strides in imaging techniques were also made during the 1960's. Nuclear medicine departments flourished around the world, especially in the United States. There was a shift from the use of radionuclides for therapeutic purposes to diagnostic purposes; radiopharmaceuticals emitting gammas instead of betas were emphasized. This prompted several members of the Society of Nuclear Medicine (SNM) to improve the methods of estimating radiation absorbed dose. Current deficiencies identified at the time included incomplete descriptions of radionuclide emissions, inconsistent methods of estimating dose, inadequate models of the human body, and inaccurate and limited biokinetic information. Hence, "The Society's ad hoc committee on dose calculations" was organized to address these concerns and held its first meeting in 1964.

Over the course of three years, several meetings were held; during the second meeting the name Medical Internal Radiation Dose (MIRD) Committee was chosen. The objective of the committee, stated at its first meeting is (Smith 1968):

> To provide the best possible estimate of absorbed dose to patients resulting from the diagnostic or therapeutic use of internally administered radiopharmaceuticals with the restriction that the committee make no judgment as to the medical significance of the estimated absorbed dose.

The committee proposed to develop, collect, and critically evaluate information pertaining to (Smith 1968):

1. Formulae, units and symbols that are consistent for absorbed-dose calculations by either manual or computer techniques.
2. Physical and nuclear decay-scheme data needed as input for the formulae developed.
3. Metabolic data on the distribution and life-times of radiopharmaceuticals at the total-body, specific-organ, sub-organ and

micro-organ level where necessary as well as the influence on the patient's age and clinical state on these variables.
4. Chemical, radiochemical and radionuclide purity and stability and physical characteristics of radiopharmaceuticals when they are apt to affect the absorbed dose to the patient.
5. Accuracy of the calibration methods used for determining the activity of a radiopharmaceutical.
6. Anatomical and physiological data for patients of various ages and body types.

At the third meeting, Loevinger presented his approach to a unified beta-gamma dose calculation method; this work was later published by Loevinger and Berman (1968a). The first MIRD pamphlet, which contained general dose equations and dose equations for a uniform isotropic model, was published by Loevinger and Berman (1968b). A revised version (Loevinger and Berman 1976) was published to include the S-value and residence time parameters.

The first MIRD Committee documents were accepted worldwide and regarded as valuable works in internal dosimetry. Further publications by the MIRD Committee clarified dose equations, decay scheme data, absorbed and specific absorbed fractions (SAFs), S-values, biological data acquisition and analysis, and dose estimates. To date, there are 21 MIRD Pamphlets (including three revisions) and five books (including one revision). These are listed in Table 2.1 and Table 2.2, respectively.

Table 2.1: List of MIRD pamphlets.

Number	Title	Reference
1	A schema for absorbed-dose calculations for biologically distributed radionuclides	Loevinger and Berman 1968b
1 Revised	A revised schema for calculating the absorbed dose from biologically distributed radionuclides	Loevinger and Berman 1976
2	Energy deposition in water by photons from point isotropic sources	Berger 1968
3	Absorbed fractions for photon dosimetry	Brownell et al. 1968
4	Radionuclide decay schemes and nuclear parameters for use in radiation-dose estimation	Dillman 1969
5	Estimates of absorbed fractions for monoenergetic photon sources uniformly distributed in various organs of a heterogeneous phantom	Snyder et al. 1969
5 Revised	Estimates of specific absorbed fractions for photon sources uniformly distributed in various organs of a heterogeneous phantom	Snyder et al. 1978
6	Radionuclide decay schemes and nuclear parameters for use in radiation-dose estimation, Part 2	Dillman 1970
7	Distribution of absorbed dose around point sources of electrons and beta particles in water and other media	Berger 1971
8	Absorbed fractions for small volumes containing photon-emitting radioactivity	Ellett and Humes 1971
9	Radiation dose to humans from Se-75-L-Selenomethionine	Lathrop et al. 1972
10	Radionuclide decay schemes and nuclear parameters for use in radiation-dose estimation	Dillman and Von der Lage 1975
11	"S," absorbed dose per unit cumulated activity for selected radionuclides and organs	Snyder et al. 1975
12	Kinetic models for absorbed dose calculations	Berman 1977
13	Specific absorbed fractions for photon sources uniformly distributed in the heart chambers and heart wall of a heterogeneous phantom	Coffey et al. 1981
14	A dynamic urinary bladder model for radiation dose calculations	Thomas et al. 1992
14 Revised	A dynamic urinary bladder model for radiation dose calculations	Thomas et al. 1999

Table 2.1 continued: List of MIRD pamphlets.

Number	Title	Reference
15	Radionuclide S values in a revised dosimetric model of the adult head and brain	Bouchet et al. 1999a
16	Techniques for quantitative radiopharmaceutical biodistribution data acquisition and analysis for use in human radiation dose estimates	Siegel et al. 1999
17	The dosimetry of nonuniform activity distributions-radionuclide S values at the voxel level	Bolch et al. 1999
18	Administered cumulated activity for ventilation studies	Thomas 2001

Table 2.2: List of MIRD books.

Title	Reference
MIRD primer for absorbed dose calculations	Loevinger et al. 1988
MIRD: radionuclide data and decay schemes	Weber et al. 1989a
MIRD primer for absorbed dose calculations: revised	Loevinger et al. 1991
MIRD cellular S values: self-absorbed dose per unit cumulated activity for selected radionuclides and monoenergetic electron and alpha particle emitters incorporated into different cell compartments	Howell et al. 1997
MIRD head and brain dosimetry: absorbed fractions of energy and absorbed dose per unit cumulated activity within pediatric and adult head and brain models for use in nuclear medicine internal dosimetry	Bouchet et al. 1999b

The MIRD Committee utilized the works of others, especially for biological data and mathematical phantoms. The lack of biological data was, and remains, of particular concern. Nuclear medicine departments were enlisted to try to fill some of this void; the series of MIRD Dose Estimate Reports was the outcome. Internal dosimetry of nuclear medicine procedures was further aided in 1977 when, on a directive by the editor of the

Journal of Nuclear Medicine, dosimetry data were required from authors submitting articles describing new radiopharmaceuticals.

Table 2.3: List of MIRD dose estimate reports.

Number	Title	Reference
1	Selenium-75-L-selenomethionine	Lathrop et al. 1973
2	Summary of current radiation dose estimates to humans from 66Ga-, 68Ga-, and 72Ga-citrate	Cloutier et al. 1973b
3	Summary of current radiation dose estimates to humans with various liver conditions from 99mTc-sulfur colloid	Atkins et al. 1975
4	Summary of current radiation dose estimates to humans with various liver conditions from 198Au-colloidal gold	Cloutier et al. 1975
5	Summary of current radiation dose estimates to humans from 123I, 124I, 125I, 126I, 130I, 131I, and 132I as sodium iodide	Thomas et al. 1975
6	Summary of current radiation dose estimates to humans from 197Hg- and 203Hg-labeled chlormerodrin	Blau et al. 1975
7	Summary of current radiation dose estimates to humans from 123I, 124I, 126I, 130I, and 131I as sodium rose Bengal	Eary et al. 1975
8	Summary of current radiation dose estimates to normal humans from 99mTc as sodium pertechnetate	Lathrop et al. 1976
9	Estimates of radiation absorbed doses from radioxenons in lung imaging	Atkins et al. 1980
10	Radiation absorbed dose from albumin microspheres labeled with technetium-99m	Blau et al. 1982
11	Radiation absorbed doses from iron-52, iron-55, and iron-59 used to study ferrokinetics	Robertson et al. 1983
12	Radiation absorbed dose from Tc-99m diethylenetriaminepentaacetic acid (DTPA)	Thomas et al. 1984
13	Radiation absorbed dose from Tc-99m labeled bone imaging agents	Weber et al. 1989b
14	Radiation absorbed dose from technetium-99m-labeled red blood cells	Atkins et al. 1990
15	Radiation absorbed dose estimates for radioindium-labeled autologous platelets	Robertson et al. 1992
16	Radiation absorbed dose from technetium-99m-diethylenetriaminepentaacetic acid aerosol	Atkins et al. 1992

Table 2.3 continued: List of MIRD dose estimate reports.

Number	Title	Reference
17	Radiation absorbed dose estimates from inhaled krypton-81m gas in lung imaging	Atkins et al. 1993
18	Radiation absorbed dose estimates for indium-111-labeled B72.3, an IgG antibody to ovarian and colorectal cancer	Mardirossian et al. 1998
19	Radiation absorbed dose estimates from 18F-FDG	Hays et al. 2002

Initial dose estimates were calculated using a mathematical model developed by Snyder and others (1969) that contained both male and female organs. This model has been adjusted over the years, and several new mathematical models have been developed, including ones for children and pregnant women. As the models are refined, the accuracy of internal dose estimates improves.

Also begun in the 1960's was the first international symposium on internal dosimetry for nuclear medicine procedures. Since 1969 seven meetings of the International Radiopharmaceutical Dosimetry Symposia have been held; the meetings occur every few years with the most recent in 2002 (Seventh International Radiopharmaceutical Dosimetry Symposium 2002). About the same time as the first symposium was held and the MIRD Committee was being established, a center for internal dosimetry information was founded. The Radiation Internal Dose Information Center (RIDIC) has become a resource center for the most recent information on internal dosimetry techniques and internal dose estimates (Radiation Internal Dose Information Center 2002).

The review of internal dosimetry essentially ends here. The extent and accuracy of internal dosimetry techniques and estimates are continuously evaluated; the advances in this field in the 1980's and 1990's cannot be presented here in detail. However, an important area of continuing development lies in imaging anatomy and physiology of health and disease. CT and MRI provide details of patient anatomy with far better resolution than previously achievable. Single photon emission computed tomography (SPECT) and PET are used to study metabolic function and can provide information concerning the uptake and distribution of radionuclides.

2.3 Fundamentals of MIRD

The radiation absorbed dose, which may be abbreviated to dose, is defined as the amount of energy absorbed from ionizing radiation per unit mass. Computation of dose requires knowledge of the biological distribution of the radionuclide within a subject, knowledge of the physical properties of the radionuclide, and the use of a mathematical model representing the subject for whom the dose is calculated. The biological distribution of the radionuclide is the information obtained which describes the duration, location, and amount of activity of the radionuclide within a subject. The physical properties of the radionuclide equate to the energy released for each type and frequency of transition of the radionuclide. The mathematical model is a set of parameters defined for a subject that relate to the fraction of energy released by the radionuclide that is absorbed in the tissue of that subject. These requirements are related as follows (Smith 1970):

$$\begin{aligned} absorbed\ dose = &\{biological\ properties\ of\ the\ radionuclide\ within\ the\ subject\}\times \\ &\{physical\ properties\ of\ the\ radionuclide\}\times \\ &\{mathematical\ properties\ of\ the\ model\} \end{aligned} \qquad (2.1).$$

2.3.1 A unified theory

The first method of calculating dose was based on classifying radiation emissions as either non-penetrating (alphas, betas, electrons, low-energy photons) or penetrating (photons). Sets of equations were produced covering point beta particle, point gamma ray, distributed beta particle, and distributed gamma ray sources for point, line, surface, and volume situations (Loevinger 1970). Generality of absorbed dose equations was not possible. Decades of research in internal dosimetry were finally culminated when a unified theory for calculating radiation absorbed dose was published in 1968 (Loevinger and Berman 1968a). This work provided a formalism for internal dosimetry that could be applied to all radionuclides and models, regardless of the classification of emissions, and was the basis for the first MIRD publication (Loevinger and Berman 1968b).

According to the unified theory, it is possible to ignore the statistical fluctuations that occur when considering very small volumes containing only a few atoms or radiation interactions and to focus only on macroscopic compositions and changes (Loevinger and Berman 1968a). The material in which the energy is deposited is commonly referred to as the target, while the material from which the ionizing radiation originates is referred to

as the source. Hence, the average absorbed dose to a target region irradiated by a source region is given as:

$$\overline{D}_{(target \leftarrow source)} = \left(\frac{\widetilde{A}_{source}}{m_{target}} \right) \cdot \sum_i \Delta_i \phi_{i(target \leftarrow source)} \qquad (2.2)$$

where $\overline{D}$ = the mean radiation absorbed dose (mGy);
$\tilde{A}$ = cumulated activity (MBq h);
m = mass (kg);
i = type of radiation emitted;
Δ = mean energy emitted per nuclear transition (originally termed the equilibrium dose constant) (mGy kg MBq^{-1} h^{-1}); and
ϕ = absorbed fraction, or AF.

It should be noted that a target region could also be considered a source region. In this case, the dose to the target region from itself is termed the self-dose; it is almost always the largest contributor to an organ's total absorbed dose. As well, the total body could be considered a source region when the radionuclide is uniformly distributed throughout the body.

The cumulated activity is simply the time integral from zero to infinity of the activity within the source region:

$$\widetilde{A}_{source} = \int_0^\infty A_{source}(t)\, dt \qquad (2.3)$$

where A = activity (MBq); and
t = time (h).

The mean energy emitted per nuclear transition and the AF are calculated respectively as:

$$\Delta_i = K \cdot n_i E_i \qquad (2.4)$$

where K = constant (0.5757 when E is expressed in MeV);

n = the mean number of particles or photons emitted per disintegration; and
E = the mean energy per particle or photon (MeV).

and:

$$\phi = \frac{amount\ of\ energy\ absorbed\ in\ the\ target\ region}{amount\ of\ energy\ released\ from\ the\ source\ region} \qquad (2.5).$$

Equation (2.2) can also be written as:

$$\overline{D}_{(target \leftarrow source)} = \widetilde{A}_{source} \cdot \sum_i \Delta_i \Phi_{i(target \leftarrow source)} \qquad (2.6)$$

where $\Phi = \frac{\phi}{m_{target}}$ (2.7)

= specific absorbed fraction, or SAF (kg^{-1}).

The concept of the SAF was introduced by Loevinger and Berman (1968a) as an extension of the AF developed by Ellett and others in 1964.

Equations (2.2) and (2.6) are general dose equations; other dose equations derived from these may be considered special cases (Loevinger and Berman 1968b). The size or uniformity of the source or target regions, the source activity, and the absorbing material do not limit these equations (Loevinger and Berman 1968b).

2.3.2 The uniform isotropic model and reciprocity theorem

The *uniform isotropic model* requires that the target and source regions are in a homogeneous absorbing material large enough to make edge effects negligible, and that the radioactivity is uniformly distributed in the source region (Loevinger and Berman 1968b). Within this model exist useful reciprocal relations presented here for the

historical value they played in the development of internal dosimetry. The *reciprocity theorem* is valid for any pair of regions in the uniform isotropic model such that:

a) the SAF is independent of which region is designated as the source or the target

$$\Phi_{i(region\ 1 \leftarrow region\ 2)} = \Phi_{i(region\ 2 \leftarrow region\ 1)} = \Phi_{i(region\ 1 \leftrightarrow region\ 2)} \tag{2.8}$$

b) the mean radiation absorbed dose per unit cumulated activity is independent of which region is designated as the source or the target

$$\frac{\overline{D}_{(region\ 1 \leftarrow region\ 2)}}{\widetilde{A}_{region\ 2}} = \frac{\overline{D}_{(region\ 2 \leftarrow region\ 1)}}{\widetilde{A}_{region\ 1}} \tag{2.9}.$$

Equations (2.2) and (2.6) may then be written, respectively, as:

$$\overline{D}_{(target \leftarrow source)} = \left(\frac{\widetilde{A}_{source}}{m_{target}} \right) \cdot \sum_i \Delta_i \phi_{i(target \leftrightarrow source)} \tag{2.10}$$

and:

$$\overline{D}_{(target \leftarrow source)} = \widetilde{A}_{source} \cdot \sum_i \Delta_i \Phi_{i(target \leftrightarrow source)} \tag{2.11}.$$

In other words, the dose received at a point from a uniform distribution of activity within a volume is equivalent to the average absorbed dose received by that volume from the same amount of activity concentrated at that point (Brownell et al. 1968). These equations are theoretically valid in the presence of scattered radiation; although the conditions of the uniform isotropic model may not be found in practice, it is believed that the reciprocity dose equations may be used without substantial error (Loevinger and Berman 1968b).

2.3.3 Constructing the MIRD equations

The MIRD equations began a new era in internal dosimetry. The unified theory became the standard for calculating absorbed dose estimates and was the basis from which future developments in dose equations stemmed. However, to fully comprehend the MIRD equations, one must first become familiar with its components. The three requirements for calculating the absorbed dose – biological, physical, and mathematical – are clearly displayed in Equations (2.10) and (2.11). These essential components are discussed separately.

2.3.3.1 Physical properties of radionuclides

2.3.3.1.1 Decay schemes

The physical properties required in calculating dose estimates are the types and energies of the emissions per transition of the radionuclide. Until work on radionuclide decay schemes was undertaken by the MIRD Committee, the decay schemes available were generally lacking information on Auger and conversion electrons, as well as x-rays (Smith et al. 1965; Schlafke-Stelson et al. 1995). Absolute yields of gamma rays were difficult to obtain because they were presented as relative intensities (Schlafke-Stelson et al. 1995).

Detailed decay schemes for internal dosimetry were begun by Dillman and others (1969; 1970; 1975). These decay schemes listed the prominent emissions and their absolute intensities as well as the mean energy emitted per nuclear transition for

radionuclides used in nuclear medicine. Current nuclear and atomic decay data in the MIRD format may be obtained for over 200 radionuclides either from the data published by Weber and others (1989a) or from the National Nuclear Data Center (2002).

2.3.3.1.2 Classifications of radionuclide emissions

As stated earlier, the two customary classifications of ionizing radiation are non-penetrating (np) and penetrating (p). Non-penetrating radiation refers to those emissions for which the majority of the energy is absorbed within the source. Originally intended for alpha and beta particles, non-penetrating emissions also include positrons, Auger electrons, conversion electrons, and low-energy photons. In the case of low-energy photons, an upper limit of 11.3 keV was proposed by Loevinger and others (1956) as it corresponds to 95% of the energy absorption in water within 10 mm of the site of emission.

2.3.3.2 Mathematical properties of models

2.3.3.2.1 Phantoms: the mathematical models

Absorbed doses are calculated through the use of anthropomorphic phantoms – mathematical descriptions that approximate in size, shape, and composition the human body. Geometrical structures form the body and internal organs and tissues; minor features are neglected. These structures represent the target and source regions for which AFs are calculated; the regions are fixed in position and mass.

The earliest calculations of AFs for penetrating radiation represented the body as ellipsoids or spheres (Ellett et al. 1964; Ellett et al. 1965; Reddy et al. 1967; Brownell et al. 1968). The first mathematical model, a hermaphrodite adult, was introduced in MIRD Pamphlet No. 5 and approximated a "standard man" (Snyder et al. 1969). The model contained 22 internal organs, homogeneous in composition and density, that were considered source organs for monoenergetic, uniformly distributed photons. Absorbed fractions for 25 target organs and 16 source organs were tabulated for 12 monoenergetic photon sources ranging from 10 keV to 4 MeV. These organs were contained within three principal sections of the total body: the head, the trunk, and the legs. This work improved upon previous calculations of AFs by taking into account the actual size, shape, composition, and density of human organs.

The 'MIRD phantom' has been used as the basis for the development of several new mathematical models. For example, Cristy and Eckerman (1987) developed mathematical models for children ages 0, 1, 5, 10, and 15 years and for an adult male. More recently, Stabin and others (1995) produced mathematical models for a non-pregnant woman and a woman at 3, 6, and 9 months gestation. Table 2.4 lists the mathematical models used primarily in the dose estimates in the MIRD schema.

Table 2.4: Mathematical models

Models	Title	Reference
Adult male/female	Estimates of absorbed fractions for monoenergetic photon sources uniformly distributed in various organs of a heterogeneous phantom	Snyder et al. 1969
Adult male/female, revised	Estimates of specific absorbed fractions for photon sources uniformly distributed in various organs of a heterogeneous phantom	Snyder et al. 1978
Adult male/female	A tabulation of dose equivalent per microcurie-day for source and target organs of an adult for various radionuclides	Snyder et al. 1974
Newborn, 1, 5, 10, and 15 year old	Mathematical phantoms representing children of various ages for use in estimates of internal dose	Cristy 1980
Newborn, 1, 5, 10, 15 year old male and adult female, adult male	Specific absorbed fractions of energy at various ages from internal photon sources	Cristy and Eckerman 1987
Adult female, 3, 6, and 9 months gestation	Mathematical models and specific absorbed fractions of photon energy in the nonpregnant adult female and at the end of each trimester of pregnancy	Stabin et al. 1995

Several organs and tissues of the body have been modeled specifically for use in internal dose estimates. Examples are the heart wall and chambers (Coffey et al. 1981), the peritoneal cavity (Watson et al. 1989), the urinary bladder (Thomas et al. 1992; Thomas et al. 1999), the prostate gland (Stabin 1994a), and the head and brain (Bouchet et al. 1999a).

The most recent development in anthropomorphic phantoms is the introduction of voxel (volume element) phantoms. These are models based on images produced from CT

or MRI scans; the human anatomy is imaged and the data stored in voxel format. The voxels are grouped to form organs and structures within the body and form higher resolution three-dimensional models than previously achieved. The first voxel phantom produced by Zubal and others (1994) yielded a 128×128×246 matrix with an isotropic cubic voxel resolution of 4 mm. It has been proposed that voxel phantoms will eventually replace the existing sets of anthropomorphic phantoms commonly used today (Stabin et al. 1999).

2.3.3.2.2 Absorbed and specific absorbed fractions: penetrating radiation

The AF was introduced by Ellett and others (1964; 1965) to facilitate the calculation of absorbed dose from gamma rays. Later extended by Loevinger and Berman (1968a) to the concept of the SAF, these parameters represent the fraction of photon energy absorbed in a target region that is emitted from a source region. The calculations of absorbed and SAFs are complicated functions that depend on several factors. These factors include the shape, mass, and composition of the source and target regions, the distance between the regions, the composition of the medium through which the photon is traveling, and the probabilities of photon interactions for a given photon energy (Schlesinger 1978).

Calculation of the AFs for photons is not easily determined because the majority of the energy is absorbed outside the source volume. Determinations of the AF and SAF have been made extensively through the use of Monte Carlo techniques (Ellett et al.

1964; Ellett et al. 1965; Reddy et al. 1967; Brownell et al. 1968; Snyder et al. 1969). When this method does not produce appropriate values of ϕ_i or Φ_i, the point isotropic function reported by Berger (1968) may be used to calculate these values directly:

$$\Phi_{point}(x) = \left[\frac{\mu_{en}}{\rho} \cdot \frac{e^{-\mu x}}{4\pi x^2}\right] \cdot B_{en}(\mu x) \tag{2.12}$$

where Φ_{point} = point isotropic specific absorbed fraction (kg^{-1});
x = the distance between pairs of points in the source and target (cm);
μ_{en} = linear energy absorption coefficient of primary photons (cm^{-1});
μ = linear energy attenuation coefficient of primary photons (cm^{-1});
ρ = mass density (kg cm^{-3}); and
B_{en} = point isotropic energy absorption build-up factor.

This equation describes the AF of an isotropic point source within an infinite uniform absorber such that the energy absorbed around that point is a function only of the distance from that source (Loevinger et al. 1968b).

For any target and source regions, the SAF is the mean of the point isotropic SAF for all pairs of points within the target and source regions (Loevinger et al. 1991):

$$\Phi_{i\,p(target \leftarrow source)} = \frac{1}{v_{target} \cdot v_{source}} \int_{target} \int_{source} \Phi_{i\,p}(x)\, dv_{source}\, dv_{target} \tag{2.13}$$

where v = volume (cm^3).

Most AFs are tabulated for unit density materials, so the *density transformation rule* may be employed for tissues of different densities (Loevinger et al. 1968a). This rule states that for the uniform isotropic model, the AFs are independent of density provided that for each region, the size and shape are specified in terms of mass per unit area (Loevinger et al. 1968a; Loevinger et al. 1968b). This may be shown to be true by examining the

relation between a volume v of density ρ of a region. The original volume transformed for a new volume, v', and density, ρ' (given that ρx=ρ'x') yields the relation:

$$\begin{aligned} v &= \iiint dx\,dy\,dz = \rho^{-3} \iiint d(\rho x)\,d(\rho y)\,d(\rho z) \\ &= \left(\frac{\rho'}{\rho}\right)^3 \iiint dx'\,dy'\,dz' \\ &= \left(\frac{\rho'}{\rho}\right)^3 v' \end{aligned} \qquad (2.14).$$

Since m=ρv and $\Phi = \phi/m$, it follows that:

$$m = \left(\frac{\rho'}{\rho}\right)^2 m' \qquad (2.15)$$

and:

$$\Phi' = \left(\frac{\rho'}{\rho}\right)^2 \Phi \qquad (2.16).$$

Hence, the tabulated values of SAFs for unit density materials may be extended for mass densities that were not specifically calculated (e.g. – lung or bone densities).

2.3.3.2.3 Absorbed and specific absorbed fractions: non-penetrating radiation

Calculation of the AF for non-penetrating radiation is relatively simple because the range of these emissions in soft tissue is on the order of millimeters (Cloutier and Watson 1987). Hence, non-penetrating radiation distributed within a source is defined as depositing all its energy within that source and none outside:

$$\phi_{np(target \leftarrow target)} = 1 \qquad (2.17)$$

$$\phi_{np(target \leftarrow source)} = 0 \tag{2.18}$$

for the AF, and:

$$\Phi_{np(target \leftarrow target)} = \frac{1}{m_{target}} \tag{2.19}$$

$$\Phi_{np(target \leftarrow source)} = 0 \tag{2.20}$$

for the SAF.

As noted previously, the total body may be considered a source, yielding the SAF from the total body to all targets:

$$\Phi_{np(target \leftarrow tb)} = \frac{1}{m_{tb}} \tag{2.21},$$

which follows from electronic equilibrium conditions.

2.3.3.2.4 S-values

The AFs were recalculated in 1974 using the methods developed in MIRD Pamphlet No. 5, but with a more realistic phantom and better statistical results (Snyder et al. 1974). The primary method of calculating AFs for photons was the Monte Carlo technique. When the coefficient of variation of these results exceeded 50%, the point isotropic specific absorbed fraction was used. Unlike MIRD Pamphlet No. 5, therefore, values were reported for each case. The advantage of the Monte Carlo technique is that it can take into account the approximate size, shape, position, density, and composition of the organs and the surrounding materials (Snyder et al. 1974). It is more difficult to

simulate the various densities, compositions, and shapes of the organs with the point isotropic specific absorbed fraction.

In addition to recalculating the SAFs, the tabulated quantity S was introduced by Snyder and others (1974; 1975) as the absorbed dose per unit cumulated activity:

$$S_{(target \leftarrow source)} = \sum_i \Delta_i \Phi_{i(target \leftarrow source)} \tag{2.22}$$

where S = S-value (mGy MBq^{-1} h^{-1}).

The S-values could be divided according to the classifications of ionizing radiation as:

$$S_{(target \leftarrow source)} = S_{np(target \leftarrow source)} + S_{p(target \leftarrow source)} \tag{2.23}.$$

This quantity simplified calculations by tabulating the mean energy emitted per nuclear transition and the SAF for selected radionuclides given specific source and target pairs. The dose equation then becomes:

$$\overline{D}_{(target \leftrightarrow source)} = \widetilde{A}_{source} \cdot S_{(target \leftrightarrow source)} \tag{2.24},$$

which is a simplified form of Equation (2.11).

2.3.3.3 Biological properties of radiopharmaceuticals

2.3.3.3.1 Reference Man

While the theoretical equations for internal dosimetry were being developed, an equally important line of work acquiring biological information was growing in parallel. The significant events that occurred in this field are revealed in the introduction to the Report of the Task Group on Reference Man (ICRP 1975) and are summarized here.

In the late 1940's it was recognized that a set of biological parameters needed to be defined for use in internal dosimetry calculations. The ICRP advanced much of the developments in this area. Probably one of the most important events in this field was the *Chalk River Conference on Permissible Doses* held in Chalk River, Ontario, Canada in 1949. The objective was to formalize values that could be applied to the average individual, named 'Standard Man'. Data concerning the masses of organs were accepted, as well as data on the chemical composition of the total body and various tissues. However, it was stated in the conference proceedings that much effort needed to be focused on obtaining more accurate data on the chemical compositions of the body and its tissues. Finally, it was decided that the patterns of intake and excretion as well as the duration of occupational exposure should be averages for the normal activity of an individual in the Temperate Zone.

Work on Standard Man was prolific; these values were modified three times between 1950 and 1954, each at different conferences. Two reports by the International Sub-Committee II on Permissible Dose for Internal Radiation then followed, one in 1954 and one in 1959. The first report contained data on 15 naturally occurring elements in the human body; the second contained data on 46 elements. The 1959 report contained a listing of the concentrations of 44 elements in 36 tissues, as well as data concerning elimination and deposition parameters. This report consisted of the most detailed technical description of Standard Man and was widely used as the basis for dose estimation.

Further work began in 1963 when the Task Group was established by Committee II of the ICRP to revise and extend the concept of Standard Man. It was suggested by the ICRP that the name be changed from 'Standard Man' to 'Reference Man'. The Task Group was assigned the duty of reviewing and adapting the specifications defined for Standard Man to account for the current needs of health physicists. The product, *Report of the Task Group on Reference Man* (ICRP 1975), is the defining document of biological data for dosimetry calculations.

The guidelines of the Task Group are quoted here, as they should be recognized in understanding the extent and importance of this report (ICRP 1975):

> (a) It was agreed that the Task Group would limit its attention to those characteristics of man which are known to be important or which are likely to be significant for estimation of dose from sources of radiation within or outside the body. ...
>
> (b) The Task Group agreed that it is neither feasible nor necessary to specify Reference Man as representative of a well-defined population group. ... Reference Man is defined as being between 20-30 years of age, weighing 70 kg, is 170 cm in height, and lives in a climate with an average temperature of from 10° to 20°C. He is a Caucasian and is a Western European or North American in habitat and custom.
>
> (c) The Task Group agreed that it was not feasible to define Reference Man as an "average" or a "median" individual of a specified population group and that it was not necessary that he be defined in any such precise statistical sense. ... Only a very few individuals of any population will have characteristics which approximate closely those of Reference Man, however he is defined. The importance of the Reference Man concept is that his characteristics are defined rather precisely, and thus if adjustments for individual difference are made, there is a known basis for the dose estimation procedure and for the estimation of the adjustment factor needed for a specified type of individual. ...
>
> (d) Ideally, each characteristic which is specified should have some indication of the range of this parameter in the population. ... Except for a few characteristics – such as weight, height, etc. – which are obtained

> rather easily, it is likely that the health physicist will have to be content with data which embody all these imperfections for some time to come.
>
> (e) The Task Group agreed to distinguish carefully the values specified for Reference Man from others quoted to indicate the extent and variety of the data available on each characteristic.

The Task Group recognized its own limitations in providing this compendium, but laid the foundation for the gathering of biological data by the health physics community. The authors advised that "it remains for the various organizations with control of radiation exposure at the national or regional levels to determine what modification of Reference Man, if any, may be appropriate for the population at risk." As well, they hoped that this publication would be useful despite its imperfections, and that it would be improved upon and extended in the future.

Currently, new anatomical and physiological reference data are under review. The document, *Draft ICRP report: basic anatomical and physiological data for use in radiological protection: reference values* (ICRP 2002) is near completion. It will offer revised and extended reference values from those published in 1975. In addition, it will provide information on variations of these 'normal' values caused by differences in age, gender, race, or other factors.

2.3.3.3.2 Radiopharmaceutical biodistribution

In order to ascertain the absorbed dose to a subject from a radiopharmaceutical, it is necessary to quantify the biodistribution of the drug throughout the tissues of the body.

The distribution of the radiopharmaceutical will depend on its chemical form, the method of administration, the age and sex of the subject, as well as the metabolic function of the subject's organs and tissues in their healthy or diseased states.

Direct measurements of biological uptake, retention, and washout of the radiopharmaceutical may be achieved by obtaining bioassay samples and through serial images of organ activity. SPECT and PET commonly provide three-dimensional radiopharmaceutical distribution data in voxel format. Biological distribution data are initially acquired through animal experiments, where the animal is sacrificed at predetermined intervals after administration of the radiopharmaceutical and the organs harvested for counting (Stabin 1994b). Animal data are then extrapolated to humans, usually according to the percent of activity found in the organ compared to the total body. Should the radiopharmaceutical be approved for use in humans, bioassay and imaging studies performed on human subjects provide further information as to the biodistribution of the drug.

The data acquired must be processed to determine the total activity accumulated in those regions identified as sources, including the total body. Numerical and analytical methods, or a combination thereof, may be employed to determine the cumulated activity within each source. Alternatively, a compartmental model can be fit to the data when it is difficult to obtain an adequate representation of the time-course of the drug within

multiple organs of the body. The activities determined from these methods are used to estimate the absorbed dose to the subject from the administered radiopharmaceutical.

2.3.3.3.3 Residence times

It is often convenient to describe the biological distribution in a source region according to its fractional distribution within the body. This parameter, referred to as the residence time, may be described as the mean time that the radiopharmaceutical spends in a region (Berman 1977). It represents the biokinetic properties of the radiopharmaceutical within the body and is calculated as:

$$\tau_{source} = \frac{\int_0^\infty A_{source}(t)\,dt}{\int_0^\infty U_{th}(t)\,dt} = \frac{\tilde{A}_{source}}{A_0} \qquad (2.25)$$

where τ = residence time (h);
U = rate of administration (MBq h^{-1}); and
A_0 = administered activity (MBq).

The absorbed dose found in Equation (2.24) is now displayed as:

$$\overline{D}_{(target \leftrightarrow source)} = A_0 \cdot \tau_{source} \cdot S_{(target \leftrightarrow source)} \qquad (2.26),$$

but can be rearranged to yield the mean dose to a target from a source per unit administered activity:

$$\frac{\overline{D}_{(target \leftrightarrow source)}}{A_0} = \tau_{source} \cdot S_{(target \leftrightarrow source)} \qquad (2.27).$$

2.3.4 The full equation

The simplest situation for calculating the absorbed dose involves a radiopharmaceutical deposited in a single source emitting a single type of radiation. The common situation, however, involves a radiopharmaceutical deposited in several sources emitting multiple types of radiation. Equation (2.27) is the usual working equation for calculating the dose to a target from a source for any radiopharmaceutical emitting any type of radiation. The mean absorbed dose to the target per unit administered activity requires summing the doses from the individual sources:

$$\frac{\overline{D}_{(target)}}{A_0} = \sum_{source} \tau_{source} \cdot S_{(target \leftarrow source)} \qquad (2.28).$$

For those situations where individual sources are not identified, the dose to the target may be calculated based on the assumption of uniform distribution of the activity within the total body:

$$\frac{\overline{D}_{(target)}}{A_0} = \tau_{tb} \cdot S_{(target \leftarrow tb)} \qquad (2.29)$$

where tb = total body.

2.3.5 Adjustments to the equations

Although Equation (2.28) is the fundamental dose equation, adjustments have been proposed over the years. Three main adjustments are presented here as they have been accepted and incorporated for use in absorbed dose calculations.

2.3.5.1 Remainder of the body

2.3.5.1.1 The formally exact solutions

Until the 1970's, the MIRD schema allowed only two situations in which the dose to a target could be calculated. As shown Equations (2.28) and (2.29), the dose was either the result of summing individual doses from regions identified as sources, or the dose was that given from the uniform distribution of the radionuclide within the total body. The first situation allowed for biological data obtained or approximated for those regions identified as sources to be employed in the estimation of dose. The second situation only considered the overall retention and excretion of the radionuclide within the total body. At the time, there was no method available to calculate the dose to a target from those regions not identified as sources because there was no AF encompassing those regions in the remainder of the body. Hence, the work of Loevinger and Berman was expanded by Smith (1970), Roedler and others (1972), and Cloutier and others (1973c) to take into account the irradiation of a target from the remaining activity distributed throughout the body.

Roedler and others (1972) illustrated in detail a revision of the MIRD schema in order to include the dose to a target from those regions not identified as sources. Using different terms, the formally exact solution to the problem of calculating the dose to a target from the remainder of the body was developed as an extension of Equation (2.2) in three steps. The first step assumed that the radioactivity not allocated to those regions identified as sources was distributed uniformly throughout the entire body, and that its

cumulated activity was equal to that defined for the total body. The errors in this assumption are that the remaining activity is distributed throughout the total body and that it has an effective half-life equivalent to that of the total body.

The second error in the first step was corrected in the second step, where a cumulated activity for the remainder of the body was calculated (Roedler et al. 1972):

$$\tilde{A}_{rb} = \tilde{A}_{tb} - \sum_{source=1}^{target} \tilde{A}_{source} \qquad (2.30)$$

where rb = remainder of the body.

The first error in the first step, however, manifests itself in two ways. By redistributing the remaining activity throughout the entire body, those regions identified as sources are assigned additional activity. Conversely, the remaining regions are assigned less activity than they should be. Therefore, the third step proposed by Roedler and others (1972) offered a correction term for the overestimate of activity in the source regions as well as a new term correcting the underestimate of activity throughout the remaining regions. The overestimate of activity in a source region is given as:

$$\tilde{A}'_{source} = \tilde{A}_{rb} \cdot \left(\frac{m_{source}}{m_{rb}} \right) \qquad (2.31),$$

while the underestimate of activity in the remaining regions is corrected by the new term:

$$\tilde{A}'_{tb} = \tilde{A}_{rb} \cdot \left(\frac{m_{tb}}{m_{rb}} \right) \qquad (2.32)$$

where Ã' = corrected cumulated activity (MBq h); and

$$m_{rb} = m_{tb} - \sum_{source=1}^{target} m_{source} \qquad (2.33)$$

= mass of the remainder of the body (kg).

Thus, Roedler and others (1972) merged the two original, yet incomplete, methods of calculating the dose to a target to arrive at an exact solution. This solution includes the dose to a target from activity distributed throughout the remainder of the body.

Smith (1970) presented, as an example, an equation for calculating the dose to the spleen when the spleen and the liver are identified as sources:

$$\overline{D}_{spleen} = \frac{\widetilde{A}_{spleen}}{m_{spleen}} \cdot \sum_i \Delta_{i\,np} \phi_{i\,np(spleen \leftarrow spleen)} + \frac{\widetilde{A}_{spleen}}{m_{spleen}} \cdot \sum_i \Delta_{i\,p} \phi_{i\,p(spleen \leftarrow spleen)} + \frac{\widetilde{A}_{liver}}{m_{spleen}} \cdot \sum_i \Delta_{i\,p} \phi_{i\,p(spleen \leftarrow liver)} + \left\{ \frac{\widetilde{A}_{tb} - \left(\widetilde{A}_{spleen} + \widetilde{A}_{liver} \right)}{m_{spleen}} \right\} \cdot \sum_i \Delta_{i\,p} \phi_{i\,p(spleen \leftarrow tb)} \quad (2.34).$$

Although Smith did not explicitly develop this as a revision of the MIRD schema, Equation (2.34) can be written in a general format using the SAF that applies to any target region given any number of source regions:

$$\overline{D}_{target} = \widetilde{A}_{target} \cdot \sum_i \Delta_{i\,np} \Phi_{i\,np(target \leftarrow target)} + \widetilde{A}_{target} \cdot \sum_i \Delta_{i\,p} \Phi_{i\,p(target \leftarrow target)} + \sum_{source=1}^{f} \left(\widetilde{A}_{source} \cdot \sum_i \Delta_{i\,p} \Phi_{i\,p(target \leftarrow source)} \right) + \left\{ \widetilde{A}_{tb} - \left(\widetilde{A}_{target} + \sum_{source=1}^{f} \widetilde{A}_{source} \right) \right\} \cdot \sum_i \Delta_{i\,p} \Phi_{i\,p(target \leftarrow tb)} \quad (2.35)$$

where f = last source excluding the target as a source.

The last source, f, excludes the target region as a source region. The first two terms in Equation (2.35) correspond to the target region's self-dose from the non-penetrating and penetrating components of the absorbed dose. The third term corresponds to the penetrating dose received from all the regions identified as sources. The fourth term represents the penetrating component of the dose to the target region from the activity that is found in the remainder of the body, assuming uniform distribution.

Equation (2.34) attempted to include all regions of the mathematical model which were not identified specifically as sources, but within which the remaining activity known to reside in the body may be assumed to be uniformly distributed. Although an improvement, this formula in not an exact solution as it uses the AF for the total body. This example falls into the second approximation described by Roedler and others (1972).

About the same time, Cloutier and others (1973c) developed the same exact solution as Roedler and others (1972), but used the symbols and terms commonly employed in the MIRD schema:

$$\overline{D}_{target} = \widetilde{A}_{target} \cdot \sum_i \Delta_{i\,np} \Phi_{i\,np(target \leftarrow target)} + \sum_{source=1}^{target} \left\{ \left[\widetilde{A}_{source} - \widetilde{A}_{rb} \cdot \left(\frac{m_{source}}{m_{rb}} \right) \right] \cdot \sum_i \Delta_{i\,p} \Phi_{i\,p(target \leftarrow source)} \right\} + \widetilde{A}_{rb} \cdot \left(\frac{m_{tb}}{m_{rb}} \right) \cdot \sum_i \Delta_{i\,p} \Phi_{i\,p(target \leftarrow tb)} \qquad (2.36),$$

hereby referred to as Dose Equation 1a.

Cloutier and others (1973c) also published a second method of obtaining the same result by revising the total body AF:

$$\phi_{p(target \leftarrow rb)} = \phi_{p(target \leftarrow tb)} \cdot \left(\frac{m_{tb}}{m_{rb}} \right) - \phi_{p(target \leftarrow target)} \cdot \left(\frac{m_{target}}{m_{rb}} \right) - \sum_{source=1}^{f} \phi_{p(target \leftarrow source)} \cdot \left(\frac{m_{source}}{m_{rb}} \right) \tag{2.37}$$

where $\phi_{p\,(target \leftarrow rb)}$ = absorbed fraction from the remainder of the body to the target.

The calculation of the SAF from the remainder of the body to the target is analogous to that of the AF. Thus, the exact solution may also be written as:

$$\overline{D}_{target} = \widetilde{A}_{target} \cdot \sum_{i} \Delta_{i\,np} \Phi_{i\,np(target \leftarrow target)} + \sum_{source=1}^{target} \widetilde{A}_{source} \cdot \sum_{i} \Delta_{i\,p} \Phi_{i\,p(target \leftarrow source)} + \widetilde{A}_{rb} \cdot \sum_{i} \Delta_{i\,p} \Phi_{i\,p(target \leftarrow rb)} \tag{2.38},$$

hereby referred to as Dose Equation 1b.

2.3.5.1.2 Differences in the formally exact solutions explained

Dose Equation 1a (2.36) and Dose Equation 1b (2.38) are equivalent; the difference lies in the reasoning of the approach. The initial assumption for both methods is that the administered radioactivity is distributed uniformly throughout the body. In order to arrive at Dose Equation 1a (2.36), the concentration of the radiopharmaceutical in a region is assumed to be estimated as the cumulated activity in the total body weighted according to the mass of the region. However, when activity concentrations in regions identified as sources are measured at levels higher or lower than their expected uniform concentrations, they are defined as having excess activity. This excess, as

described in Equation (2.31), must then be removed. The correction alters the cumulated activities of all sources containing penetrating radiations so that they appear uniform; the revised cumulated activities in the source regions can be positive or negative. The cumulated activity in the remainder of the body is then scaled to be a uniform cumulated activity in the total body, as in Equation (2.32).

To arrive at Dose Equation 1b (2.38), it is recognized that the data obtained and processed for estimating the dose to a target are the cumulated activities for different sources in the body. These values are real and positive; cumulated activities cannot physically be negative. In revising the cumulated activities as done in Dose Equation 1a (2.36), the actual data obtained becomes obscured. Altering the AFs, on the other hand, leaves the measured data intact. In this case, whatever cumulated activity is unaccounted for ($\tilde{A}_{rb}$) is related only to those regions not already measured. Following the initial assumption, the cumulated activity in the remainder of the body should be a mass-weighted value of the cumulated activity uniformly distributed in the remaining regions. This can be demonstrated by examining the property of additivity of the SAF (Snyder et al. 1974):

$$\Phi_{p(V\leftarrow W)} = \sum_j \Phi_{p(X_j\leftarrow W)} \cdot \left(\frac{m_{X_j}}{m_V}\right) = \sum_k \Phi_{p(V\leftarrow Y_k)} \cdot \left(\frac{m_{Y_k}}{m_W}\right) \tag{2.39}$$

where $\{X_j\}_{j=1}^{a}$ and $\{Y_k\}_{k=1}^{b}$ are any sets of discrete organs or regions of the body;

V = region comprised of the totality of collective X; and
W = region comprised of the totality of collective Y.

Equation (2.39) expresses the conservation of energy. In other words, if energy is emitted uniformly in region W, then in each subregion of W the energy emitted is proportional to the mass of the subregion as compared to the mass of the entire region and the energy is additive among the regions. If one considers V a target and W the total body, then Equation (2.39) becomes:

$$\Phi_{p(target \leftarrow tb)} = \sum_{k} \Phi_{p(target \leftarrow Y_k)} \cdot \left(\frac{m_{Y_k}}{m_{tb}} \right) \tag{2.40},$$

and it is apparent that the collective regions, Y_k, contribute to the SAF for the total body by their weighted masses. The collective regions are comprised of those regions identified as sources and any regions not identified as sources. Note that the target region itself may or may not be identified as a source region. Obviously not all regions are identified as sources; usually only those regions with large uptakes or those about which some information is known or can be approximated are considered to be sources.

Now consider a single source region, Y_1, within the total body:

$$\begin{aligned} \Phi_{p(target \leftarrow tb)} &= \Phi_{p(target \leftarrow Y_1)} \cdot \left(\frac{m_{Y_1}}{m_{tb}} \right) + \sum_{k=2}^{b} \Phi_{p(target \leftarrow Y_k)} \cdot \left(\frac{m_{Y_k}}{m_{tb}} \right) \\ &= \Phi_{p(target \leftarrow Y_1)} \cdot \left(\frac{m_{Y_1}}{m_{tb}} \right) + \Phi_{p(target \leftarrow tb - Y_1)} \cdot \left(\frac{m_{tb} - m_{Y_1}}{m_{tb}} \right) \end{aligned} \tag{2.41}.$$

Expansion of Equation (2.41) to consider multiple source regions yields:

$$\Phi_{p(target \leftarrow tb)} = \sum_{k=1}^{n} \Phi_{p(target \leftarrow Y_k)} \cdot \left(\frac{m_{Y_k}}{m_{tb}} \right) + \sum_{k=n+1}^{b} \Phi_{p(target \leftarrow Y_k)} \cdot \left(\frac{m_{Y_k}}{m_{tb}} \right)$$

$$= \sum_{k=1}^{n} \Phi_{p(target \leftarrow Y_k)} \cdot \left(\frac{m_{Y_k}}{m_{tb}} \right) + \Phi_{p\left(target \leftarrow tb - \sum_{k=1}^{n} Y_k \right)} \cdot \left(\frac{m_{tb} - \sum_{k=1}^{n} m_{Y_k}}{m_{tb}} \right) \qquad (2.42)$$

where n = last identified source; and
< b.

Equation (2.42) can be written with common MIRD symbols as:

$$\Phi_{p(target \leftarrow tb)} = \sum_{source} \Phi_{p(target \leftarrow source)} \cdot \left(\frac{m_{source}}{m_{tb}} \right) + \Phi_{p(target \leftarrow rb)} \cdot \left(\frac{m_{rb}}{m_{tb}} \right) \qquad (2.43)$$

given that $\{Y_k\}_{k=1}^{n}$ is the discrete set of regions identified as sources within the total body and that $\{Y_k\}_{k=n+1}^{b}$ is the discrete set of regions not identified as sources (i.e. - the remainder of the body). The SAF for each region identified as a source is a mass-weighted sub-set of the total SAF. Similarly, the SAF for those regions not identified as sources is a mass-weighted sub-set for the remaining regions. Rearrangement of Equation (2.43) produces the desired AF for the remainder of the body:

$$\Phi_{p(target \leftarrow rb)} = \left[\Phi_{p(target \leftarrow tb)} - \sum_{source=1}^{target} \Phi_{p(target \leftarrow source)} \cdot \left(\frac{m_{source}}{m_{tb}} \right) \right] \cdot \left(\frac{m_{tb}}{m_{rb}} \right) \qquad (2.44)$$

and is equivalent to Equation (2.37).

Thus, a formally exact solution can be derived through different logical paths. The first path attempts to keep the distribution of activity within the body uniform by altering the measured activities in the source regions. The second path determines the

SAF for the remainder of the body and leaves undisturbed the measured data for those regions identified as sources.

2.3.5.1.3 The formally exact solutions using S-values

Dose Equation 1a (2.36) and Dose Equation 1b (2.38) offer two possible methods for calculating the mean absorbed dose to a target. Although they yield equivalent results, differences emerge in their uses. If knowledge of the penetrating and non-penetrating self-dose components is desired, only Dose Equation 1b (2.38) is capable of producing this information. Dose Equation 1a (2.36), which revises the cumulated activities to render 'uniform' distributions, cannot give a correct penetrating self-dose component. As well, implicit in both equations is the presumption that the mean absorbed dose being calculated is for a target which is also identified as a source; it is not possible to obtain the dose to a target when it is not already identified as a source. This is due to the fact that the corrections for the remainder of the body, which concern those regions not identified as sources, only deal with penetrating radiation. As mentioned previously, the remaining cumulated activity is assumed to be uniformly distributed throughout the body to all those regions not specifically measured. When calculating the dose to one of these regions, the theoretical amount of cumulated activity situated in that region would yield a self-dose. Thus, the non-penetrating portion for that region must somehow be included.

Coffey and Watson (1979) solved this problem with the introduction of two new equations involving the S-values. They also proposed two solutions; the first revised the cumulated activities:

$$\overline{D}_{target} = \sum_{source=1}^{g}\left[\tilde{A}_{source} - \tilde{A}_{rb}\cdot\left(\frac{m_{source}}{m_{rb}}\right)\right]\cdot S_{(target\leftarrow source)} + \tilde{A}_{rb}\cdot\left(\frac{m_{tb}}{m_{rb}}\right)\cdot S_{(target\leftarrow tb)} \qquad (2.45),$$

and the second revised the S-values:

$$\overline{D}_{target} = \sum_{source=1}^{g}\tilde{A}_{source}\cdot S_{(target\leftarrow source)} + \tilde{A}_{rb}\cdot S_{(target\leftarrow rb)} \qquad (2.46)$$

where g = last source.

Equations (2.45) and (2.46) will hereby be referred to as Dose Equation 2a and Dose Equation 2b, respectively. The last source, g, may or may not include the target region as a source region. The S-value from the remainder of the body to the target is analogous to that of the AF found in Equation (2.37), but is presented here for clarity:

$$S_{(target\leftarrow rb)} = S_{(target\leftarrow tb)}\cdot\left(\frac{m_{tb}}{m_{rb}}\right) - \sum_{source=1}^{g} S_{(target\leftarrow source)}\cdot\left(\frac{m_{source}}{m_{rb}}\right) \qquad (2.47).$$

As seen in Equations (2.22) and (2.23), the S-value is the sum of all the penetrating and non-penetrating emissions, thereby guaranteeing that the non-penetrating component of the mean absorbed dose is included in either the $S_{(target\leftarrow source)}$ or $S_{(target\leftarrow tb)}$ values. If the target is identified as a source, then the non-penetrating component of the S-value from the total body to the target is subtracted in calculating the remainder of the body S-value. Therefore, Dose Equation 2a (2.45) and Dose Equation 2b (2.46) are flexible in that they can be used whether the target is identified as a source or whether it

is a region for which data were not obtained. As well, Dose Equation 2b (2.46) provides the self-dose in one term if the target is also a source.

There are thus four formally exact equations for calculating the mean absorbed dose to a target. The solutions provided by Cloutier and others (1973c) maintain independent parameters for the penetrating and non-penetrating components (Dose Equation 1a (2.36) and Dose Equation 1b (2.38)), but exclude the condition when the target is not identified as a source. On the other hand, the solutions provided by Coffey and Watson (1978) simplify the calculations by using the S-values instead of the SAFs (Dose Equation 2a (2.45) and Dose Equation 2b (2.46)).

2.3.5.2 Walled organs

Snyder and others (1974) provided two exceptions to the rules concerning the SAFs for non-penetrating emissions. The first exception occurs when the source is the contents of an organ with walls (i.e. – the heart, the gastrointestinal tract, and the urinary bladder). In this case, the energy contribution to the wall from the non-penetrating emissions of its contents is taken as half that which the contents receives from itself. This results in a dose to the *surface* of the wall. This was later expressed in MIRD Pamphlet No. 11 (Snyder et al. 1975) as:

$$\Phi_{np(wall \leftarrow contents)} = \frac{1}{2 \cdot m_{contents}} \qquad (2.48).$$

Therefore, when the target is a walled organ, two potential sources of non-penetrating radiation exist: the wall itself and the contents contained within it. For all walled organs except the heart, S-values for wall irradiating wall are not provided; only S-values for contents irradiating wall are provided. For these walled organs, the non-penetrating component of the S-value for wall irradiating wall is contained within the total body S-value, as discussed earlier. Analogous to Equation (2.48), the non-penetrating component of the S-value for contents irradiating wall is:

$$S_{np(wall \leftarrow contents)} = \sum_i \frac{\Delta_{i\,np}}{2 \cdot m_{contents}} \qquad (2.49).$$

2.3.5.3 Bone marrow

The second exception provided by Snyder and others (1974) occurs when the target is the bone marrow. The skeletal system consists of bone, bone marrow, periosteum, cartilage, teeth, and blood vessels (ICRP 1995). The bone structure, for the purposes of MIRD dosimetry, is a complex matrix of red marrow and trabecular bone commonly surrounded by cortical bone. Snyder and others (1974) divided bone into six target regions pertaining to red bone marrow, yellow bone marrow, cortical bone, trabecular bone, cortical bone surface, and trabecular bone surface. Only the first four targets were considered sources. The SAFs for these structures were based mainly on calculations by Spiers (1968) rather than on the standard assumptions found in Equations (2.19) and (2.20). Over the past three decades several revisions in the biological data and mathematical model of the skeleton have occurred. The most recently published skeletal

model for the adult provides S-values for 22 different bone sites, yielding skeletal averaged S-values for seven source organs and six target organs (Bouchet et al. 2000). Further explanations as to the calculation of SAFs for bone may be found in theses and other references (Spiers 1970; Eckerman and Stabin 2000; Bolch et al. 2002).

2.3.5.4 Patient-specific cases

Presently, the SAFs are available only for the organs contained within the anthropomorphic phantoms derived for a standard subject. In cases when a mathematical model is not representative of an actual subject, the SAFs can be adjusted to produce patient-specific values. Brownell and others (1968) alluded to a transformation in the case when the target is the source; the relation between the mass of the target and the AF depends on the target shape. Snyder (1970) reported that the AF is expected to vary as the cube root of the mass considering that the mean free path length of photons within a sphere is proportional to the radius of the sphere. Snyder and others (1975) as well as Yamaguchi and others (1975; 1978) further addressed this issue and provide a method for scaling the SAFs based on a comparison of the transformed and original target masses. Snyder and others (1975) explained that, to a first approximation, when a source irradiates a target at a distance, the SAF should be independent of mass. As the source approaches the target, the automatic scaling disappears for photons. In the case where the source becomes the target, the scaling for penetrating radiation varies as the ratio of the masses to the two-thirds power:

$$\Phi''_{p(target \leftarrow target)} = \Phi_{p(target \leftarrow target)} \left(\frac{m''_{target}}{m_{target}} \right)^{-2/3} \tag{2.50}$$

or:

$$S''_{p(target \leftarrow target)} = S_{p(target \leftarrow target)} \left(\frac{m''_{target}}{m_{target}} \right)^{-2/3} \tag{2.51},$$

where Φ'' = patient-specific specific absorbed fraction (kg^{-1});
S'' = patient-specific S-value (mGy MBq h^{-1}); and
m'' = patient-specific mass (kg).

This is apparent when examining the point isotropic specific absorbed fraction found in Equation (2.12). Assuming spherical geometry:

$$m = \rho \cdot \frac{4}{3} \pi r^3 \text{ or } r = \left(\frac{3m}{4\pi\rho} \right)^{1/3} \tag{2.52}$$

so that:

$$\Phi_{point}(x) \propto \frac{r}{m} \propto m^{-2/3} \tag{2.53}$$

where r = radius (cm).

No method is available to calculate patient-specific S-values when the source is not the target (Snyder et al. 1975); it is not possible to predict how the S-value would change†. Therefore:

$$\Phi''_{p(target \leftarrow source)} = \Phi_{p(target \leftarrow source)} \tag{2.54}$$

and:

$$S''_{p(target \leftarrow source)} = S_{p(target \leftarrow source)} \tag{2.55}$$

The transformation of the SAF for non-penetrating radiation simply varies as the ratio of the masses:

$$\Phi''_{np(target\leftarrow target)} = \Phi_{np(target\leftarrow target)}\left(\frac{m''_{target}}{m_{target}}\right)^{-1} = \frac{1}{m''_{target}} \tag{2.56}$$

or:

$$S''_{np(target\leftarrow target)} = S_{np(target\leftarrow target)}\left(\frac{m''_{target}}{m_{target}}\right)^{-1} \tag{2.57}.$$

Therefore, the full patient-specific S-value appears as such:

$$S''_{(target\leftarrow target)} = S_{np(target\leftarrow target)}\left(\frac{m''_{target}}{m_{target}}\right)^{-1} + S_{p(target\leftarrow target)}\left(\frac{m''_{target}}{m_{target}}\right)^{-2/3} \tag{2.58}.$$

Patient-specific SAF and S-values are scaled versions of the mathematical model values according to a ratio of the target masses defined for the model and measured in the patient. Therefore, the individualization of the dose calculation is with respect to the self-dose component of the total dose to the organ. Although the patient-specific adjustment provides a closer dose estimate to an actual patient, it should still be regarded as a modified value based on a model.

2.4 Applications of MIRD

Absorbed dose calculations are generally performed for three purposes: 1) in a retrospective study, a dose estimate to a particular patient from a particular administration

of a radiopharmaceutical is desired, 2) in a prospective study, the dose estimate from a trace administration of a radiopharmaceutical prior to the administration of a larger activity is required, or 3) in a class study, a dose estimate to a class of individuals is performed without reference to individual differences (Loevinger 1969). The MIRD schema provides a reasonable approach for calculating these doses and has been accepted as a useful technique in internal dosimetry (Watson et al. 1993).

Radiation absorbed dose estimates are performed routinely for diagnostic, therapeutic, and research purposes. Class studies are performed for the approval of radiopharmaceuticals for common use and are used as an evaluation of risk for the general population for a given procedure. These dose estimates are often used in prospective studies as an estimate of the efficacy of radiation therapy. However, the application of radiation doses calculated for a mathematical model to an individual in some cases has resulted in a lack of correlation between the expected and observed radiation effects (Stabin 1999).

A recent trend in the dosimetry community has focused attention on obtaining patient-specific doses (Wessels and Siegel 1997; Mattsson and Johansson 1999; Stabin et al. 1999; Howell et al. 1999; Zanzonico 2000). Patient-specific dosimetry attempts to take into consideration variations in an individual's characteristics, such as age, weight, biokinetics, and pathological conditions. Using information obtained specifically on an individual's anatomy and biokinetics allows for a better estimation of radiation absorbed

dose to the individual, rather than to the mathematical model. As more radiopharmaceuticals emerge for diagnostic imaging and radiation therapy, the priority is shifting towards detailed individual dosimetry for radiological protection and optimization of treatment.

2.4.1 Effective dose equivalent and effective dose

The effective dose equivalent (EDE) and the effective dose (ED) are numerical quantities developed by the ICRP to express non-uniform dose distributions as comparable whole-body doses. The EDE, introduced in 1977, was originally intended for use in radiation protection of occupationally exposed adults in order to estimate the risk from stochastic effects; non-stochastic effects were not considered. It was calculated by assigning weighting factors to six organs, with the remaining organs lumped together, and summing these organ-weighted doses. The ED replaced the EDE in 1991 (ICRP 1991) and considered 13 tissues and included the total detriment rather than just the risk of fatal cancer. A clarification of the colon weighting factor in the ED to include the upper and lower large intestines and the use of the dose to the thymus as a surrogate for the dose to the esophagus was later provided by the ICRP (1994). The EDE and ED are calculated as:

$$EDE = \sum_T w_T (EDE) \cdot \left(\sum_R w_R \cdot D_{T,R} \right) \tag{2.59}$$

and:

$$ED = \sum_T w_T(ED) \cdot \left(\sum_R w_R \cdot D_{T,R} \right) \tag{2.60}$$

where EDE = effective dose equivalent (mSv);
ED = effective dose (mSv);
w_T = tissue weighting factor;
w_R = radiation weighting factor; and
$D_{T,R}$ = mean absorbed dose in target organ T from radiation type R.

The radiation weighting factors take into account the relative biological effectiveness (RBE) of the type of radiation involved in the dose estimate and may be found in ICRP 60 (1991). For photons, electrons and positrons (the most common types of radiation found in diagnostic and therapeutic procedures), the radiation weighting factor is equal to 1.0. The tissue weighting factors for the EDE and the ED can be obtained from ICRP 26 (1977), ICRP 60 (1991), and ICRP 67 (1994).

A controversy over the use of the EDE and the ED in diagnostic and nuclear medicine procedures has arisen. Due to several factors, the opinion of the MIRD Committee is that "it is inappropriate to use the effective dose equivalent for individual patients undergoing nuclear medicine procedures" (Poston 1993). These factors pertain to the approach taken by the ICRP in selecting the values of the risk coefficients used to calculate the tissue weighting factors. The MIRD Committee points to the fact that the risk coefficients were derived from Japanese A-bomb survivor data, which involve high dose and dose-rate exposures contrary to the typical low dose and dose-rate exposures delivered in nuclear medicine procedures (Poston 1994). As well, the Committee expresses concern over the choice of a single weighting factor per organ selected from a

wide range of values, especially since it may vary according to age, sex, dose, dose rate, and other factors (Poston 1993). Stabin and others (1993) have also commented that people are opposed to the use of these quantities in medicine for this reason.

Several prominent members of the Health Physics community immediately protested the MIRD Committee's position (Harding et al. 1994; Shields and Lawson 1994; Clarke 1994; Thomson et al. 1994). The primary counterpoint expressed by these and other individuals is that the EDE and ED are useful parameters for comparing the relative risk of the dose received from different procedures. Clarke (1994) refers to the ICRP publication *Protection of the patient in nuclear medicine* (ICRP 1987) which stated that the EDE could be used as a comparison tool:

> When radiopharmaceuticals are administered, individual organs may receive very different doses. In order to facilitate a comparison between different types of radiological investigations, the effective dose equivalent is a convenient measure.

ICRP 52 (1987) also recognized that the distribution of age and sex in a patient population differs from that of a working population, but that the weighting factors are a broad average such that "the effective dose equivalent can only be an approximate indicator of the risk to either the individual worker or the individual nuclear medicine patient".

It is accepted on both sides of the argument that the EDE and ED are not appropriate for therapeutic purposes where non-stochastic effects exist (Poston 1993; Johansson et al. 1993; Harding et al. 1994; Watson 1994; Toohey and Stabin 1999). The

MIRD Committee consents that as a comparison of risk for a collective population for various exposures, the EDE may be useful (Poston 1994). The Committee and others assert that organ doses must be reported and evaluated as the fundamentally important quantity used to estimate the effects of exposure on the patient (Poston 1993; Stabin et al. 1993; Poston 1994; Toohey and Stabin 1999), and that the use of the EDE in evaluating the absolute risk to a patient is questionable (Poston 1994). However, the EDE and ED are routinely reported in dose estimates to patients and are most likely considered "... as a guide to associated risk" (Thomson et al. 1994).

2.4.2 Dosimetry software programs

Computer programs facilitate the calculations of absorbed dose, especially when a large number of source and target organs are considered or when calculations for more than one phantom are desired. Several programs are available to this end; examples of these programs are MIRD #S (Butler et al. 1976; Butler et al. 1977), CAMIRD (Feller et al. 1976; Bellina and Guzzardi 1980) and MIRDOSE (Stabin 1996). MIRDOSE is probably the most prevalent dosimetry software in the world, and is among the most frequently cited in nuclear medicine publications (Anonymous 2000). The most recent version, MIRDOSE 3, allows the user to choose from over 200 radionuclides, 10 mathematical models, and 26 source organs, for which residence times as input parameters are required. Options for using the ICRP 30 gastrointestinal tract model (ICRP 1979) and a dynamic bladder model (Cloutier et al. 1973a) are included when calculating absorbed dose, and the distribution of dose through the skeleton may be

viewed. The MIRDOSE software program employs Equations (2.46) and (2.47) in its calculation of absorbed dose. Calculation of the self-dose to unit density spheres is also available, although it is independent of the phantoms.

Other software programs exist which are intended for use in calculating the absorbed dose to tumors. MABDOSE (Johnson 1988; Johnson et al. 1999a; Johnson et al. 1999b) is probably the most documented software tool for use in absorbed dose calculations to organs, including tumors. Similar to MIRDOSE, users are requested to choose a radionuclide, a mathematical model, and source organs. Additionally, tumors may be placed within the anthropomorphic phantom using a graphical interface; a spherical geometry is assumed and characterized by a radius entered by the user. Monte Carlo simulations are then run in order to obtain the S-values for penetrating radiation. These are used in conjunction with the cumulated activities to provide dose estimates for each organ and the tumors.

More recently, efforts have been directed at combining anatomical data from computerized images with dose-point kernel or Monte Carlo based techniques for calculating absorbed doses (Furhang et al. 1996; Kolbert et al. 1997; Yoriyaz et al. 2001). This work is aimed at improving treatment planning by combining patient anatomical with physiological images. Transport codes are run with voxel phantoms; computations of dose distributions for these purposes are on the order of several hours (Yoriyaz et al.

2001), but one should expect these computation times to decrease as more powerful computers are introduced.

2.5 Limitations and accuracy of MIRD

2.5.1 Limitations of MIRD

The MIRD schema is beautiful in its simplicity. Originally separate and tedious, equations for beta and gamma absorbed doses have been combined. Absorbed doses can now be calculated for men, women, and children of specific ages and for a few select nationalities.

Despite the amazing advances made in internal dosimetry over the last 60 years, there are limitations that affect the accuracy of radiation absorbed dose estimates. Some of these limitations are the consequence of producing this practical schema. These limitations include: 1) the assumption of uniform activity distribution within a target, 2) the assumption of uniform activity distribution within the remainder of the body, 3) the assumption that each region is homogeneous in composition and density, 4) the assumption that non-penetrating radiation emissions are completely absorbed within the source, and 5) the use of generalized S-values for subjects who vary in age, size, and metabolic function (Loevinger 1990; Kassis 1992; Howell et al. 1999). Fortunately, some of these limitations are becoming less of a problem with the development of the voxel phantoms. For example, subregions of an organ may accumulate varying amounts of the radiopharmaceutical, as illustrated by the accumulation of mercury in the kidney,

which is much higher in the cortex than in the medulla (Smith 1966; Blau et al. 1975). Currently, the dose gradient produced as a result of different regional radiopharmaceutical uptake is ignored (Howell et al. 1999); calculations with voxel phantoms allow for smaller dose distributions to be accounted for, producing dose distributions on an enhanced level. The use of voxel phantoms also obviates the need for generalized S-values and can take into account the full range of non-penetrating radiation emissions.

To date, the physical properties of radionuclides are well characterized and much effort is placed on continuously improving the mathematical properties of models, both at the macroscopic and microscopic scales. However, these are only two of the three requirements for calculating radiation absorbed doses; a void still exists in the knowledge of biological properties of most radiopharmaceuticals, and the uncertainty in this component is far greater (Loevinger 1969; Stabin 1999; Wilder et al. 1999). It has been noted in the literature for decades that there is a deficiency in biokinetic data available for dosimetric estimates of both routinely used and new radiopharmaceuticals (Seltzer et al. 1964; Smith 1970; Roedler et al. 1972; Trott 1977; Nosslin 1981; Weber 1990). As well, the main source of biokinetic data used for dosimetric purposes is that obtained from different species of animals, and these data cannot be consistently extrapolated to humans (Smith 1966; Roedler et al. 1972; Weber 1990). The modest amount of biokinetic data obtained in man has been broadly applied to women and children, with little regard to the metabolic differences corresponding to sex or age (Seltzer et al. 1964; Smith 1966;

Kereiakes et al. 1972; ICRP 1988; Stabin 1994b; Stabin and Gelfand 1998). However, the metabolism of radiopharmaceuticals for children, infants, and pregnant women can be quite different from that of an adult, especially taking into consideration radionuclide uptake and washout, as well as pathological states (ICRP 1993; Russel et al. 1997). Therefore, the collection and continual assessment of biokinetic data for routinely used and new radiopharmaceuticals is highly encouraged (Roedler et al. 1972; Kereiakes 1976; Wooten 1983; Graham and Bigler 1984; ICRP 1988; Weber 1990).

2.5.2 Accuracy of absorbed dose estimates

Having recognized that there are limitations inherent in the MIRD schema, it is useful to quantify the accuracy of any absorbed dose estimate obtained by this method. In a comparison of well-established residence times for ^{75}Se-selenomethionine and ^{67}Ga-citrate in animals and men, it was reported that in some cases the residence times in the total body and organs agreed within 50%, while in others they differed by a factor of two to seven (Kaul 1980). It has also been reported that the radiopharmaceutical concentration in a given human organ may differ by a factor ranging from about 2 to 100 (Seltzer et al. 1964; Kaul 1980). Therefore, given the accuracy of the physical, mathematical, and biological components required for estimating an absorbed dose, it is estimated that an accuracy to a factor of two is all that can be expected (Roedler et al. 1972; Kaul et al. 1980; Loevinger 1990; Howell et al. 1999). Considering, however, that the average doses in diagnostic and research cases are low, the administration of

radiopharmaceuticals for these purposes is considered to be safe (Kassis 1992; Stabin and Gelfand 1998).

Finally, with the focus now on therapeutic radiopharmaceuticals, the interest in obtaining more accurate biological data has heightened (Watson 1999). Radiopharmaceutical dosimetry for therapeutic purposes is intended to provide precise dosimetric treatment for diseased tissues while sparing normal tissues from unnecessary damage. Understanding the biological distribution of a radiopharmaceutical within the body and its variations according to various physical parameters such as sex, age, height, weight, nationality, diet, and pathological condition of the patient is very important. Hence, accurate dosimetric information, including well-defined biological distribution data, is necessary to achieve the highest quality treatment for each individual patient.

2.6 Conclusion

The MIRD Committee and others have succeeded in producing a unified and effective method for calculating internal doses from radiopharmaceuticals. The development of complex mathematical models and research into the biological and physiological properties of human beings have furthered the field of internal dosimetry. The MIRD schema has been accepted and employed worldwide, and will continue to be an integral part of diagnostic and therapeutic dose estimates. However, this technique is used to determine the *average* radiation absorbed doses to organs and tissues. Therefore,

the limitations of the MIRD schema and the accuracy of the calculated doses must be considered when judging the quality of any radiation absorbed dose estimate.

Footnotes:

† Personal communication, Michael Stabin 24 April 2001.

Chapter 3: Analysis of the MIRD Equations

3.1 Introduction

Refinement of the MIRD schema is a continual process; periodically adjustments are reviewed and accepted as part of the process to simplify the method or to improve its accuracy. Several of these adjustments were discussed previously because they have been accepted and incorporated for use in absorbed dose calculations. There are, however, some more recent suggestions proposed here which could further improve the dose estimates obtained through the MIRD schema.

3.2 Remainder of the body and walled organs revisited

As discussed in Chapter 2, one exception to the rules concerning the SAFs for non-penetrating emissions occurs when calculating the dose to a walled organ from its contents. The SAF or S-value to the wall in this situation is taken as half that which the contents receives from itself, as given in Equations (2.48) and (2.49); the dose to the walls from the contents utilizes this SAF or S-value. The resulting dose represents the dose to the surface of the wall and is not equivalent to the mean dose to the wall[†]. Therefore, the non-penetrating dose to the walls from the contents (the surface dose) and the non-penetrating dose to the walls from the walls (the mean self-dose) should not be summed. Furthermore, if the non-penetrating component of the SAF for contents

irradiating wall is subtracted from the total body SAF in calculating the remainder of the body SAF, the non-penetrating component of the total body SAF is incorrectly reduced (Stabin and Sparks 1999). The same is true for the S-value. Both situations may be resolved by simply utilizing only the penetrating component of the SAF or S-value for the contents irradiating wall:

$$\Phi_{(wall \leftarrow contents)} = \Phi_{p(wall \leftarrow contents)} = \sum_i \frac{\phi_{i\,p(wall \leftarrow contents)}}{m_{wall}} \tag{3.1}$$

or:

$$S_{(wall \leftarrow contents)} = S_{p(wall \leftarrow contents)} = \sum_i \frac{\Delta_{i\,p} \cdot \phi_{i\,p(wall \leftarrow contents)}}{m_{wall}} \tag{3.2}.$$

3.3 Patient-specific cases revisited

3.3.1 Considerations for patient-specific doses

As stated previously, the absorbed doses incurred in diagnostic medicine are generally low, and the benefits of the diagnostic information outweigh the potential risks associated with the dose. This is not the case in therapeutic medicine, as the ideal treatment involves maximizing radiation damage of diseased tissue while minimizing damage to healthy tissue. Thus, the drive behind patient-specific dosimetry is to provide more detailed organ doses that are realistic for the individual patient. Furthermore, the dosimetry community can use patient-specific dosimetry in evaluation of accidental

internal exposures, as well as in the investigation of variations in the patient population to provide a range of dose estimates.

However, use of patient-specific dose calculations has thus far been limited. Patient-specific dose estimates are not routinely performed in investigations of new radiopharmaceuticals and are therefore not generally reported. In addition, patient-specific information with regards to organ mass is not usually collected; activity concentration (activity per unit mass of tissue) at a level within the center of the organ is generally the value most often obtained. When patient-specific doses are desired, they are calculated by hand after the total dose has been calculated. Therefore, patient-specific equations, although in use, have not been incorporated into the main MIRD schema.

3.3.2 Application within the formally exact solutions

In the MIRD schema for calculating absorbed doses, there are four formally exact solutions for calculating the dose to a target organ from a source organ, as found in Dose Equations 1a (2.36), 1b (2.38), 2a (2.45), and 2b (2.46). These four equations are equivalent given that the dose is calculated for a standard anthropomorphic model when the target organ is considered a source organ. When a patient-specific dose is desired, however, the SAF (or S-value) is adjusted according to a ratio of the patient to model target masses. Incorrect application of this patient-specific value in these dose equations

can lead to inaccurate doses. In this situation, the usefulness of these four dose equations diverges and the significance of their structure emerges.

As discussed previously, Dose Equations 1a and 1b separate the non-penetrating and penetrating terms while Dose Equations 2a and 2b combine them. Additionally, Dose Equations 1a and 1b are not applicable when the target is not a source; Dose Equations 2a and 2b are valid whether the target is a source or not. However, simple replacement of the SAF or S-value with the patient-specific term does not yield a correct dose equation in any case.

Consider Dose Equation 1a with the revised SAF (Φ"):

$$\overline{D}_{target} = \widetilde{A}_{target} \cdot \sum_i \Delta_{inp} \Phi''_{inp(target \leftarrow target)} + \sum_{source=1}^{target} \left\{ \left[\widetilde{A}_{source} - \widetilde{A}_{rb} \cdot \left(\frac{m_{source}}{m_{rb}} \right) \right] \cdot \sum_i \Delta_{ip} \Phi''_{ip(target \leftarrow source)} \right\} + \widetilde{A}_{rb} \cdot \left(\frac{m_{tb}}{m_{rb}} \right) \cdot \sum_i \Delta_{ip} \Phi_{ip(target \leftarrow tb)} \quad (3.3).$$

It is apparent that the non-penetrating component of the adjusted SAF is applied only to the cumulated activity of the target itself; this is correct. However, the penetrating component of the adjusted SAF is applied to the 'uniform' cumulated activity of the target, not to its true cumulated activity. This leads to the term:

$$\left[\widetilde{A}_{target} - \widetilde{A}_{rb} \cdot \left(\frac{m_{target}}{m_{rb}} \right) \right] \cdot \sum_i \Delta_{ip} \Phi''_{ip(target \leftarrow target)} \quad (3.4)$$

rather than:

$$\widetilde{A}_{target} \cdot \sum_i \Delta_{i\,p} \Phi''_{i\,p(target \leftarrow target)} - \widetilde{A}_{rb} \cdot \left(\frac{m_{target}}{m_{rb}} \right) \cdot \sum_i \Delta_{i\,p} \Phi_{i\,p(target \leftarrow target)} \qquad (3.5).$$

This is unacceptable because patient-specific adjustments are with respect to the self-dose component only. The same result occurs in Dose Equation 1b when the adjusted SAF is applied in the remainder of the body SAF calculation.

Now consider Dose Equation 2a with the adjusted S-value (S"):

$$\overline{D}_{target} = \sum_{source=1}^{g} \left[\widetilde{A}_{source} - \widetilde{A}_{rb} \cdot \left(\frac{m_{source}}{m_{rb}} \right) \right] \cdot S''_{(target \leftarrow source)} + \widetilde{A}_{rb} \cdot \left(\frac{m_{tb}}{m_{rb}} \right) \cdot S_{(target \leftarrow tb)} \qquad (3.6).$$

In this case both the non-penetrating and penetrating components of the adjusted S-value are applied to the 'uniform' cumulated activity of the target, not to its true cumulated activity. This leads to the term:

$$\left[\widetilde{A}_{target} - \widetilde{A}_{rb} \cdot \left(\frac{m_{target}}{m_{rb}} \right) \right] \cdot S''_{(target \leftarrow target)} \qquad (3.7)$$

rather than:

$$\widetilde{A}_{target} \cdot S''_{(target \leftarrow target)} - \widetilde{A}_{rb} \cdot \left(\frac{m_{target}}{m_{rb}} \right) \cdot S_{(target \leftarrow target)} \qquad (3.8).$$

The same type of error occurs in equation (3.7) as in equation (3.4); the patient-specific adjustments are applied to terms other than those relating to the self-dose. The same result occurs in Dose Equation 2b when the adjusted S-value is applied in the remainder of the body S-value calculation.

3.3.3 Comparison of the formally exact solutions

The inappropriate application of the patient-specific term is unavoidable when Dose Equations 1a and 2a are used to estimate absorbed doses to targets when they are also sources. The same incorrect results would occur in Dose Equations 1b and 2b, but can be avoided if patient-specific values are applied cautiously (i.e. – not in the calculation of the remainder of the body). The error in the dose in either case will depend on several factors: 1) the radionuclide of interest (which determines the AF and hence the SAF and S-value), 2) the target organ of interest, 3) the distribution of radionuclide throughout the body, and 4) the ratio of the patient-specific to mathematical model target masses.

3.3.3.1 Methods

In order to examine the magnitude of the error incurred in the incorrect use of a patient-specific S-value, ratios of incorrect to correct patient-specific doses were calculated. These ratios are:

$$\overline{D}_{ratio\,1} = \frac{\begin{array}{l}\widetilde{A}_{target} \cdot \sum_i \Delta_{inp} \Phi''_{inp(target \leftarrow target)} + \\ \left[\widetilde{A}_{target} - \widetilde{A}_{rb} \cdot \left(\frac{m_{target}}{m_{rb}}\right)\right] \cdot \sum_i \Delta_{ip} \Phi''_{ip(target \leftarrow target)} + \\ \sum_{source=1}^{f} \left\{\left[\widetilde{A}_{source} - \widetilde{A}_{rb} \cdot \left(\frac{m_{source}}{m_{rb}}\right)\right] \cdot \sum_i \Delta_{ip} \Phi''_{ip(target \leftarrow source)}\right\} + \\ \widetilde{A}_{rb} \cdot \left(\frac{m_{tb}}{m_{rb}}\right) \cdot \sum_i \Delta_{ip} \Phi_{ip(target \leftarrow tb)}\end{array}}{\begin{array}{l}\widetilde{A}_{target} \cdot \sum_i \Delta_{inp} \Phi''_{inp(target \leftarrow target)} + \\ \widetilde{A}_{target} \cdot \sum_i \Delta_{ip} \Phi''_{ip(target \leftarrow target)} - \widetilde{A}_{rb} \cdot \left(\frac{m_{target}}{m_{rb}}\right) \cdot \sum_i \Delta_{ip} \Phi_{ip(target \leftarrow target)} \\ \sum_{source=1}^{f} \left\{\left[\widetilde{A}_{source} - \widetilde{A}_{rb} \cdot \left(\frac{m_{source}}{m_{rb}}\right)\right] \cdot \sum_i \Delta_{ip} \Phi''_{ip(target \leftarrow source)}\right\} + \\ \widetilde{A}_{rb} \cdot \left(\frac{m_{tb}}{m_{rb}}\right) \cdot \sum_i \Delta_{ip} \Phi_{ip(target \leftarrow tb)}\end{array}} \qquad (3.9)$$

for Dose Equations 1a and 1b, and:

$$\overline{D}_{ratio\,2} = \frac{\begin{array}{l}\left[\widetilde{A}_{target} - \widetilde{A}_{rb} \cdot \left(\frac{m_{target}}{m_{rb}}\right)\right] \cdot S''_{(target \leftarrow target)} + \\ \sum_{source=1}^{f} \left[\widetilde{A}_{source} - \widetilde{A}_{rb} \cdot \left(\frac{m_{source}}{m_{rb}}\right)\right] \cdot S_{(target \leftarrow source)} + \widetilde{A}_{rb} \cdot \left(\frac{m_{tb}}{m_{rb}}\right) \cdot S_{(target \leftarrow tb)}\end{array}}{\begin{array}{l}\widetilde{A}_{target} \cdot S''_{(target \leftarrow target)} - \widetilde{A}_{rb} \cdot \left(\frac{m_{target}}{m_{rb}}\right) \cdot S_{(target \leftarrow target)} + \\ \sum_{source=1}^{f} \left[\widetilde{A}_{source} - \widetilde{A}_{rb} \cdot \left(\frac{m_{source}}{m_{rb}}\right)\right] \cdot S_{(target \leftarrow source)} + \widetilde{A}_{rb} \cdot \left(\frac{m_{tb}}{m_{rb}}\right) \cdot S_{(target \leftarrow tb)}\end{array}} \qquad (3.10)$$

for Dose Equations 2a and 2b.

The radionuclides examined in this study were ^{3}H, ^{32}P, ^{60}Co, ^{67}Ga, ^{90}Y, ^{99m}Tc, ^{123}I, ^{131}I, ^{137}Cs, and ^{201}Tl, which are commonly found in diagnostic imaging, therapy, or industrial applications. The targets investigated within the adult male, adult non-pregnant female, and newborn mathematical models (Christy and Eckerman 1987; Stabin et al. 1995) were the brain, breasts, kidneys, liver, lungs, and thyroid. The testes were investigated for the adult male and newborn mathematical models; the uterus and ovaries were investigated for the adult non-pregnant female and newborn mathematical models. In each case, only the target organ and the remainder of the body were considered as sources. The S-values were obtained from the MIRDOSE 3 dosimetry software program (Stabin 1996) and the target masses for the adult male, adult non-pregnant female, and newborn were obtained from Stabin (1996), with the exception of the adult non-pregnant female lung mass and total body mass. Rather, the actual masses used in determining the adult non-pregnant female AFs were used (0.800 kg and 56.912 kg for the lungs[‡] and total body[§], respectively). The mean energies emitted per nuclear transition for the non-penetrating emissions of the radionuclides were obtained from the MIRD decay schemes from the National Nuclear Data Center (2001), with the exception of ^{67}Ga and ^{90}Y, which were obtained from Dillman (1970) and (1969), respectively. In all cases, the non-penetrating radiations consisted of particulate radiation in addition to photons whose energy was below 11.3 keV.

The cumulated activity in each target was calculated as a factor, Z, of the cumulated activity in the total body, which was assumed to be distributed evenly by mass:

$$\tilde{A}_{target} = Z \times \left(\frac{m_{target}}{m_{tb}} \right) \tilde{A}_{tb} \qquad (3.11),$$

where Z = factor of the uniform distribution.

Hence, Z=1 would represent a uniform distribution. The cumulated activity of the remainder of the body is thus defined:

$$\tilde{A}_{rb} = \left[1 - Z \times \left(\frac{m_{target}}{m_{tb}} \right) \right] \times \tilde{A}_{tb} \qquad (3.12).$$

A range of Z producing cumulated activities in the target organ from one-quarter to four times the uniform distribution was selected. Finally, the ratio of the patient-specific to mathematical model target masses was defined as a constant:

$$\beta = \frac{m''_{target}}{m_{target}} \qquad (3.13).$$

The effect of the patient-specific target mass on the dose ratio was examined by varying β; a patient-specific target mass which is one-half to twice that of the model's target mass was investigated.

3.3.3.2 Results

The extent to which the calculated doses deviated from the true doses is displayed in graphs of the adult male and newborn brains. Figure 3.1 and Figure 3.2 display the dose ratios, $\bar{D}_{ratio\ 1}$, as β increases while Figure 3.3 and Figure 3.4 display the dose ratios,

$\bar{D}_{ratio\ 2}$, as β increases. The dose ratios and their corresponding deviations from the true dose, in percent, are displayed; a dose ratio of 1.0 signifies no deviation from the true dose.

Figure 3.1: $\bar{D}_{ratio\ 1}$ vs. β with Z=0.25 for the adult male brain.

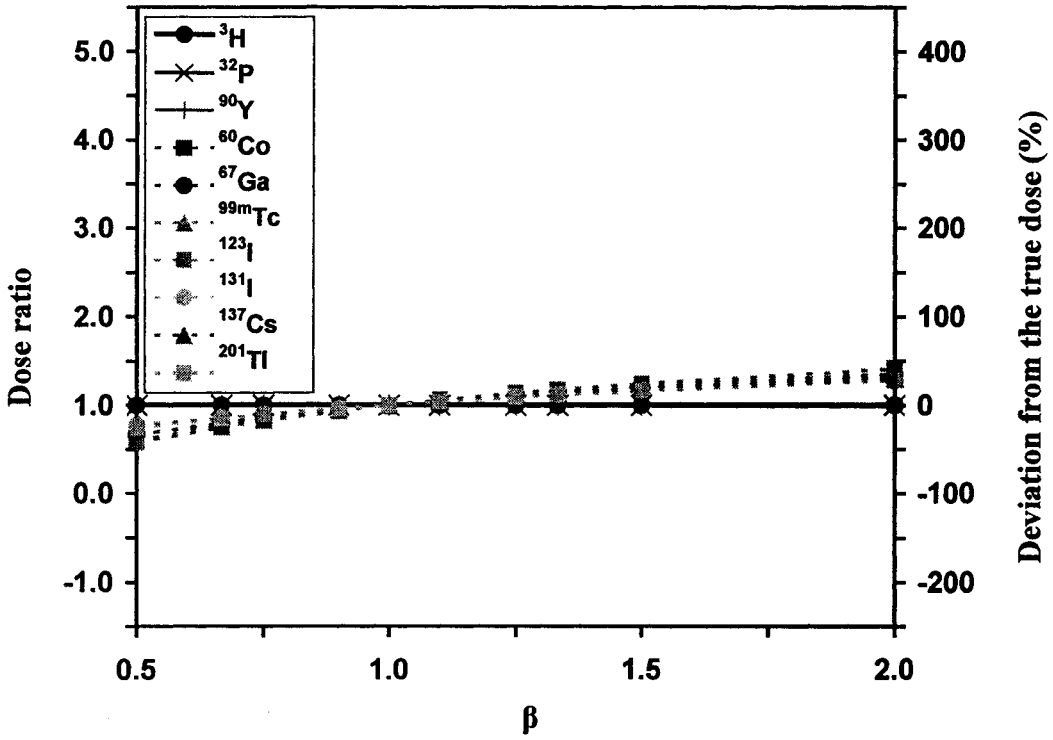

Figure 3.2: $\bar{D}_{ratio\ 1}$ vs. β with Z=0.25 for the newborn brain.

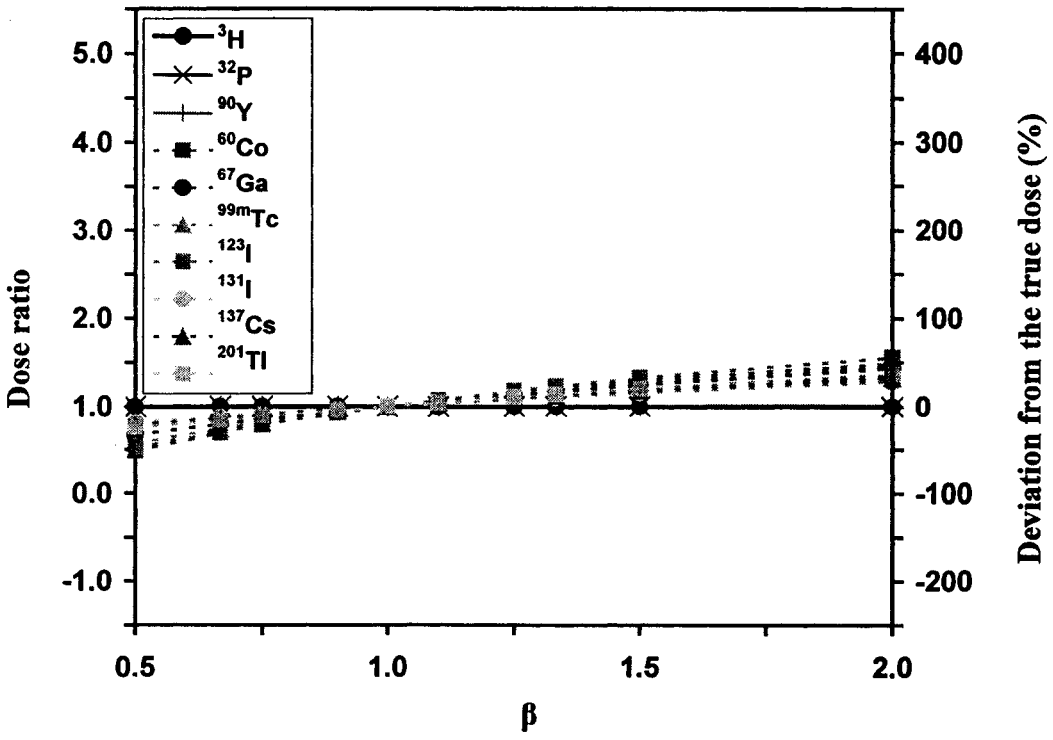

Figure 3.3: $\bar{D}_{ratio\,2}$ vs. β with Z=0.25 for the adult male brain.

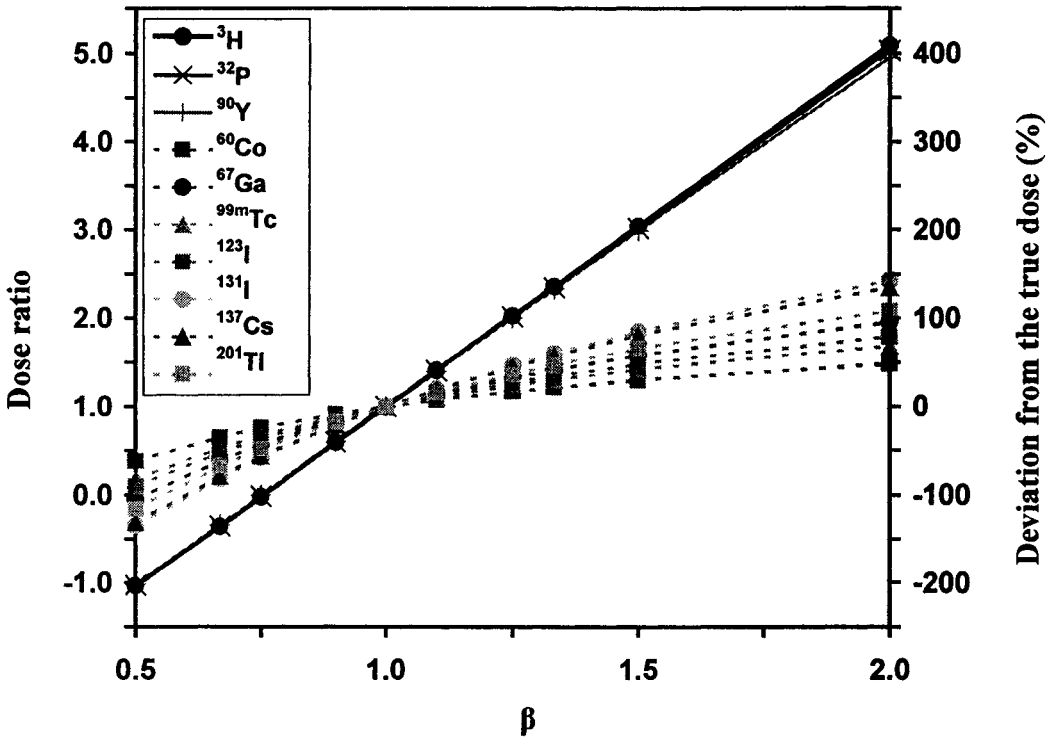

Figure 3.4: $\bar{D}_{ratio\,2}$ vs. β with Z=0.25 for the newborn brain.

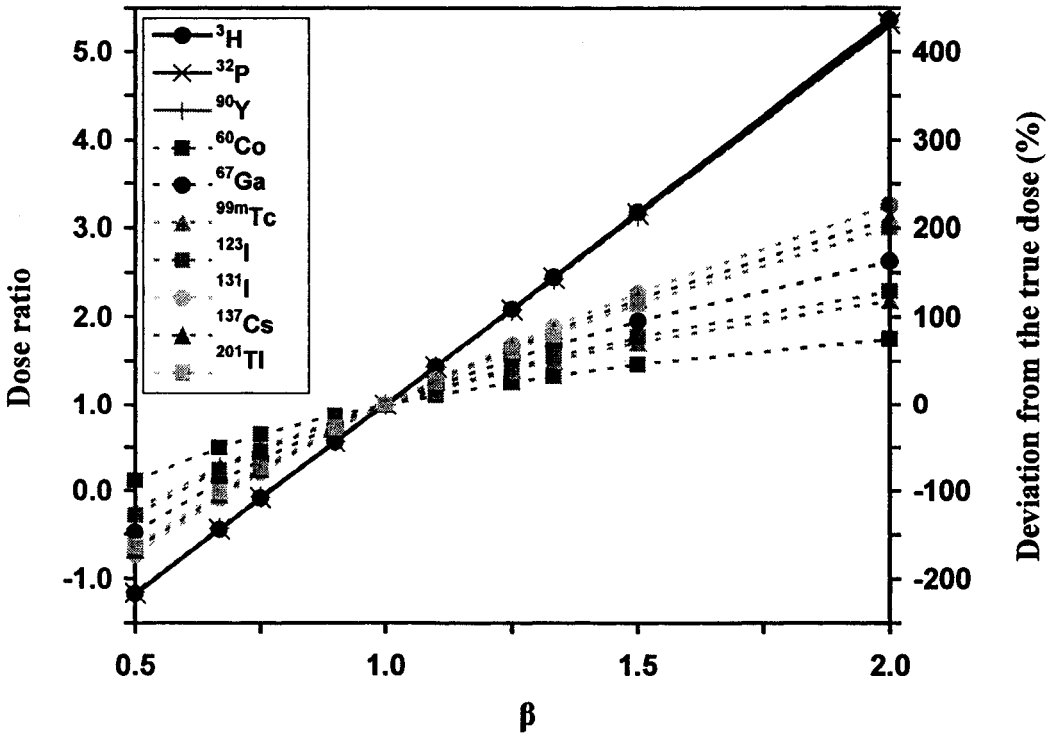

It is apparent from Figures 3.1 and 3.2 that ^{3}H, ^{32}P, and ^{90}Y produce little to no errors in $\bar{D}_{ratio\ 1}$. These radionuclides are mainly non-penetrating emitters, so little error would be expected because this incorrect patient-specific dose equation contains only inappropriate penetrating radiation terms, as seen in Equation (3.4). Otherwise, when β is low both $\bar{D}_{ratio\ 1}$ and $\bar{D}_{ratio\ 2}$ are low; when β is high both $\bar{D}_{ratio\ 1}$ and $\bar{D}_{ratio\ 2}$ are high. The errors in $\bar{D}_{ratio\ 2}$, as seen in Figures 3.3 and 3.4, are larger than those in $\bar{D}_{ratio\ 1}$ because both non-penetrating and penetrating radiation terms are affected in that incorrect patient-specific dose equation, as shown in Equation (3.7). The incorrect patient-specific dose equation can even yield negative ratios in $\bar{D}_{ratio\ 2}$, depending on the magnitude of the inapplicable non-penetrating and penetrating radiation terms.

Figures 3.5 and 3.6 display the dose ratios, $\bar{D}_{ratio\ 1}$, as Z increases while Figures 3.7 and 3.8 display the dose ratios, $\bar{D}_{ratio\ 2}$, as Z increases. Again, the deviation of the dose ratio from 1.0 is shown as a percent difference on the right axis of the graph.

Figure 3.5: $\bar{D}_{ratio\ 1}$ **vs. Z for the adult male brain.**

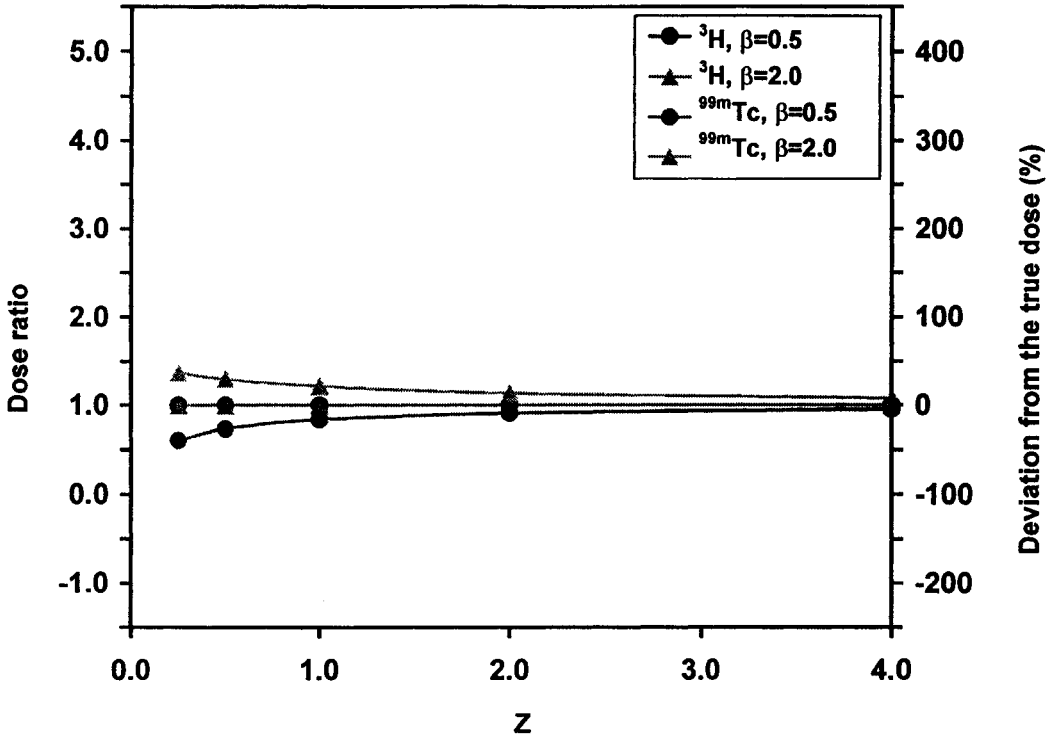

Figure 3.6: $\bar{D}_{ratio\ 1}$ **vs. Z for the newborn brain.**

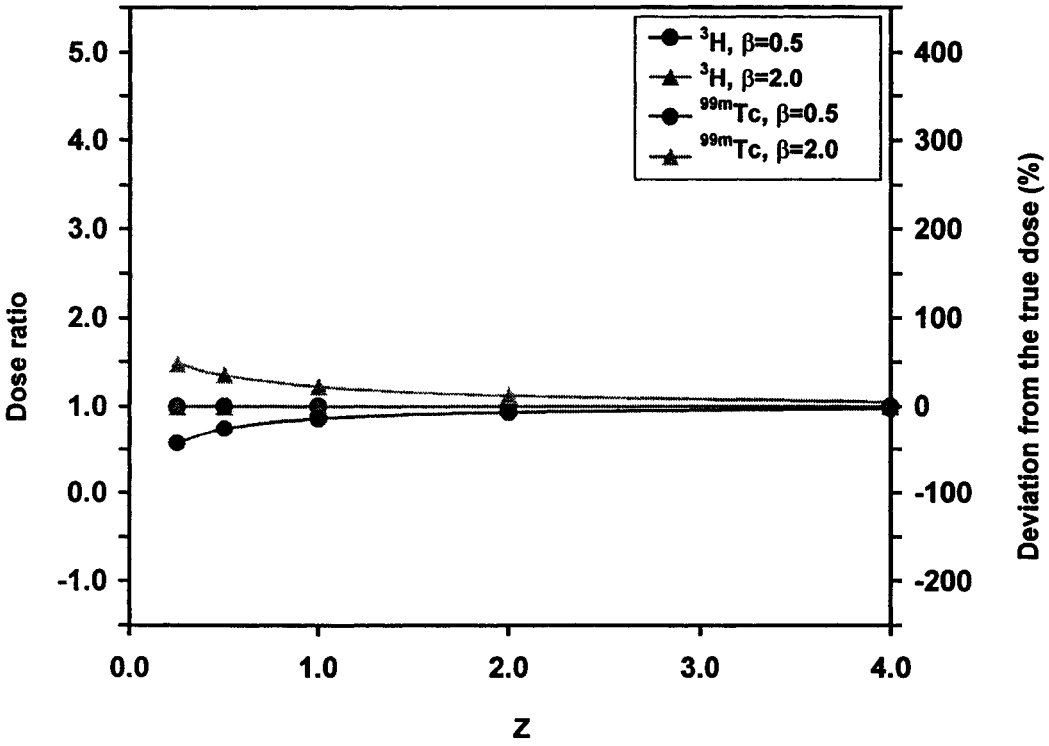

Figure 3.7: $\bar{D}_{ratio\,2}$ vs. Z for the adult male brain.

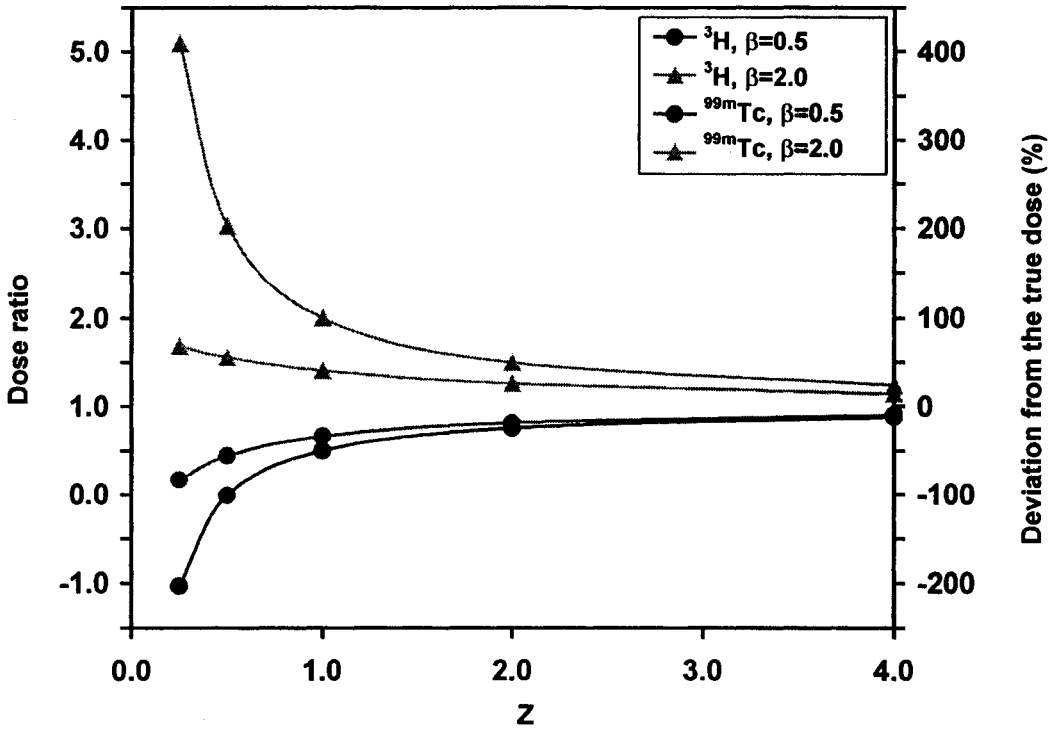

Figure 3.8: $\bar{D}_{ratio\,2}$ vs. Z for the newborn brain.

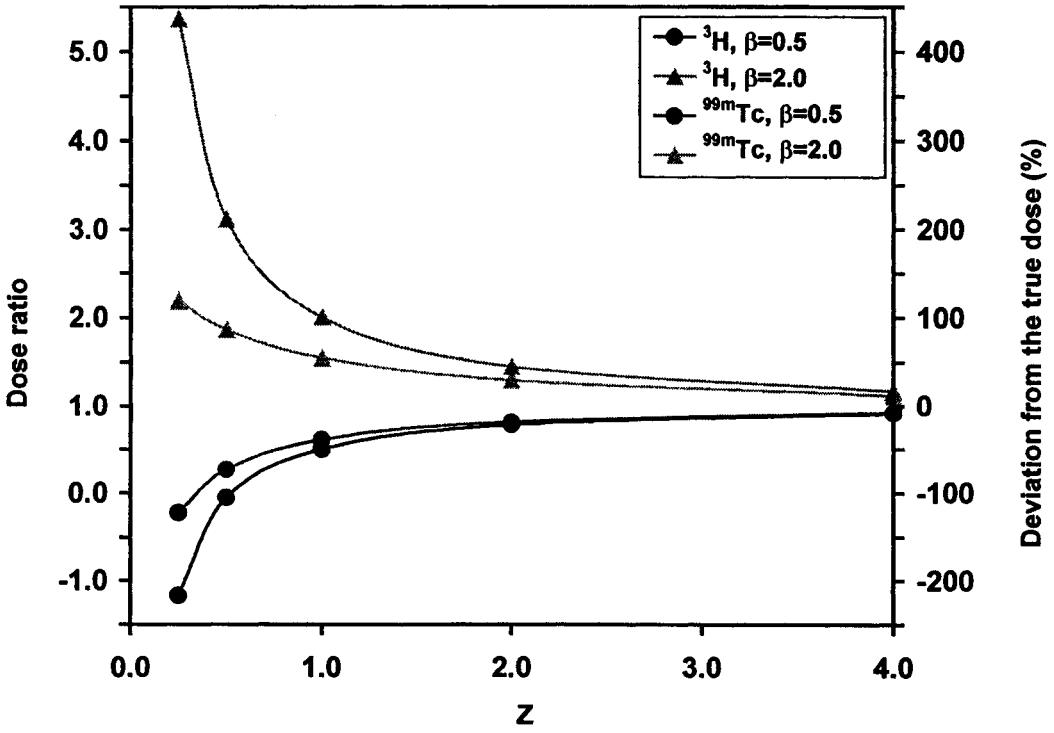

Again it is clear that the deviations of the dose ratios are larger for $\bar{D}_{ratio\ 2}$ than for $\bar{D}_{ratio\ 1}$. As well, the incorrect patient-specific dose approaches the correct dose (a dose ratio equal to 1.0) as Z increases.

It is apparent from Figures 3.1 to 3.8 that the radioisotopes can be separated into two categories: those that are mainly non-penetrating radiation emitters and those that are both non-penetrating and penetrating radiation emitters. The radionuclides investigated were thus separated into two categories:

category 1: non-penetrating (^{3}H, ^{32}P, ^{90}Y)

category 2: non-penetrating and penetrating (^{60}Co, ^{67}Ga, ^{99m}Tc, ^{123}I, ^{131}I, ^{137}Cs, ^{201}Tl)

Based on these two categories, the average dose ratios were calculated for all organs and all radionuclides examined in this study and are displayed in Tables 3.1 to 3.3. As mentioned previously, the ovaries and uterus were not included for the adult male and the testes were not included for the adult non-pregnant female.

Table 3.1: Dose ratios (mean ± standard deviation) for the adult male averaged for all organs examined in this study.

Z	β	Dose ratio			
		$\bar{D}_{ratio\ 1}$		$\bar{D}_{ratio\ 2}$	
		Category 1	**Category 2**	**Category 1**	**Category 2**
0.25	0.50	1.00 ± 0.00	0.85 ± 0.10	-1.01 ± 0.01	0.28 ± 0.30
	0.67	1.00 ± 0.00	0.91 ± 0.06	-0.34 ± 0.01	0.60 ± 0.18
	0.90	1.00 ± 0.00	0.98 ± 0.02	0.60 ± 0.00	0.90 ± 0.05
	1.00	1.00 ± 0.00	1.00 ± 0.00	1.00 ± 0.00	1.00 ± 0.00
	1.10	1.00 ± 0.00	1.02 ± 0.02	1.40 ± 0.00	1.09 ± 0.04
	1.33	1.00 ± 0.00	1.06 ± 0.04	2.34 ± 0.01	1.26 ± 0.14
	2.00	1.00 ± 0.01	1.14 ± 0.10	5.01 ± 0.05	1.57 ± 0.32
1.00	0.50	1.00 ± 0.00	0.93 ± 0.04	0.50 ± 0.00	0.68 ± 0.08
	0.67	1.00 ± 0.00	0.96 ± 0.03	0.67 ± 0.00	0.80 ± 0.05
	0.90	1.00 ± 0.00	0.99 ± 0.01	0.90 ± 0.00	0.95 ± 0.02
	1.00	1.00 ± 0.00	1.00 ± 0.00	1.00 ± 0.00	0.00 ± 0.00
	1.10	1.00 ± 0.00	1.01 ± 0.01	1.10 ± 0.00	1.05 ± 0.02
	1.33	1.00 ± 0.00	1.03 ± 0.02	1.33 ± 0.00	1.14 ± 0.05
	2.00	1.00 ± 0.00	1.08 ± 0.06	2.00 ± 0.00	1.35 ± 0.14
4.00	0.50	1.00 ± 0.00	0.98 ± 0.01	0.88 ± 0.00	0.90 ± 0.01
	0.67	1.00 ± 0.00	0.99 ± 0.01	0.92 ± 0.00	0.94 ± 0.01
	0.90	1.00 ± 0.00	1.00 ± 0.00	0.98 ± 0.00	0.98 ± 0.00
	1.00	1.00 ± 0.00	1.00 ± 0.00	1.00 ± 0.00	1.00 ± 0.00
	1.10	1.00 ± 0.00	1.00 ± 0.00	1.02 ± 0.00	1.02 ± 0.00
	1.33	1.00 ± 0.00	1.01 ± 0.01	1.08 ± 0.00	1.06 ± 0.01
	2.00	1.00 ± 0.00	1.04 ± 0.02	1.24 ± 0.01	1.15 ± 0.04

Table 3.2: Dose ratios (mean ± standard deviation) for the adult non-pregnant female averaged for all organs examined in this study.

Z	β	Dose ratio			
		$\bar{D}_{ratio\ 1}$		$\bar{D}_{ratio\ 2}$	
		Category 1	**Category 2**	**Category 1**	**Category 2**
0.25	0.50	1.00 ± 0.00	0.87 ± 0.10	-1.02 ± 0.02	0.31 ± 0.31
	0.67	1.00 ± 0.00	0.92 ± 0.06	-0.35 ± 0.01	0.61 ± 0.19
	0.90	1.00 ± 0.00	0.98 ± 0.02	0.60 ± 0.00	0.90 ± 0.05
	1.00	1.00 ± 0.00	1.00 ± 0.00	1.00 ± 0.00	1.00 ± 0.00
	1.10	1.00 ± 0.00	1.02 ± 0.01	1.40 ± 0.00	1.08 ± 0.04
	1.33	1.00 ± 0.00	1.05 ± 0.04	2.35 ± 0.02	1.24 ± 0.14
	2.00	1.00 ± 0.01	1.12 ± 0.10	5.07 ± 0.06	1.53 ± 0.32
1.00	0.50	1.00 ± 0.00	0.94 ± 0.04	0.50 ± 0.00	0.69 ± 0.08
	0.67	1.00 ± 0.00	0.96 ± 0.03	0.67 ± 0.00	0.81 ± 0.06
	0.90	1.00 ± 0.00	0.99 ± 0.01	0.90 ± 0.00	0.95 ± 0.02
	1.00	1.00 ± 0.00	1.00 ± 0.00	1.00 ± 0.00	1.00 ± 0.00
	1.10	1.00 ± 0.00	1.01 ± 0.01	1.10 ± 0.00	1.05 ± 0.02
	1.33	1.00 ± 0.00	1.03 ± 0.02	1.33 ± 0.00	1.14 ± 0.05
	2.00	1.00 ± 0.00	1.08 ± 0.05	2.00 ± 0.00	1.34 ± 0.14
4.00	0.50	1.00 ± 0.00	0.98 ± 0.01	0.88 ± 0.00	0.90 ± 0.01
	0.67	1.00 ± 0.00	0.99 ± 0.01	0.92 ± 0.00	0.94 ± 0.01
	0.90	1.00 ± 0.00	1.00 ± 0.00	0.98 ± 0.00	0.98 ± 0.00
	1.00	1.00 ± 0.00	1.00 ± 0.00	1.00 ± 0.00	1.00 ± 0.00
	1.10	1.00 ± 0.00	1.00 ± 0.00	1.02 ± 0.00	1.02 ± 0.00
	1.33	1.00 ± 0.00	1.01 ± 0.01	1.08 ± 0.00	1.05 ± 0.01
	2.00	1.00 ± 0.00	1.03 ± 0.02	1.24 ± 0.01	1.14 ± 0.04

Table 3.3: Dose ratios (mean ± standard deviation) for the newborn averaged for all organs examined in this study.

Z	β	Dose ratio			
		$\bar{D}_{ratio\ 1}$		$\bar{D}_{ratio\ 2}$	
		Category 1	**Category 2**	**Category 1**	**Category 2**
0.25	0.50	1.00 ± 0.00	0.91 ± 0.11	-1.03 ± 0.05	0.09 ± 0.38
	0.67	1.00 ± 0.00	0.94 ± 0.07	-0.35 ± 0.04	0.47 ± 0.24
	0.90	1.00 ± 0.00	0.99 ± 0.02	0.60 ± 0.01	0.87 ± 0.07
	1.00	1.00 ± 0.00	1.00 ± 0.00	1.00 ± 0.00	1.00 ± 0.00
	1.10	1.00 ± 0.00	1.01 ± 0.02	1.40 ± 0.01	1.12 ± 0.06
	1.33	1.00 ± 0.00	1.04 ± 0.05	2.35 ± 0.04	1.35 ± 0.19
	2.00	1.00 ± 0.01	1.10 ± 0.13	5.05 ± 1.11	1.80 ± 0.48
1.00	0.50	1.00 ± 0.00	0.96 ± 0.04	0.50 ± 0.00	0.64 ± 0.08
	0.67	1.00 ± 0.00	0.98 ± 0.02	0.67 ± 0.00	0.78 ± 0.06
	0.90	1.00 ± 0.00	0.99 ± 0.01	0.90 ± 0.00	0.94 ± 0.02
	1.00	1.00 ± 0.00	1.00 ± 0.00	1.00 ± 0.00	1.00 ± 0.00
	1.10	1.00 ± 0.00	1.01 ± 0.01	1.10 ± 0.00	1.06 ± 0.02
	1.33	1.00 ± 0.00	1.02 ± 0.02	1.33 ± 0.00	1.18 ± 0.06
	2.00	1.00 ± 0.00	1.05 ± 0.06	2.00 ± 0.00	1.44 ± 0.18
4.00	0.50	1.00 ± 0.00	0.99 ± 0.01	0.88 ± 0.01	0.90 ± 0.02
	0.67	1.00 ± 0.00	0.99 ± 0.01	0.92 ± 0.01	0.93 ± 0.01
	0.90	1.00 ± 0.00	1.00 ± 0.00	0.98 ± 0.00	0.98 ± 0.00
	1.00	1.00 ± 0.00	1.00 ± 0.00	1.00 ± 0.00	1.00 ± 0.00
	1.10	1.00 ± 0.00	1.00 ± 0.00	1.02 ± 0.00	1.02 ± 0.00
	1.33	1.00 ± 0.00	1.01 ± 0.00	1.08 ± 0.01	1.06 ± 0.01
	2.00	1.00 ± 0.00	1.02 ± 0.02	1.24 ± 0.03	1.16 ± 0.04

In all cases involving category 1 radionuclides, the dose ratios did not deviate from the expected value of 1.0 for $\bar{D}_{ratio\ 1}$. The dose ratios deviated equally and significantly for $\bar{D}_{ratio\ 2}$, regardless of the target, the mathematical model, or the radionuclide. The largest errors occurred when Z=0.25; the incorrect patient-specific dose was on average -1.02 times that of the correct dose when β=0.5 and on average 5.04 times that of the correct dose when β=2.0.

For category 2 radionuclides and all mathematical models, the dose ratios erred the most for the brain. For the adult male, the organ that was least affected was the thyroid. For the adult non-pregnant female and the newborn, the ovaries were the least affected. As well, in all cases investigated, the radionuclides that yielded the greatest differences from 1.0 were ^{123}I for $\bar{D}_{ratio\ 1}$ and ^{131}I for $\bar{D}_{ratio\ 2}$. Conversely, the radionuclides that produced the least differences were ^{131}I and ^{60}Co, respectively. The largest error for a single organ averaged for all radionuclides occurred in the newborn brain with Z=0.25 and β=2.0, where the incorrect patient-specific dose was on average 1.4 times higher than the correct dose as calculated for $\bar{D}_{ratio\ 1}$ and 2.6 times higher as calculated for $\bar{D}_{ratio\ 2}$.

3.3.3.3 Discussion

As can be seen from Tables 3.1 to 3.3, the dose ratios vary over a wide range, but similar trends in the data can be found in $\bar{D}_{ratio\ 1}$ and $\bar{D}_{ratio\ 2}$. It is apparent from Figures 3.1 to 3.4 that as β increases, the dose ratios increase. However, the absolute values of

the percent difference decrease as β approaches 1.0 (i.e. – when the patient target mass approaches the phantom target mass).

From Figures 3.5 to 3.8, it can be seen that when β is less than 1.0 and Z increases, the ratio increases towards 1.0. Accordingly, if β is greater than 1.0 and Z increases, the ratio decreases towards 1.0. Therefore, as the cumulated activity in a target organ increases, the incorrect patient-specific dose converges towards the correct dose, regardless of the amount of correction applied for patient-specific mass.

As mentioned earlier, there are no errors in the incorrect patient-specific dose equation for $\bar{D}_{ratio\ 1}$ when category 1 radionuclides are considered. This is easily explained, as the incorrect patient-specific dose equation in $\bar{D}_{ratio\ 1}$ does not alter the non-penetrating portion of the equation in patient-specific situations. In general, the errors are larger in $\bar{D}_{ratio\ 2}$. This is due to the fact that the patient-specific S-values are applied inappropriately for both non-penetrating and penetrating radiation terms.

In the event that the ratio is negative, it means that the incorrect patient-specific dose equation yielded a negative dose. The fact that negative dose ratios only occur with $\bar{D}_{ratio\ 2}$ and when β is low suggests that the incorrect non-penetrating radiation term is the contributing factor. It can be shown that it is highly improbable for $\bar{D}_{ratio\ 1}$ to yield a negative result with the parameters examined in this study. Given that the only sources

examined in this study were the target and the remainder of the body, Equation (3.9) can be reduced to:

$$\overline{D}_{ratio\,1} = \frac{\widetilde{A}_{target} \cdot \left(\sum_i \Delta_{i\,np} \Phi''_{i\,np(target \leftarrow target)} + \sum_i \Delta_{i\,p} \Phi''_{i\,p(target \leftarrow target)} \right) + \frac{\widetilde{A}_{rb}}{m_{rb}} \cdot \left[\sum_i \Delta_{i\,p} \left(m_{tb} \cdot \Phi_{i\,p(target \leftarrow tb)} - m_{target} \cdot \Phi''_{i\,p(target \leftarrow target)} \right) \right]}{\widetilde{A}_{target} \cdot \left(\sum_i \Delta_{i\,np} \Phi''_{i\,np(target \leftarrow target)} + \sum_i \Delta_{i\,p} \Phi''_{i\,p(target \leftarrow target)} \right) + \frac{\widetilde{A}_{rb}}{m_{rb}} \cdot \left[\sum_i \Delta_{i\,p} \left(m_{tb} \cdot \Phi_{i\,p(target \leftarrow tb)} - m_{target} \cdot \Phi_{i\,p(target \leftarrow target)} \right) \right]} \quad (3.14).$$

The inappropriate term in Equation (3.14), containing only penetrating radiation emission terms, is grouped as:

$$\left(m_{tb} \cdot \Phi_{i\,p(target \leftarrow tb)} - m_{target} \cdot \Phi''_{i\,p(target \leftarrow target)} \right) \quad (3.15),$$

and contains the only negative term in the numerator. Recalling Equation (2.40) that stated that the total body SAF is a mass-weighted sum of all the source SAFs, then:

$$m_{tb} \cdot \Phi_{i\,p(target \leftarrow tb)} >> m_{target} \cdot \Phi_{i\,p(target \leftarrow target)} \quad (3.16).$$

Since the smallest value of β examined in this study is 0.25, the patient-specific SAF is only 2.5 times that of the mathematical model SAF. There is no target mass greater than 40% of the total body mass; the inequality stated in Equation (3.16) holds for a patient-specific SAF. The value calculated in Equation (3.15) is therefore positive.

Furthermore, when considering only category 1 radionuclides, Equation (3.10) can be reduced to:

$$\overline{D}_{ratio\,2} = 1 + \left(\frac{\beta - 1}{Z}\right) \cdot \left[1 + \frac{m_{target}}{m_{rb}} \cdot (1 - Z)\right] \quad (3.17).$$

However:

$$\left[1 + \frac{m_{target}}{m_{rb}} \cdot (1 - Z)\right] \approx 1.0 \quad (3.18),$$

leaving:

$$\overline{D}_{ratio\,2} \approx 1 + \left(\frac{\beta - 1}{Z}\right) \quad (3.19).$$

Therefore, the value of $\bar{D}_{ratio\ 2}$ is negative for non-penetrating radiation emitters only when:

$$\beta + Z < 1.0 \quad (3.20).$$

The values calculated for $\bar{D}_{ratio\ 2}$ support Equations (3.19) and (3.20). The positive penetrating radiation terms included in $\bar{D}_{ratio\ 2}$ when considering category 2 radionuclides would dampen the negative non-penetrating radiation terms. This is seen in Figures 3.3 and 3.4.

Fortunately, in most cases the errors produced from use of the incorrect patient-specific doses are negligible, as seen in Tables 3.1 to 3.3. For example, if the patient target mass is within 10% of the mathematical model target mass, the largest difference is about 40%, while the remaining errors are generally less than 10%. These errors are within the expected accuracy of a factor of two that has been claimed for non-patient-specific dose estimates (Howell 1999). However, certain illnesses may greatly alter the

size of an organ in a diseased state, making patient-specific dose equations highly relevant.

3.4 Proposed MIRD equation

In order to incorporate the correction for walled organs and to provide a patient-specific dose equation that is unambiguous, a new MIRD dose equation is proposed here:

$$\frac{\overline{D}''_{target}}{A_0} = \tau_{target} \cdot S''_{(target \leftarrow target)} + \sum_{source=1}^{f} \tau_{source} \cdot S_{p(target \leftarrow source)} + \tau_{rb} \cdot S_{(target \leftarrow rb)} \tag{3.21}$$

where:

$$S''_{(target \leftarrow target)} = S_{np(target \leftarrow target)} \left(\frac{m''_{target}}{m_{target}} \right)^{-1} + S_{p(target \leftarrow target)} \left(\frac{m''_{target}}{m_{target}} \right)^{-2/3} \tag{3.22}$$

and:

$$S_{(target \leftarrow rb)} = S_{(target \leftarrow tb)} \cdot \left(\frac{m_{tb}}{m_{rb}} \right) - \sum_{source=1}^{f} S_{p(target \leftarrow source)} \cdot \left(\frac{m_{source}}{m_{rb}} \right) - \delta \cdot S_{(target \leftarrow target)} \cdot \left(\frac{m_{target}}{m_{rb}} \right) \tag{3.23}$$

$$m_{rb} = \sum_{source=1}^{f} m_{source} + \delta \cdot m_{target} \tag{3.24}$$

where δ = 0 if target $\neq$ source; and
1 if target = source.

Equation (3.21) solves three problems. It integrates the patient-specific dose equation into the classical MIRD equation, the self-dose is contained within the first

term, and by stating which S-values are explicitly penetrating S-values, the incorrect application of the non-penetrating dose from the contents to the walls is eliminated.

3.5 Conclusion

With increasing interest in patient-specific dosimetry, it is important to ensure that the MIRD equations are applied correctly. Inappropriate application of any adjustments to the dose equations can yield dose estimates that vary significantly from the true dose. Therefore, two refinements to the dose equations, one for walled organs and one for patient-specific cases, have lead to a newly proposed MIRD schema. In this schema, the patient-specific equation is no longer a post-estimate adjustment; it has been incorporated as an important quantity of the dose equation.

Footnotes:

† Personal communication, Evelyn Watson 30 August 2001.

‡ Personal communication, Michael Stabin 21 February 2001.

§ Personal communication, Michael Stabin 6 March 2001.

Chapter 4: Adult Dosimetry of FDG

4.1 Introduction

FDG is routinely used in PET studies; although its use is widespread, the dosimetry studies performed in the last two decades have relied mainly on biokinetic data obtained in animals. As stated previously, interest has grown in developing a more accurate quantification of the doses to patients administered radiopharmaceuticals, especially to females. Given the same administered activity and assuming similar biokinetics, a female's radiation dose will be higher than her male counterpart's due to her smaller overall body size and smaller organ sizes (Stabin 1997). This is simply due to the larger SAFs expected for smaller target masses, because the SAF is inversely proportional to the mass, as seen in Equation (2.7). According to the same report, women's effective doses averaged for all radiopharmaceuticals are about 25% higher than those for men, and women's gonad doses may be as much as 10 to 30 times higher than those for men. It has been reported that the female effective dose from FDG is 29% higher than the male, with the dose to the ovaries being 46% higher than the dose to the testes (Stabin 1997). In the case of FDG, the distribution of the radiopharmaceutical has been assumed to be the same in both men and women, without investigation into the possible differences in biokinetics between males and females. These differences, if any,

may result in an increase in the estimated radiation doses to the female patient, leading to an even greater risk to the female for the same medical procedure.

4.2 Literature review

Presently, the reported estimates of absorbed doses to adults from the administration of FDG rely on data obtained from animal biodistribution studies (Gallagher et al. 1977; Reivich et al. 1979; Brownell et al. 1980; ICRP 1988; Stabin et al. 1996; ICRP 1999) and from human subjects (Jones et al. 1982; ICRP 1988; Mejia et al. 1991; Dowd et al. 1991; Stabin et al. 1996; Deloar et al. 1998; ICRP 1999; Hays and Segall 1999; Niven et al. 2001; Hays and Segall 2002).

In the biodistribution studies of FDG by Gallagher and others (1977), four female mongrel dogs administered FDG were sacrificed; two at 60 min post-injection and two at 135 min post-injection. The activity per unit gram of tissue was determined for eight organs as well as blood, bone, urine, and muscle tissue samples. Reivich and others (1979; 1981) and Brownell and others (1980) used these data for their determinations of the absorbed doses to adults, assuming that the distribution in humans is the same as that observed in those dogs sacrificed at 60 min. Jones and others (1982) acquired data on the brain and bladder from humans, then used Gallagher's data (1977) for their remaining organ dose estimates. ICRP (1988; 1999) also used Gallagher's data (1977) in conjunction with the urine data from Jones' (1982) human subjects for its estimate of absorbed doses from FDG. Stabin and others (1996) also reported a 1992 absorbed dose

estimate based upon Gallagher's data (1977) and Jones' data (1982), but used both the brain and urinary bladder from the study by Jones and others (1982). More recently, Mejia and others (1991), Dowd and others (1991), Deloar and others (1998), Hays and Segall (1999), Niven and others (2001), and Hays and others (2002) have studied the biokinetics of FDG in several organs in human volunteers. With the exception of ICRP (1988; 1999) which lists absorbed doses for the adult, the 15 year-old, 10 year-old, five year-old, and one year-old phantoms, and Niven and others (2001) which lists brain doses for adult males and females, only absorbed doses to reference man have been published.

Table 4.1 summarizes those studies that reported absorbed doses to adults from FDG, Table 4.2 summarizes the significant biological data reported in those studies, and Table 4.3 displays the absorbed doses reported in those studies. Although biological data were measured and dose estimates were calculated by Niven and others (2001), the data are not included in Tables 4.2 and 4.3 because the data are included later in the text.

Table 4.1: Summary of studies reporting absorbed doses to adults from FDG.

Authors	Subjects	Number	Age of humans	Sex of humans	Comments
Reivich et al. 1979	dogs	2			dogs from Gallagher's study
Brownell et al. 1980	dogs	2			dogs from Gallagher's study
Reivich et al. 1981	dogs	2			dogs from Gallagher's study
Jones et al. 1982[a]	dogs	2			dogs from Gallagher's study
	humans	11	20-86 years	not reported	North American study: brain and bladder
ICRP 1988	dogs	2			dogs from Gallagher's study
	humans	11	20-86 years	not reported	humans from Jones' study
Mejia et al. 1991	humans	18	23-60 years	not reported	Japanese study: multiple organs
Dowd et al. 1991	humans	302	≥ 18 years	not reported	North American study: bladder
Stabin et al. 1996	dogs	2			dogs from Gallagher's study
	humans	11	20-86 years	not reported	humans from Jones' study
Deloar et al. 1998	humans	6	22-56 years	not reported	Japanese study: multiple organs
ICRP 1999	dogs	2			dogs from Gallagher's study
	humans	11	20-86 years	not reported	humans from Jones' study
Hays and Segall 1999	humans	5	not reported	4 male, 1 female	North American study: multiple organs
Niven et al. 2001	humans	14	53-79 years	8 male, 6 female	North American study: brain
Hays et al. 2002	humans	7	55-74 years	6 male, 1 female	North American study: multiple organs

[a] Correction appears in Jones et al. 1983

Table 4.2: Summary of studies reporting residence times for FDG.

Authors	Residence times (h)									
	Adrenals	Brain	LLI contents	Small intestine	Stomach contents	ULI contents	Heart wall	Kidneys	Liver	Lungs
Reivich et al. 1979										
Brownell et al. 1980										
Reivich et al. 1981										
Jones et al. 1982		0.105								
ICRP 1988		0.148[a]					0.098[a]	0.024[a]		
Mejia et al. 1991		0.178					0.085	0.034	0.112	0.023
Dowd et al. 1991										
Stabin et al. 1996										
Deloar et al. 1998	0.001	0.212	0.006	0.037	0.006	0.008	0.030[c]	0.036	0.119	0.076
ICRP 1999		0.148[a]					0.098[a]	0.024[a]		
Hays and Segall 1999		0.245[a]					0.133		0.161	0.084
Hays et al. 2002		0.220[a]					0.120[a]	0.030[a]	0.140[a]	0.060[a]

[a] Value was not measured by the authors.

[b] Reported for the North American mathematical model by Christy and Eckerman (1987).

[c] Value calculated from the measured data for the left ventricle; mass of left ventricle is 58.5% of the total heart wall (Coffey et al. 1981).

[d] Value is based on a two hour voiding schedule.

[e] Value was calculated from the MIRD dose estimate provided by the author and using the S-value for reference man.

[f] Value is based on clinical data; largest value calculated was 0.227 (no voiding).

Table 4.2 continued: Summary of studies reporting residence times for FDG.

Authors	Residence times (h)								
	Ovaries	Pancreas	Red marrow	Spleen	Testes	Thymus	Thyroid	Bladder contents	Total body
Reivich et al. 1979									
Brownell et al. 1980									
Reivich et al. 1981									
Jones et al. 1982								0.198	
ICRP 1988								0.317[a]	2.134[a]
Mejia et al. 1991	0.0003[a]	0.008	0.044[a]	0.010	0.001[a]			0.162[d]	2.639[a]
Dowd et al. 1991								0.193[e]	
Stabin et al. 1996									
Deloar et al. 1998[b]		0.011		0.008	0.001	0.003	0.001	0.199	2.639[a]
ICRP 1999								0.317[a]	2.134[a]
Hays and Segall 1999								0.040[f]	2.639[a]
Hays et al. 2002		0.006[a]		0.010[a]				0.130[a, d]	2.380[a]

[a] Value was not measured by the authors.

[b] Reported for the North American mathematical model by Christy and Eckerman (1987).

[c] Value calculated from the measured data for the left ventricle; mass of left ventricle is 58.5% of the total heart wall (Coffey et al. 1981).

[d] Value is based on a two hour voiding schedule.

[e] Value was calculated from the MIRD dose estimate provided by the author and using the S-value for reference man.

[f] Value is based on clinical data; largest value calculated was 0.227 (no voiding).

Table 4.3: Summary of studies reporting absorbed doses for FDG (adult male unless otherwise noted).

Authors	Absorbed doses (mGy MBq^{-1})									
	Adrenals	**Brain**	**Breasts**	**Gall-bladder**	**LLI wall**	**Small intestine**	**Stomach**	**ULI wall**	**Heart wall**	**Kidneys**
Reivich et al. 1979		0.0178							0.0397	0.0208
Brownell et al. 1980		0.0176					0.0141		0.0089	0.0143
Reivich et al. 1981		0.0216							0.0430	0.0230
Jones et al. 1982; 1983		0.0216							0.0432	0.0192
ICRP 1988 (adult male)	0.0140	0.0260	0.0110		0.0160	0.0130	0.0120	0.0130	0.0650	0.0210
ICRP 1988 (adult female)[a]	0.0150	0.0270	0.0110		0.0180	0.0170	0.0140	0.0150	0.0800	0.0250
Mejia et al. 1991[b]	0.0180	0.0290	0.0100		0.0180	0.0170	0.0150	0.0170	0.0450	0.0300
Mejia et al. 1991[c]		0.0280							0.0430	0.0260
Dowd et al. 1991										
Stabin et al. 1996	0.0130	0.0190	0.0092	0.0140	0.0170	0.0140	0.0130	0.0130	0.0600	0.0200
Deloar et al. 1998[c]	0.0160	0.0370	0.0089		0.0140	0.0140	0.0120	0.0140	0.0160	0.0280
ICRP 1999 (adult male)	0.0120	0.0280	0.0086	0.0120	0.0150	0.0130	0.0110	0.0120	0.0620	0.0210
ICRP 1999 (adult female)[a]	0.0150	0.0280	0.0110	0.0150	0.0190	0.0170	0.0140	0.0160	0.0810	0.0250
Hays and Segall 1999										
Hays et al. 2002		0.0460							0.0680	0.0210

[a] Same mathematical model as the 15 year-old.

[b] Values are for the Japanese adult mathematical model using the values measured in the Japanese subjects.

[c] Values are for the North American adult mathematical model.

[d] EDE and ED are given in units of mSv MBq^{-1}.

Table 4.3 continued: Summary of studies reporting absorbed doses for FDG (adult male unless otherwise noted).

Authors	Absorbed doses (mGy MBq^{-1})									
	Liver	Lungs	Muscle	Ovaries	Pancreas	Red marrow	Bone surfaces	Skin	Spleen	Testes
Reivich et al. 1979	0.0181	0.0181		0.0170					0.0500	
Brownell et al. 1980	0.0222	0.0211	0.0127	0.0176	0.0141			0.0100	0.0392	
Reivich et al. 1981	0.0203	0.0211		0.0143		0.0138			0.0427	0.0184
Jones et al. 1982; 1983	0.0157	0.0162		0.0151		0.0114			0.0389	0.0150
ICRP 1988 (adult male)	0.0120	0.0110		0.0150	0.0120	0.0110	0.0100		0.0120	0.0150
ICRP 1988 (adult female)[a]	0.0140	0.0130		0.0200	0.0160	0.0140	0.0120		0.0140	0.0160
Mejia et al. 1991[b]	0.0230	0.0110			0.0200	0.0120	0.0150		0.0220	0.0150
Mejia et al. 1991[c]	0.0210	0.0094			0.0180	0.0110			0.0200	0.0130
Dowd et al. 1991										
Stabin et al. 1996	0.0160	0.0170	0.0110	0.0170	0.0260	0.0130	0.0120	0.0084	0.0370	0.0130
Deloar et al. 1998[c]	0.0190	0.0180		0.0150	0.0270	0.0050	0.0071		0.0140	0.0140
ICRP 1999 (adult male)	0.0110	0.0100	0.0110	0.0150	0.0120	0.0110	0.0110	0.0080	0.0110	0.0120
ICRP 1999 (adult female)[a]	0.0140	0.0140	0.0140	0.0200	0.0160	0.0140	0.0140	0.0100	0.0140	0.0160
Hays and Segall 1999										
Hays et al. 2002	0.0240	0.0150		0.0110	0.0140	0.0110			0.0150	0.0110

[a] Same mathematical model as the 15 year-old.

[b] Values are for the Japanese adult mathematical model using the values measured in the Japanese subjects.

[c] Values are for the North American adult mathematical model.

[d] EDE and ED are given in units of mSv MBq^{-1}.

Table 4.3 continued: Summary of studies reporting absorbed doses for FDG (adult male unless otherwise noted).

Authors	Absorbed doses (mGy MBq^{-1})					
	Thymus	Thyroid	Bladder wall	Uterus	EDE[d]	ED[d]
Reivich et al. 1979			0.0781			
Brownell et al. 1980		0.0127	0.0389	0.0141		
Reivich et al. 1981			0.1176			
Jones et al. 1982; 1983			0.1135			
ICRP 1988 (adult male)		0.0097	0.1700	0.0200	0.0270	
ICRP 1988 (adult female)[a]		0.0120	0.2100	0.0260	0.0320	
Mejia et al. 1991[b]		0.0130	0.1200		0.0240	
Mejia et al. 1991[c]			0.0910			
Dowd et al. 1991						
Stabin et al. 1996	0.0120	0.0100	0.1900	0.0230	0.0300	
Deloar et al. 1998[c]	0.0110	0.0130	0.3100	0.0180		0.0290
ICRP 1999 (adult male)	0.0110	0.0100	0.1600	0.0210		0.0190
ICRP 1999 (adult female)[a]	0.0150	0.0130	0.2100	0.0260		0.0250
Hays and Segall 1999						
Hays et al. 2002			0.0730			

[a] Same mathematical model as the 15 year-old.

[b] Values are for the Japanese adult mathematical model using the values measured in the Japanese subjects.

[c] Values are for the North American adult mathematical model.

[d] EDE and ED are given in units of mSv MBq^{-1}.

4.3 Brain data

4.3.1 Materials and methods

4.3.1.1 Subjects

Eight male subjects (age: 53-77 years) and six female subjects (age: 53-79 years) undergoing clinical PET scans were included in this study. The average weight of the male subjects was 82.6 ± 17.2 kg; the average weight of the female subjects was 66.6 ± 11.4 kg. Of the male subjects, two were suspected Huntington's patients, three were suspected Alzheimer's patients, and three were controls. Of the female subjects, three were suspected Alzheimer's patients and three were controls. All subjects fasted for four hours prior to their studies, as per the clinical protocol.

4.3.1.2 PET scanning protocol

All studies were performed on the ECAT 953/31 PET Scanner (Siemens Medical Systems, Inc., Nuclear Medicine Group, 810 Innovation Drive, Knoxville, TN 37932) in the Department of Nuclear Medicine at McMaster University Medical Center. The scanner has a spatial resolution of 6 mm in all directions and an axial field of view of 10.8 cm. A 20 cm diameter, 20 cm long cylindrical uniform phantom filled with a $^{68}Ge/^{68}Ga$ solution was used to calibrate the scanner. Measurements of the phantom were performed at intervals throughout the duration of the study to ensure system stability. The variation found in the calibration measurements was determined to be 1% with no systematic trend in the calibration.

Dynamic PET studies were performed for 60 min at five min per frame over the brain of each patient; the entire organ was in view. The average injected activity per study was 177.1 MBq (range: 144.1-198.0 MBq) for the men and 179.1 MBq (range: 157.9-194.3 MBq) for the women. Images were reconstructed using a filtered backprojection algorithm and a Hann filter with a cutoff of 12 mm. Attenuation correction was calculated from a manually positioned ellipse in each of the 31 axial planes (Huang et al. 1981). The data were not decay corrected; the time course of activity was measured, including the biological and physical components.

For both male and female subjects, the Alzheimer's and control patients were studied twice, allowing for within-subject variability to be studied. These consecutive studies occurred one day apart except in one case, where the studies of a male patient occurred two weeks apart. The residence times for these duplicate studies were averaged to produce a single residence time per patient.

4.3.1.3 Description of measurements

Regions of interest (ROIs) were drawn around the brain for all planes that contained the organ. The activities and volumes determined from the ROIs were summed and a time-activity curve was produced for the entire organ volume. The time-activity curve was integrated by numerical integration using the trapezoidal rule (Siegel et al. 1999). It was assumed that the drug was fixed in the patient at completion of the scan (Huang et al. 1980) and that it decayed only by its physical half-life thereafter, according

to the method given by Smith (1966). This single exponential decay was integrated analytically (from the end of the scan to infinity) and summed with the numerical integration performed on the measured data to yield the cumulated activity.

4.3.2 Results

4.3.2.1 Residence times

The average brain volume was found to be 1340 ± 100 cm^3 for the male subjects and 1300 ± 90 cm^3 for the female subjects. Given a density of 1.03 g cm^{-3} (ICRP 1975), these volumes correspond to brain masses of 1.38 ± 0.10 kg and 1.34 ± 0.09 kg for the male and female subjects, respectively. The average brain masses of the male and females subjects are similar to the brain masses of 1.420 kg and 1.200 kg determined for the adult male and adult non-pregnant female mathematical models (Stabin 1996), respectively. The average residence times were 0.222 ± 0.033 h and 0.270 ± 0.027 h for the men and women, respectively. The data acquired for the adult males and females are displayed in Tables 4.4 and 4.5, respectively.

Table 4.4: Biological and biokinetic data obtained in adult males.

Subject (#)	Height (cm)	Weight (kg)	Age (years)	Injected activity[a] (MBq)	Brain mass[a] (kg)	Residence time[a] (h)
1	Unknown	57.3	Unknown	186.1	1.45	0.199
2	178.0	84.1	Unknown	149.5	1.24	0.245
3	187.0	93.5	56	183.2	1.55	0.244
scan 1				177.9	1.54	0.233
scan 2				188.5	1.57	0.254
4	175.0	83.8	77	183.4	1.39	0.227
scan 1				181.9	1.44	0.258
scan 2				184.9	1.35	0.195
5	180.0	84.5	76	187.6	1.41	0.255
scan 1				198.0	1.26	0.252
scan 2				177.2	1.57	0.257
6	191.0	94.2	53	169.7	1.35	0.174
scan 1				168.1	1.33	0.163
scan 2				171.3	1.36	0.185
7	177.0	106.0	72	159.2	1.25	0.178
scan 1				174.3	1.25	0.166
scan 2				144.1	1.25	0.190
8	168.0	57.5	73	188.9	1.38	0.253
scan 1				183.0	1.38	0.218
scan 2				194.8	1.37	0.288
Mean	179.4	82.6	68	176.1	1.38	0.222
SD	7.6	17.2	11	15.3	0.10	0.033

[a] The values are averaged from the duplicate studies performed on patients 3-8.

Table 4.5: Biological and biokinetic data obtained in adult females.

Subject (#)	Height (cm)	Weight (kg)	Age (years)	Injected activity[a] (MBq)	Brain mass[a] (kg)	Residence time[a] (h)
9	161.0	75.0	77	176.1	1.29	0.278
scan 1				169.2	1.33	0.278
scan 2				183.1	1.25	0.277
10	157.0	77.6	66	185.3	1.40	0.246
scan 1				187.8	1.42	0.232
scan 2				182.7	1.39	0.260
11	158.0	49.5	79	190.7	1.47	0.263
scan 1				194.2	1.46	0.313
scan 2				187.2	1.49	0.212
12	172.0	72.5	53	161.9	1.21	0.247
scan 1				166.0	1.23	0.247
scan 2				157.9	1.20	0.247
13	175.0	69.5	74	182.5	1.38	0.265
scan 1				187.6	1.42	0.266
scan 2				177.4	1.33	0.264
14	163.0	55.5	63	178.3	1.29	0.320
scan 1				171.4	1.31	0.330
scan 2				185.2	1.26	0.309
Mean	164.3	66.6	69	179.1	1.34	0.270
SD	7.5	11.4	10	10.8	0.09	0.027

[a] The values are averaged from the duplicate studies performed on patients 9-14.

Assuming no elimination of FDG from the body, the total body residence time is 2.639 h, based on the physical half-life of FDG (1.83 h). This yields average residence times of 2.417 ± 0.033 h and 2.369 ± 0.027 h for the remainder of the body for the males and females, respectively.

The typical rapid incorporation of FDG in the brain can be seen in Figure 4.1, which includes one female and one male subject. The activity in the brain, normalized to the administered activity, represents not a single plane but the entire brain volume as summed from all the PET images for the study.

Figure 4.1: Typical time-activity curves normalized to the administered activity for the adult male and female brain.

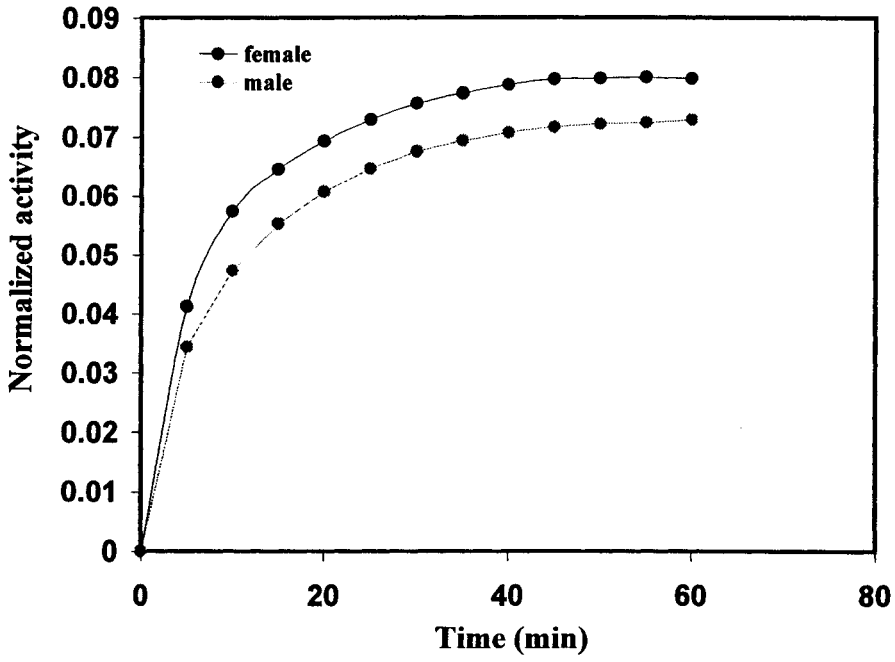

4.3.2.2 Dose estimates

The dose estimates were calculated according to Equations (3.21) and (3.23). The differences in brain masses between this patient population and the MIRDOSE phantoms were corrected for by adjusting the S-values as given in Equation (3.22). The calculated

self-dose to the brain was found to be lower for men ($3.9x10^{-2}$ mGy MBq^{-1}) than for women ($4.8x10^{-2}$ mGy MBq^{-1}). Similarly, the dose to the brain was found to be $4.2x10^{-2}$ mGy MBq^{-1} for the male subjects, which is lower than the $5.2x10^{-2}$ mGy MBq^{-1} determined for the female subjects. The patient-specific doses calculated for the brains of this patient population are given in Tables 4.6 and 4.7.

Table 4.6: Patient-specific doses calculated for the brains of the adult males.

Subject (#)	Brain (mGy MBq^{-1})	
	Self-dose	**Total dose**
1	0.0336	0.0362
2	0.0472	0.0498
3	0.0387	0.0413
4	0.0395	0.0421
5	0.0440	0.0465
6	0.0313	0.0339
7	0.0341	0.0368
8	0.0446	0.0472
Mean	0.0391	0.0417
SD	0.0058	0.0058

Table 4.7: Patient-specific doses calculated for the brains of the adult females.

Subject (#)	Brain (mGy MBq^{-1})	
	Self-dose	**Total dose**
9	0.0513	0.0548
10	0.0422	0.0457
11	0.0432	0.0467
12	0.0479	0.0514
13	0.0462	0.0497
14	0.0590	0.0625
Mean	0.0483	0.0518
SD	0.0062	0.0062

4.3.2.3 Within-subject variability

The duplicate studies performed on patients 3-8 and 9-14 allowed for within-subject variability to be studied. Figure 4.2 shows the absorbed self-doses in the duplicate studies for all 12 patients with no distinction between genders. The self-doses for several patients were nearly identical or very close in the duplicate studies, so that the mean within-subject variability was found to be within 14%. The largest difference was found to be 1.8×10^{-2} mGy MBq^{-1}, which is the exception.

Figure 4.2: The duplicate studies of six male subjects (3-8) and six female subjects (9-14) showed little variation in most cases, where the average variation was found to be within 14%.

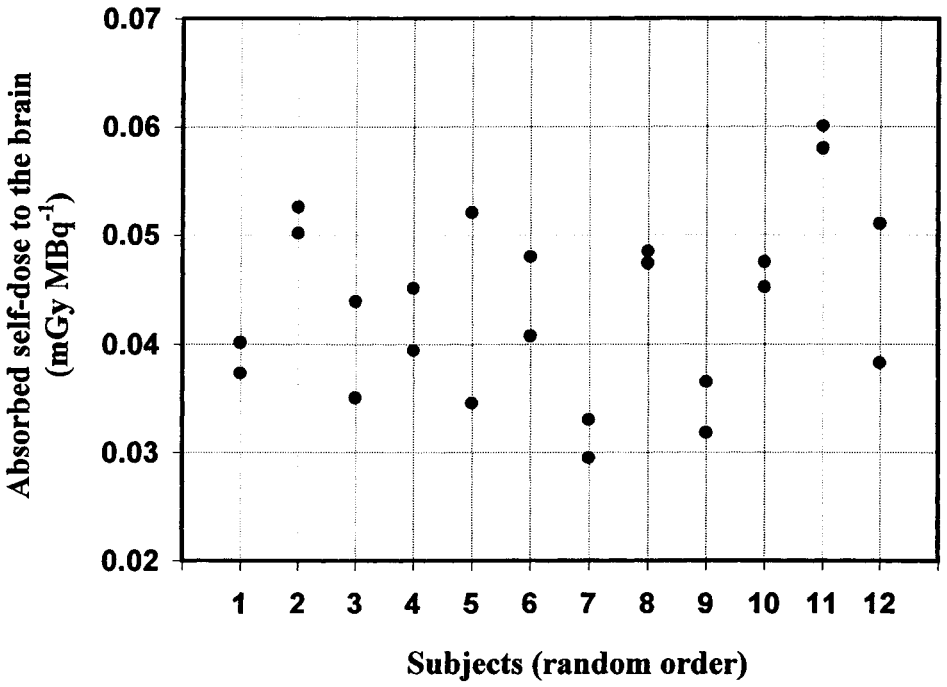

4.3.3 Discussion

The results derived from this study show a significant gender difference in the residence time ($p < 0.02$) and in the absorbed dose ($p < 0.01$) to the brain from FDG. The 22% higher residence time in the brains of females vs. males yields a 25% higher absorbed dose. As stated previously, it is known that the doses to women are higher for the same administered activity simply due to a difference in the S-values, given the same biodistribution (Stabin 1997). However, the difference in the residence time determined in this study implies a biological difference in the biodistribution of FDG in the brains of women compared to men.

The residence time determined for the male subjects in this study is similar to previously published values; the residence time determined for the female subjects is higher than any previously published values (Table 4.2). The average dose to the adult male brain obtained in this study is comparable to recently published data, as seen in Table 4.3. However, the average dose to the adult female brain obtained in this study is almost twice any previously published values for adult females. As well, an increasing trend in the dose to the brain appears over time (Table 4.3). This is probably due to the use of data obtained from human subjects rather than data obtained from animal subjects.

This is the first time within-subject variability for the radiopharmaceutical FDG has been studied. With all duplicate studies, the within-subject variability was found to have an average variation of 14%, while in 10 out of 12 studies, the average variation was less than 10%. This means that the reliability of a single dose estimate is excellent in most cases.

4.4 Heart, liver, and lung data

4.4.1 Materials and methods

4.4.1.1 Subjects

Seven male subjects (age: 44-78 years) and seven female subjects (age: 44-84 years) who had undergone heart viability research PET scans were included in this study. These patients were chosen retrospectively; the criteria for inclusion in this study were

based on weight and height characteristics similar to the adult mathematical models. The average weight and height of the male subjects were 73.6 ± 1.1 kg and 173.4 ± 8.5 cm; the adult male mathematical model weighs 73.7 kg and is 170 cm tall. The average weight and height of the female subjects were 56.9 ± 3.9 kg and 156.4 ± 6.5 cm; the adult non-pregnant female mathematical model weighs 56.9 kg[†] and is 160 cm tall (Eckerman and Christy 1995). All subjects fasted for four hours and all were given glucose solutions approximately one hour prior to their studies, as per the research protocol.

4.4.1.2 PET scanning protocol

All studies were performed on the ECAT ART PET Scanner (Siemens Medical Systems, Inc., Nuclear Medicine Group, 810 Innovation Drive, Knoxville, TN 37932) in the Cardiac PET Centre at The University of Ottawa Heart Institute. The scanner has a spatial resolution of 4 mm in all directions and an axial field of view of 16.2 cm. A 20 cm diameter, 20 cm long cylindrical uniform phantom filled with an ^{18}F-FDG solution was used to calibrate the scanner.

Dynamic PET studies were performed either for a 70 min scan at five min per frame or for a 40-70 min scan with an additional 30 min gated scan over the chest of each patient. The average injected activities were 84.9 MBq (range: 59.9-103.1 MBq) and 70.0 MBq (range: 56.7-86.9 MBq) for men and women, respectively. Images were reconstructed using a filtered backprojection algorithm and a Hann filter with a cutoff frequency of 12 mm. Attenuation correction was applied through a transmission scan

obtained immediately prior to the start of the PET scan. The data were not decay corrected.

4.4.1.3 Description of measurements

ROIs were drawn on the transmission scan outlining the lungs on all planes where the lungs were visible. Similarly, ROIs were drawn on the emission scan outlining the heart wall and the liver. Several small ROIs were drawn within the blood pool in the heart muscle to represent the heart contents. The activities and volumes determined from the ROIs on each plane were summed; these values were scaled according to the actual organ sizes as defined for the adult male and adult non-pregnant female mathematical models. As previously stated, a time-activity curve was produced for the entire organ. The time-activity curve was integrated by numerical integration using the trapezoidal rule (Siegel et al. 1999). It was assumed that the drug was fixed in the patient at completion of the scan (Huang et al. 1980) and that it decayed only by its physical half-life thereafter, according to the method given by Smith (1966). This single exponential decay was integrated analytically and summed with the numerical integration to yield the cumulated activity.

4.4.2 Results

4.4.2.1 Residence times

Given densities of 1.0298 g cm^{-3} for the heart (ICRP 1975), 1.058 g cm^{-3} for the blood (ICRP 1975), 1.053 g cm^{-3} for the liver (ICRU 1989), and 0.296 g cm^{-3} for the lung

(Christy and Eckerman 1987), the organ volumes determined from the planar images were converted to organ masses. The average organ masses of the subjects are presented in Table 4.8 and can be compared to the mathematical model organ masses in Table 4.9.

Table 4.8: Average organ masses determined in the adult male and female subjects.

Model	Organ masses (kg)			
	Heart wall	**Heart contents**	**Liver**	**Lungs**
Males	0.269 ± 0.061	0.005 ± 0.001	1.060 ± 0.359	0.353 ± 0.128
Females	0.177 ± 0.039	0.004 ± 0.001	0.831 ± 0.207	0.280 ± 0.175

Table 4.9: Organ masses of the adult mathematical models.

Model	Organ mass[a] (kg)			
	Heart wall	**Heart contents**	**Liver**	**Lung**
Males	0.315	0.454	1.910	1.000
Females	0.240	0.410	1.400	0.800[b]

[a] All organ masses were taken from Stabin (1996), with the exception of the adult female lung mass.
[b] Personal communication, Michael Stabin 21 February 2001.

The average residence times calculated for the adult males were 0.061 ± 0.012 h, 0.031 ± 0.008 h, 0.128 ± 0.036 h, and 0.073 ± 0.014 h for the heart wall, heart contents, liver, and lung, respectively. The average residence times calculated for the adult females were 0.048 ± 0.006 h, 0.035 ± 0.008 h, 0.127 ± 0.026 h, and 0.076 ± 0.024 h for the heart wall, heart contents, liver, and lung, respectively. The data acquired for the adult males and females are displayed in Tables 4.10 and 4.11.

Table 4.10: Biological and biokinetic data obtained in adult males.

Subject (#)	Height (cm)	Weight (kg)	Age (years)	Injected activity (MBq)	Residence time (h)			
					Heart wall	Heart contents	Liver	Lungs
15	182.9	72.7	78.0	71.5	0.058	0.024	0.096	0.061
16	177.8	75.0	59.0	100.4	0.053	0.033	0.147	0.082
17	157.5	72.7	44.0	84.5	0.057	0.044	0.109	0.063
18	172.7	75.0	70.0	99.1	0.056	0.027	0.112	0.063
19	167.6	72.7	73.0	59.9	0.089	0.033	0.184	0.100
20	177.8	74.1	53.0	103.1	0.059	0.020	0.088	0.064
21	177.8	72.7	78.0	75.7	0.057	0.036	0.161	0.074
Mean	173.4	73.6	65.0	84.9	0.061	0.031	0.128	0.073
SD	8.5	1.1	13.2	16.6	0.012	0.008	0.036	0.014

Table 4.11: Biological and biokinetic data obtained in adult females.

Subject (#)	Height (cm)	Weight (kg)	Age (years)	Injected activity (MBq)	Residence time (h)			
					Heart wall	Heart contents	Liver	Lungs
22	162.6	52.3	44.0	65.2	0.045	0.029	0.096	0.056
23	157.5	61.4	59.0	73.7	0.050	0.027	0.104	0.062
24	162.6	58.2	71.0	66.7	0.046	0.024	0.099	0.054
25	149.9	58.2	84.0	73.0	0.038	0.039	0.144	0.115
26	147.3	61.4	72.0	86.9	0.050	0.037	0.141	0.080
27	162.6	54.5	78.0	56.7	0.057	0.042	0.142	0.061
28	152.4	52.3	73.0	67.7	0.053	0.044	0.161	0.101
Mean	156.4	56.9	68.7	70.0	0.048	0.035	0.127	0.076
SD	6.5	3.9	13.3	9.3	0.006	0.008	0.026	0.024

Again, assuming no elimination of FDG from the body, the total body residence time is 2.639 h. This yields average residence times of 2.346 ± 0.062 h and 2.353 ± 0.055 h for the remainder of the body for the males and females, respectively.

The characteristic uptake and gradual washout of FDG in several organs are illustrated for a male subject (Figure 4.3) and a female subject (Figure 4.4). The activity in these organs, normalized to the administered activity, represents the entire organ volumes as calculated from the summed PET images for the study.

Figure 4.3: Typical time-activity curves normalized to the administered activity for several adult male organs.

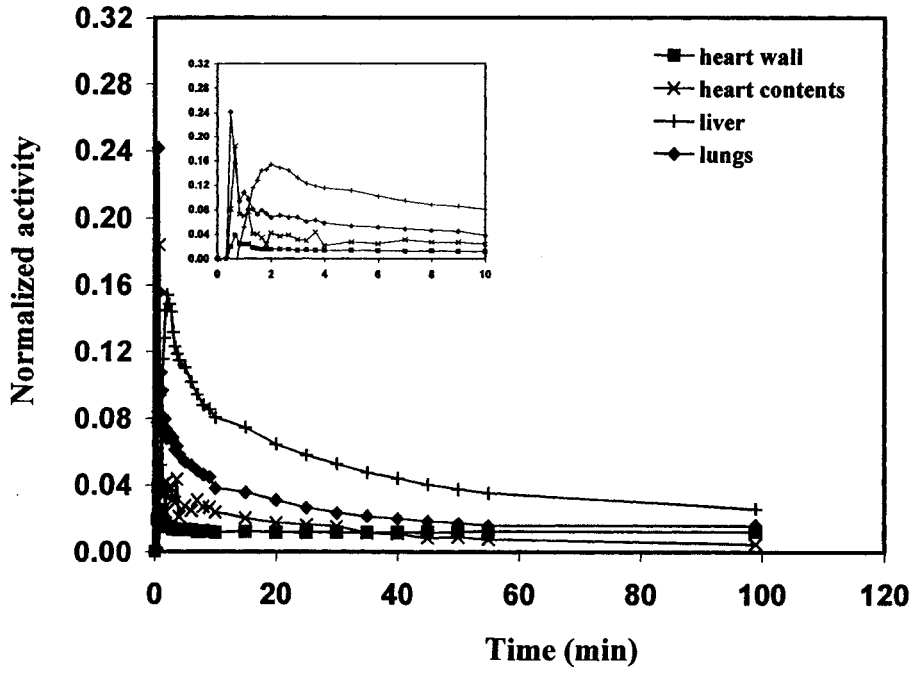

Figure 4.4: Typical time- activity curves normalized to the administered activity for several adult female organs.

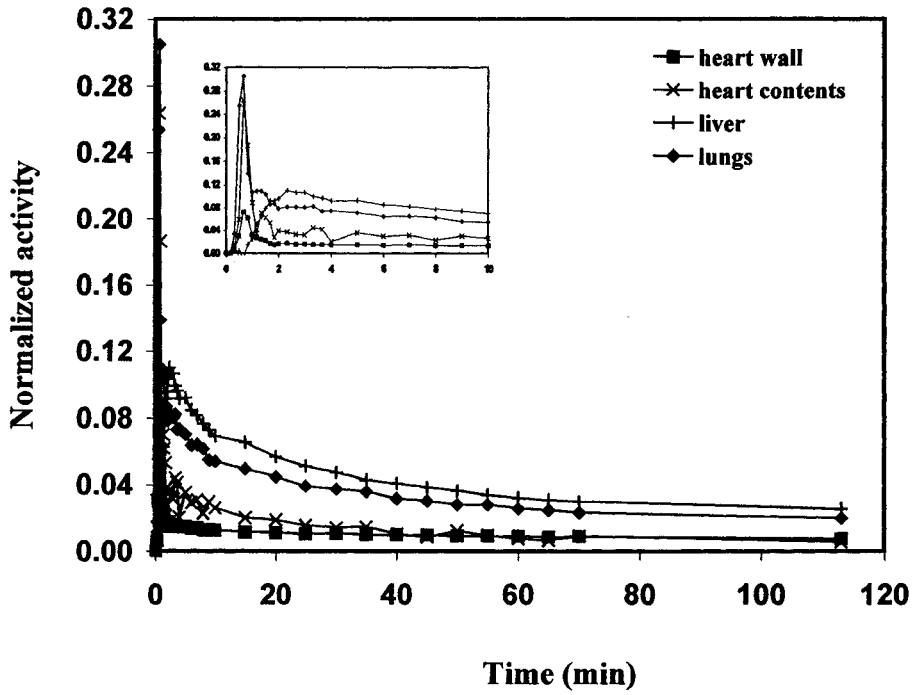

4.4.2.2 Dose estimates

Equations (3.21) and (3.23) were used in calculating the absorbed dose. Because the entire organ masses were not measured, patient-specific dose calculations could not be performed. Therefore, there were effectively no adjustments to the S-values; the doses calculated are related to the reference adult male and adult non-pregnant female mathematical models. The doses calculated for the organs of this patient population are given in Tables 4.12 and 4.13.

Table 4.12: Doses calculated for the heart wall, liver, and lungs of the adult males.

Subject (#)	Heart wall (mGy MBq^{-1})		Liver (mGy MBq^{-1})		Lungs (mGy MBq^{-1})	
	Self-dose	Total dose	Self-dose	Total dose	Self-dose	Total dose
15	0.0333	0.0419	0.0121	0.0177	0.0107	0.0177
16	0.0305	0.0402	0.0186	0.0241	0.0144	0.0215
17	0.0326	0.0429	0.0138	0.0194	0.0110	0.0181
18	0.0322	0.0412	0.0142	0.0197	0.0110	0.0181
19	0.0512	0.0610	0.0232	0.0289	0.0175	0.0250
20	0.0337	0.0420	0.0111	0.0167	0.0112	0.0181
21	0.0327	0.0427	0.0203	0.0258	0.0129	0.0202
Mean	0.0352	0.0445	0.0162	0.0218	0.0127	0.0198
SD	0.0071	0.0073	0.0046	0.0046	0.0025	0.0027

Table 4.13: Doses calculated for the heart wall, liver, and lungs of the adult females.

Subject (#)	Heart wall (mGy MBq^{-1})		Liver (mGy MBq^{-1})		Lungs (mGy MBq^{-1})	
	Self-dose	Total dose	Self-dose	Total dose	Self-dose	Total dose
22	0.0336	0.0447	0.0160	0.0231	0.0123	0.0211
23	0.0373	0.0483	0.0172	0.0244	0.0138	0.0226
24	0.0339	0.0445	0.0165	0.0236	0.0118	0.0206
25	0.0286	0.0417	0.0238	0.0311	0.0255	0.0344
26	0.0373	0.0497	0.0234	0.0306	0.0177	0.0268
27	0.0423	0.0549	0.0236	0.0308	0.0134	0.0227
28	0.0397	0.0531	0.0266	0.0339	0.0224	0.0316
Mean	0.0361	0.0481	0.0210	0.0282	0.0167	0.0257
SD	0.0045	0.0048	0.0043	0.0044	0.0054	0.0054

4.4.3 Discussion

The results derived from this study show a significant sex difference in the residence time of the heart wall ($p < 0.03$). The largest residence time for the adult males is actually an outlier as determined by the boxplot technique (Milton and Arnold 1995);

once removed the average residence time becomes 0.057± 0.002 h and is still significantly different from the adult female residence time ($p < 0.01$). There is also a significant gender difference in the absorbed doses to the lungs ($p < 0.03$) and the liver ($p < 0.03$) from FDG. There is no statistical difference in the residence time of the lungs or the liver for females vs. males; the higher S-value for the respective organ is the primary contributor to the higher dose. Again, this is expected given the same biological distribution (Stabin 1997). Interestingly, the 27% higher residence time of the heart wall in the males is balanced by the 31% higher S-value in the females, leading to comparable absorbed doses. Nonetheless, the difference in the residence time of the heart wall determined in this study implies a biological difference in the biodistribution of FDG in women compared to men.

The residence times determined for the male and female subjects for the lungs and liver are similar to previously published values (Table 4.2). However, the residence times previously published for the heart wall vary drastically, from 0.030 to 0.133 h; the residence times determined for the male and female subjects are between these values.

The average dose to the adult male heart wall determined in this study is comparable to previously published data (heart wall: 0.0449 ± 0.0201 mGy MBq^{-1}), as seen in Table 4.3. However, the average dose to the adult female heart wall obtained in this study is less than half any previously published values (0.0805 ± 0.0007 mGy MBq^{-1}). This large difference is not due to the omission of the dose to the surface of the

heart wall from the heart contents. The non-penetrating dose to the walls from the contents would contribute an increase in either the male or female absorbed dose estimates of on average only 11%. Rather, the use of a heart wall residence time obtained in male subjects to calculate the absorbed dose to female subjects would be the primary contributor for the overestimate of the dose previously reported for females. Another important contributing factor is the use of different mathematical models. The only studies that have published absorbed doses to females are by ICRP, which used the hermaphrodite 15 year-old child/adult female mathematical model; this study used the adult non-pregnant female mathematical model.

The average doses to the adult male liver and lungs determined in this study are higher than previously published data (liver: 0.0179 ± 0.0043 mGy MBq^{-1}; lungs: 0.0157 ± 0.0043 mGy MBq^{-1}), as seen in Table 4.3. In contrast, the average doses for the adult female subjects are almost twice as high for their respective organs (liver: 0.0140 ± 0.0000 mGy MBq^{-1}; lungs: 0.0135 ± 0.0007 mGy MBq^{-1}). Again, a major contributing factor for the difference in the results determined in this study compared to previously published results is the fact that data were measured in female subjects rather than being extrapolated from male subjects or animals.

4.5 Comprehensive dosimetry calculations

4.5.1 Additional residence times

The residence times for organs not measured have traditionally been either lumped in with the remainder of the body residence time or were assigned values based on the assumption of uniform distribution (i.e. – based on the organ's relative mass). For calculations of absorbed doses to the male and female subjects in this study, several approaches have been taken which combine measured residence times with previously measured or calculated residence times. This method provides a range of possible dose estimates.

4.5.1.1 Organs

Several key organs have been identified with the uptake of FDG: brain, heart wall, kidneys, liver, lungs, pancreas, spleen, and urinary bladder contents. Several of these organs have been examined in various studies. For subjects 1-8 and 9-14, the heart wall, heart contents, liver, and lung residence times obtained from subjects 15-21 and 22-28 were used, with male and female values respectively. Similarly, for subjects 15-21 and 22-28, the average brain residence times obtained from subjects 1-8 and 9-14 were used, with male and female values respectively.

With the exception of case 1, residence times for the kidneys, pancreas, and spleen were averaged from the measured data reported by Mejia and others (1991) and

Deloar and others (1998). Previously published residence times for the urinary bladder contents vary widely, from 0.040 h (Hays and Segall 1999) to 0.317 (ICRP 1988; ICRP 1999). Therefore, five scenarios were developed:

case 1: calculated assuming uniform distribution but using brain, heart wall, heart contents, lung, and liver data measured by Niven and others.

case 2: same as case 1, but using previously published residence times for the kidneys, pancreas, and spleen.

cases 3 and 4: same as case 2, but using a bladder contents residence time averaged from the measured data reported by Jones and others (1982), Mejia and others (1991), Dowd and others (1991), and Deloar and others (1998).

case 5: same as case 2, but using a urinary bladder contents residence time averaged from the residence times reported by Hays and Segall (1999) at voiding periods of 144 min and 288 min. The data provided by Hays and Segall (1999) correlate to voiding periods of 2.4 h and 4.8 h; the age-related bladder voiding model (ICRP 1999) for the adult is 3.5 h.

4.5.1.2 Total body and remainder of the body

The assumption that the cumulated activity in the total body is calculated assuming instantaneous uptake and no washout is most likely an overestimate, as urinary excretion of FDG would reduce the activity in the total body. Therefore, the residence time of 2.639 h was used in cases 1 to 3, while the previously reported value of 2.134 h

was used for the total body residence time in cases 4 and 5. Summaries of these residence times are presented in Tables 4.14 to 4.18.

Table 4.14: Summary of residence times for case 1.

Subject (#)	Sex	Residence times (h)									
		Brain	Heart wall	Heart contents	Kidneys	Liver	Lungs	Pancreas	Spleen	Bladder contents	Total body
1	male	0.199	0.061	0.031	0.011	0.128	0.073	0.003	0.007	0.008	2.639
2	male	0.245	0.061	0.031	0.011	0.128	0.073	0.003	0.007	0.008	2.639
3	male	0.244	0.061	0.031	0.011	0.128	0.073	0.003	0.007	0.008	2.639
4	male	0.227	0.061	0.031	0.011	0.128	0.073	0.003	0.007	0.008	2.639
5	male	0.255	0.061	0.031	0.011	0.128	0.073	0.003	0.007	0.008	2.639
6	male	0.174	0.061	0.031	0.011	0.128	0.073	0.003	0.007	0.008	2.639
7	male	0.178	0.061	0.031	0.011	0.128	0.073	0.003	0.007	0.008	2.639
8	male	0.253	0.061	0.031	0.011	0.128	0.073	0.003	0.007	0.008	2.639
9	female	0.278	0.048	0.035	0.013	0.127	0.076	0.004	0.007	0.007	2.639
10	female	0.246	0.048	0.035	0.013	0.127	0.076	0.004	0.007	0.007	2.639
11	female	0.263	0.048	0.035	0.013	0.127	0.076	0.004	0.007	0.007	2.639
12	female	0.247	0.048	0.035	0.013	0.127	0.076	0.004	0.007	0.007	2.639
13	female	0.265	0.048	0.035	0.013	0.127	0.076	0.004	0.007	0.007	2.639
14	female	0.320	0.048	0.035	0.013	0.127	0.076	0.004	0.007	0.007	2.639
15	male	0.222	0.058	0.024	0.011	0.096	0.061	0.003	0.007	0.008	2.639
16	male	0.222	0.053	0.033	0.011	0.147	0.082	0.003	0.007	0.008	2.639
17	male	0.222	0.057	0.044	0.011	0.109	0.063	0.003	0.007	0.008	2.639
18	male	0.222	0.056	0.027	0.011	0.112	0.063	0.003	0.007	0.008	2.639
19	male	0.222	0.089	0.033	0.011	0.184	0.100	0.003	0.007	0.008	2.639

Table 4.14 continued: Summary of residence times for case 1.

Subject (#)	Sex	Residence times (h)									
		Brain	Heart wall	Heart contents	Kidneys	Liver	Lungs	Pancreas	Spleen	Bladder contents	Total body
20	male	0.222	0.089	0.033	0.011	0.088	0.064	0.003	0.007	0.008	2.639
21	male	0.222	0.059	0.020	0.011	0.161	0.074	0.003	0.007	0.008	2.639
22	female	0.270	0.045	0.029	0.013	0.096	0.056	0.004	0.007	0.007	2.639
23	female	0.270	0.050	0.027	0.013	0.104	0.062	0.004	0.007	0.007	2.639
24	female	0.270	0.046	0.024	0.013	0.099	0.054	0.004	0.007	0.007	2.639
25	female	0.270	0.038	0.039	0.013	0.144	0.115	0.004	0.007	0.007	2.639
26	female	0.270	0.050	0.037	0.013	0.141	0.080	0.004	0.007	0.007	2.639
27	female	0.270	0.057	0.042	0.013	0.142	0.061	0.004	0.007	0.007	2.639
28	female	0.270	0.053	0.044	0.013	0.161	0.101	0.004	0.007	0.007	2.639

Table 4.15: Summary of residence times for case 2.

Subject (#)	Sex	Residence times (h)									
		Brain	Heart wall	Heart contents	Kidneys	Liver	Lungs	Pancreas	Spleen	Bladder contents	Total body
1	male	0.199	0.061	0.031	0.035	0.128	0.073	0.010	0.009	0.008	2.639
2	male	0.245	0.061	0.031	0.035	0.128	0.073	0.010	0.009	0.008	2.639
3	male	0.244	0.061	0.031	0.035	0.128	0.073	0.010	0.009	0.008	2.639
4	male	0.227	0.061	0.031	0.035	0.128	0.073	0.010	0.009	0.008	2.639
5	male	0.255	0.061	0.031	0.035	0.128	0.073	0.010	0.009	0.008	2.639
6	male	0.174	0.061	0.031	0.035	0.128	0.073	0.010	0.009	0.008	2.639
7	male	0.178	0.061	0.031	0.035	0.128	0.073	0.010	0.009	0.008	2.639
8	male	0.253	0.061	0.031	0.035	0.128	0.073	0.010	0.009	0.008	2.639
9	female	0.278	0.048	0.035	0.035	0.127	0.076	0.010	0.009	0.007	2.639
10	female	0.246	0.048	0.035	0.035	0.127	0.076	0.010	0.009	0.007	2.639
11	female	0.263	0.048	0.035	0.035	0.127	0.076	0.010	0.009	0.007	2.639
12	female	0.247	0.048	0.035	0.035	0.127	0.076	0.010	0.009	0.007	2.639
13	female	0.265	0.048	0.035	0.035	0.127	0.076	0.010	0.009	0.007	2.639
14	female	0.320	0.048	0.035	0.035	0.127	0.076	0.010	0.009	0.007	2.639
15	male	0.222	0.058	0.024	0.035	0.096	0.061	0.010	0.009	0.008	2.639
16	male	0.222	0.053	0.033	0.035	0.147	0.082	0.010	0.009	0.008	2.639
17	male	0.222	0.057	0.044	0.035	0.109	0.063	0.010	0.009	0.008	2.639
18	male	0.222	0.056	0.027	0.035	0.112	0.063	0.010	0.009	0.008	2.639
19	male	0.222	0.089	0.033	0.035	0.184	0.100	0.010	0.009	0.008	2.639

Table 4.15 continued: Summary of residence times for case 2.

Subject (#)	Sex	Residence times (h)									
		Brain	Heart wall	Heart contents	Kidneys	Liver	Lungs	Pancreas	Spleen	Bladder contents	Total body
20	male	0.222	0.089	0.033	0.035	0.088	0.064	0.010	0.009	0.008	2.639
21	male	0.222	0.059	0.020	0.035	0.161	0.074	0.010	0.009	0.008	2.639
22	female	0.270	0.045	0.029	0.035	0.096	0.056	0.010	0.009	0.007	2.639
23	female	0.270	0.050	0.027	0.035	0.104	0.062	0.010	0.009	0.007	2.639
24	female	0.270	0.046	0.024	0.035	0.099	0.054	0.010	0.009	0.007	2.639
25	female	0.270	0.038	0.039	0.035	0.144	0.115	0.010	0.009	0.007	2.639
26	female	0.270	0.050	0.037	0.035	0.141	0.080	0.010	0.009	0.007	2.639
27	female	0.270	0.057	0.042	0.035	0.142	0.061	0.010	0.009	0.007	2.639
28	female	0.270	0.053	0.044	0.035	0.161	0.101	0.010	0.009	0.007	2.639

Table 4.16: Summary of residence times for case 3.

Subject (#)	Sex	Residence times (h)									
		Brain	Heart wall	Heart contents	Kidneys	Liver	Lungs	Pancreas	Spleen	Bladder contents	Total body
1	male	0.199	0.061	0.031	0.035	0.128	0.073	0.010	0.009	0.188	2.639
2	male	0.245	0.061	0.031	0.035	0.128	0.073	0.010	0.009	0.188	2.639
3	male	0.244	0.061	0.031	0.035	0.128	0.073	0.010	0.009	0.188	2.639
4	male	0.227	0.061	0.031	0.035	0.128	0.073	0.010	0.009	0.188	2.639
5	male	0.255	0.061	0.031	0.035	0.128	0.073	0.010	0.009	0.188	2.639
6	male	0.174	0.061	0.031	0.035	0.128	0.073	0.010	0.009	0.188	2.639
7	male	0.178	0.061	0.031	0.035	0.128	0.073	0.010	0.009	0.188	2.639
8	male	0.253	0.061	0.031	0.035	0.128	0.073	0.010	0.009	0.188	2.639
9	female	0.278	0.048	0.035	0.035	0.127	0.076	0.010	0.009	0.188	2.639
10	female	0.246	0.048	0.035	0.035	0.127	0.076	0.010	0.009	0.188	2.639
11	female	0.263	0.048	0.035	0.035	0.127	0.076	0.010	0.009	0.188	2.639
12	female	0.247	0.048	0.035	0.035	0.127	0.076	0.010	0.009	0.188	2.639
13	female	0.265	0.048	0.035	0.035	0.127	0.076	0.010	0.009	0.188	2.639
14	female	0.320	0.048	0.035	0.035	0.127	0.076	0.010	0.009	0.188	2.639
15	male	0.222	0.058	0.024	0.035	0.096	0.061	0.010	0.009	0.188	2.639
16	male	0.222	0.053	0.033	0.035	0.147	0.082	0.010	0.009	0.188	2.639
17	male	0.222	0.057	0.044	0.035	0.109	0.063	0.010	0.009	0.188	2.639
18	male	0.222	0.056	0.027	0.035	0.112	0.063	0.010	0.009	0.188	2.639
19	male	0.222	0.089	0.033	0.035	0.184	0.100	0.010	0.009	0.188	2.639

Table 4.16 continued: Summary of residence times for case 3.

Subject (#)	Sex	Residence times (h)									
		Brain	Heart wall	Heart contents	Kidneys	Liver	Lungs	Pancreas	Spleen	Bladder contents	Total body
20	male	0.222	0.089	0.033	0.035	0.088	0.064	0.010	0.009	0.188	2.639
21	male	0.222	0.059	0.020	0.035	0.161	0.074	0.010	0.009	0.188	2.639
22	female	0.270	0.045	0.029	0.035	0.096	0.056	0.010	0.009	0.188	2.639
23	female	0.270	0.050	0.027	0.035	0.104	0.062	0.010	0.009	0.188	2.639
24	female	0.270	0.046	0.024	0.035	0.099	0.054	0.010	0.009	0.188	2.639
25	female	0.270	0.038	0.039	0.035	0.144	0.115	0.010	0.009	0.188	2.639
26	female	0.270	0.050	0.037	0.035	0.141	0.080	0.010	0.009	0.188	2.639
27	female	0.270	0.057	0.042	0.035	0.142	0.061	0.010	0.009	0.188	2.639
28	female	0.270	0.053	0.044	0.035	0.161	0.101	0.010	0.009	0.188	2.639

Table 4.17: Summary of residence times for case 4.

Subject (#)	Sex	Residence times (h)									
		Brain	Heart wall	Heart contents	Kidneys	Liver	Lungs	Pancreas	Spleen	Bladder contents	Total body
1	male	0.199	0.061	0.031	0.035	0.128	0.073	0.010	0.009	0.188	2.134
2	male	0.245	0.061	0.031	0.035	0.128	0.073	0.010	0.009	0.188	2.134
3	male	0.244	0.061	0.031	0.035	0.128	0.073	0.010	0.009	0.188	2.134
4	male	0.227	0.061	0.031	0.035	0.128	0.073	0.010	0.009	0.188	2.134
5	male	0.255	0.061	0.031	0.035	0.128	0.073	0.010	0.009	0.188	2.134
6	male	0.174	0.061	0.031	0.035	0.128	0.073	0.010	0.009	0.188	2.134
7	male	0.178	0.061	0.031	0.035	0.128	0.073	0.010	0.009	0.188	2.134
8	male	0.253	0.061	0.031	0.035	0.128	0.073	0.010	0.009	0.188	2.134
9	female	0.278	0.048	0.035	0.035	0.127	0.076	0.010	0.009	0.188	2.134
10	female	0.246	0.048	0.035	0.035	0.127	0.076	0.010	0.009	0.188	2.134
11	female	0.263	0.048	0.035	0.035	0.127	0.076	0.010	0.009	0.188	2.134
12	female	0.247	0.048	0.035	0.035	0.127	0.076	0.010	0.009	0.188	2.134
13	female	0.265	0.048	0.035	0.035	0.127	0.076	0.010	0.009	0.188	2.134
14	female	0.320	0.048	0.035	0.035	0.127	0.076	0.010	0.009	0.188	2.134
15	male	0.222	0.058	0.024	0.035	0.096	0.061	0.010	0.009	0.188	2.134
16	male	0.222	0.053	0.033	0.035	0.147	0.082	0.010	0.009	0.188	2.134
17	male	0.222	0.057	0.044	0.035	0.109	0.063	0.010	0.009	0.188	2.134
18	male	0.222	0.056	0.027	0.035	0.112	0.063	0.010	0.009	0.188	2.134
19	male	0.222	0.089	0.033	0.035	0.184	0.100	0.010	0.009	0.188	2.134

Table 4.17 continued: Summary of residence times for case 4.

Subject (#)	Sex	Residence times (h)									
		Brain	Heart wall	Heart contents	Kidneys	Liver	Lungs	Pancreas	Spleen	Bladder contents	Total body
20	male	0.222	0.089	0.033	0.035	0.088	0.064	0.010	0.009	0.188	2.134
21	male	0.222	0.059	0.020	0.035	0.161	0.074	0.010	0.009	0.188	2.134
22	female	0.270	0.045	0.029	0.035	0.096	0.056	0.010	0.009	0.188	2.134
23	female	0.270	0.050	0.027	0.035	0.104	0.062	0.010	0.009	0.188	2.134
24	female	0.270	0.046	0.024	0.035	0.099	0.054	0.010	0.009	0.188	2.134
25	female	0.270	0.038	0.039	0.035	0.144	0.115	0.010	0.009	0.188	2.134
26	female	0.270	0.050	0.037	0.035	0.141	0.080	0.010	0.009	0.188	2.134
27	female	0.270	0.057	0.042	0.035	0.142	0.061	0.010	0.009	0.188	2.134
28	female	0.270	0.053	0.044	0.035	0.161	0.101	0.010	0.009	0.188	2.134

Table 4.18: Summary of residence times for case 5.

Subject (#)	Sex	Residence times (h)									
		Brain	Heart wall	Heart contents	Kidneys	Liver	Lungs	Pancreas	Spleen	Bladder contents	Total body
1	male	0.199	0.061	0.031	0.035	0.128	0.073	0.010	0.009	0.155	2.134
2	male	0.245	0.061	0.031	0.035	0.128	0.073	0.010	0.009	0.155	2.134
3	male	0.244	0.061	0.031	0.035	0.128	0.073	0.010	0.009	0.155	2.134
4	male	0.227	0.061	0.031	0.035	0.128	0.073	0.010	0.009	0.155	2.134
5	male	0.255	0.061	0.031	0.035	0.128	0.073	0.010	0.009	0.155	2.134
6	male	0.174	0.061	0.031	0.035	0.128	0.073	0.010	0.009	0.155	2.134
7	male	0.178	0.061	0.031	0.035	0.128	0.073	0.010	0.009	0.155	2.134
8	male	0.253	0.061	0.031	0.035	0.128	0.073	0.010	0.009	0.155	2.134
9	female	0.278	0.048	0.035	0.035	0.127	0.076	0.010	0.009	0.155	2.134
10	female	0.246	0.048	0.035	0.035	0.127	0.076	0.010	0.009	0.155	2.134
11	female	0.263	0.048	0.035	0.035	0.127	0.076	0.010	0.009	0.155	2.134
12	female	0.247	0.048	0.035	0.035	0.127	0.076	0.010	0.009	0.155	2.134
13	female	0.265	0.048	0.035	0.035	0.127	0.076	0.010	0.009	0.155	2.134
14	female	0.320	0.048	0.035	0.035	0.127	0.076	0.010	0.009	0.155	2.134
15	male	0.222	0.058	0.024	0.035	0.096	0.061	0.010	0.009	0.155	2.134
16	male	0.222	0.053	0.033	0.035	0.147	0.082	0.010	0.009	0.155	2.134
17	male	0.222	0.057	0.044	0.035	0.109	0.063	0.010	0.009	0.155	2.134
18	male	0.222	0.056	0.027	0.035	0.112	0.063	0.010	0.009	0.155	2.134
19	male	0.222	0.089	0.033	0.035	0.184	0.100	0.010	0.009	0.155	2.134

Table 4.17 continued: Summary of residence times for case 5.

Subject (#)	Sex	Residence times (h)									
		Brain	Heart wall	Heart contents	Kidneys	Liver	Lungs	Pancreas	Spleen	Bladder contents	Total body
20	male	0.222	0.089	0.033	0.035	0.088	0.064	0.010	0.009	0.155	2.134
21	male	0.222	0.059	0.020	0.035	0.161	0.074	0.010	0.009	0.155	2.134
22	female	0.270	0.045	0.029	0.035	0.096	0.056	0.010	0.009	0.155	2.134
23	female	0.270	0.050	0.027	0.035	0.104	0.062	0.010	0.009	0.155	2.134
24	female	0.270	0.046	0.024	0.035	0.099	0.054	0.010	0.009	0.155	2.134
25	female	0.270	0.038	0.039	0.035	0.144	0.115	0.010	0.009	0.155	2.134
26	female	0.270	0.050	0.037	0.035	0.141	0.080	0.010	0.009	0.155	2.134
27	female	0.270	0.057	0.042	0.035	0.142	0.061	0.010	0.009	0.155	2.134
28	female	0.270	0.053	0.044	0.035	0.161	0.101	0.010	0.009	0.155	2.134

4.5.2 Dose estimates

Again, Equations (3.21) to (3.23) were used in calculating the absorbed dose estimates. For patients 1-14, patient-specific dose calculations were performed for the brain. Otherwise, the doses calculated are related to the reference adult male and adult non-pregnant female mathematical models. The weighting factors for the EDE and the ED were obtained from ICRP 26 (1977) and ICRP 67 (1994), respectively, although the uterus was eliminated as an organ for the male subjects. The doses calculated for the organs of these patient populations are given in Table 4.19.

Table 4.19: Summary of the average absorbed doses corresponding to the residence times stated in five different cases.

Organ	Absorbed dose (mGy MBq^{-1})			
	Case 1		Case 2	
	Male	Female	Male	Female
Adrenals	0.0141 ± 0.0002	0.0175 ± 0.0002	0.0146 ± 0.0002	0.0180 ± 0.0002
Brain	0.0411 ± 0.0041	0.0539 ± 0.0046	0.0411 ± 0.0041	0.0539 ± 0.0046
Breasts	0.0102 ± 0.0001	0.0127 ± 0.0001	0.0101 ± 0.0001	0.0126 ± 0.0001
Gall bladder	0.0151 ± 0.0004	0.0176 ± 0.0003	0.0153 ± 0.0004	0.0178 ± 0.0003
Lower large intestine	0.0131 ± 0.0003	0.0161 ± 0.0003	0.0129 ± 0.0003	0.0159 ± 0.0003
Small intestine	0.0136 ± 0.0002	0.0153 ± 0.0002	0.0135 ± 0.0002	0.0153 ± 0.0002
Stomach	0.0132 ± 0.0001	0.0163 ± 0.0001	0.0134 ± 0.0001	0.0165 ± 0.0001
Upper large intestine	0.0134 ± 0.0002	0.0166 ± 0.0002	0.0134 ± 0.0002	0.0165 ± 0.0002
Heart wall	0.0452 ± 0.0062	0.0474 ± 0.0034	0.0452 ± 0.0062	0.0475 ± 0.0034
Kidneys	0.0139 ± 0.0001	0.0173 ± 0.0001	0.0291 ± 0.0001	0.0323 ± 0.0001
Liver	0.0214 ± 0.0030	0.0277 ± 0.0031	0.0216 ± 0.0030	0.0279 ± 0.0031
Lungs	0.0195 ± 0.0017	0.0252 ± 0.0038	0.0195 ± 0.0017	0.0252 ± 0.0038
Muscle	0.0114 ± 0.0001	0.0140 ± 0.0002	0.0114 ± 0.0001	0.0139 ± 0.0002
Ovaries	0.0000 ± 0.0000	0.0163 ± 0.0003	0.0000 ± 0.0000	0.0161 ± 0.0003
Pancreas	0.0149 ± 0.0002	0.0194 ± 0.0002	0.0282 ± 0.0002	0.0321 ± 0.0002
Red marrow	0.0126 ± 0.0001	0.0158 ± 0.0001	0.0126 ± 0.0001	0.0157 ± 0.0001
Bone surfaces	0.0134 ± 0.0001	0.0166 ± 0.0002	0.0133 ± 0.0001	0.0165 ± 0.0002
Skin	0.0091 ± 0.0001	0.0113 ± 0.0001	0.0091 ± 0.0001	0.0112 ± 0.0001
Spleen	0.0141 ± 0.0001	0.0172 ± 0.0001	0.0168 ± 0.0001	0.0204 ± 0.0001
Testes	0.0109 ± 0.0002	0.0000 ± 0.0000	0.0108 ± 0.0002	0.0000 ± 0.0000
Thymus	0.0132 ± 0.0002	0.0162 ± 0.0001	0.0131 ± 0.0002	0.0161 ± 0.0001
Thyroid	0.0123 ± 0.0002	0.0138 ± 0.0002	0.0122 ± 0.0002	0.0136 ± 0.0002
Urinary bladder wall	0.0131 ± 0.0002	0.0136 ± 0.0002	0.0130 ± 0.0002	0.0135 ± 0.0002
Uterus	0.0000 ± 0.0000	0.0162 ± 0.0003	0.0000 ± 0.0000	0.0160 ± 0.0003
EDE[a]	0.0172 ± 0.0006	0.0218 ± 0.0006	0.0187 ± 0.0006	0.0234 ± 0.0006
ED[a]	0.0137 ± 0.0003	0.0176 ± 0.0005	0.0138 ± 0.0003	0.0176 ± 0.0005

[a] EDE and ED are given in units of mSv MBq^{-1}.

Table 4.19 continued: Summary of the average absorbed doses corresponding to the residence times stated in five different cases.

Organ	Absorbed dose (mGy MBq^{-1})			
	Case 3		Case 4	
	Male	Female	Male	Female
Adrenals	0.0137 ± 0.0002	0.0169 ± 0.0002	0.0110 ± 0.0002	0.0135 ± 0.0002
Brain	0.0409 ± 0.0041	0.0536 ± 0.0046	0.0403 ± 0.0041	0.0529 ± 0.0046
Breasts	0.0094 ± 0.0001	0.0117 ± 0.0001	0.0073 ± 0.0001	0.0090 ± 0.0001
Gall bladder	0.0145 ± 0.0004	0.0169 ± 0.0003	0.0117 ± 0.0004	0.0136 ± 0.0003
Lower large intestine	0.0144 ± 0.0003	0.0178 ± 0.0003	0.0113 ± 0.0003	0.0139 ± 0.0003
Small intestine	0.0134 ± 0.0002	0.0153 ± 0.0002	0.0102 ± 0.0002	0.0118 ± 0.0002
Stomach	0.0125 ± 0.0001	0.0154 ± 0.0001	0.0097 ± 0.0001	0.0118 ± 0.0001
Upper large intestine	0.0131 ± 0.0002	0.0162 ± 0.0002	0.0100 ± 0.0002	0.0124 ± 0.0002
Heart wall	0.0449 ± 0.0062	0.0470 ± 0.0034	0.0437 ± 0.0062	0.0456 ± 0.0034
Kidneys	0.0288 ± 0.0001	0.0319 ± 0.0001	0.0274 ± 0.0001	0.0303 ± 0.0001
Liver	0.0213 ± 0.0030	0.0275 ± 0.0031	0.0203 ± 0.0030	0.0262 ± 0.0031
Lungs	0.0191 ± 0.0017	0.0247 ± 0.0038	0.0179 ± 0.0017	0.0232 ± 0.0038
Muscle	0.0111 ± 0.0001	0.0135 ± 0.0002	0.0086 ± 0.0001	0.0104 ± 0.0002
Ovaries	0.0000 ± 0.0000	0.0178 ± 0.0003	0.0000 ± 0.0000	0.0139 ± 0.0003
Pancreas	0.0278 ± 0.0002	0.0315 ± 0.0002	0.0262 ± 0.0002	0.0296 ± 0.0002
Red marrow	0.0121 ± 0.0001	0.0151 ± 0.0001	0.0094 ± 0.0001	0.0117 ± 0.0001
Bone surfaces	0.0125 ± 0.0001	0.0156 ± 0.0002	0.0097 ± 0.0001	0.0121 ± 0.0002
Skin	0.0085 ± 0.0001	0.0105 ± 0.0001	0.0065 ± 0.0001	0.0080 ± 0.0001
Spleen	0.0164 ± 0.0001	0.0199 ± 0.0001	0.0151 ± 0.0001	0.0183 ± 0.0001
Testes	0.0115 ± 0.0002	0.0000 ± 0.0000	0.0089 ± 0.0002	0.0000 ± 0.0000
Thymus	0.0122 ± 0.0002	0.0149 ± 0.0001	0.0097 ± 0.0002	0.0116 ± 0.0001
Thyroid	0.0112 ± 0.0002	0.0125 ± 0.0002	0.0085 ± 0.0002	0.0094 ± 0.0002
Urinary bladder wall	0.0408 ± 0.0002	0.0582 ± 0.0002	0.0379 ± 0.0002	0.0554 ± 0.0002
Uterus	0.0000 ± 0.0000	0.0211 ± 0.0003	0.0000 ± 0.0000	0.0172 ± 0.0003
EDE[a]	0.0197 ± 0.0005	0.0252 ± 0.0005	0.0177 ± 0.0005	0.0225 ± 0.0005
ED[a]	0.0148 ± 0.0004	0.0193 ± 0.0005	0.0127 ± 0.0003	0.0164 ± 0.0005

[a] EDE and ED are given in units of mSv MBq^{-1}.

Table 4.19 continued: Summary of the average absorbed doses corresponding to the residence times stated in five different cases.

Organ	Absorbed dose (mGy MBq^{-1})	
	Case 5	
	Male	Female
Adrenals	0.0112 ± 0.0002	0.0137 ± 0.0002
Brain	0.0403 ± 0.0041	0.0529 ± 0.0046
Breasts	0.0074 ± 0.0001	0.0091 ± 0.0001
Gall bladder	0.0118 ± 0.0004	0.0138 ± 0.0003
Lower large intestine	0.0110 ± 0.0003	0.0136 ± 0.0003
Small intestine	0.0103 ± 0.0002	0.0117 ± 0.0002
Stomach	0.0098 ± 0.0001	0.0120 ± 0.0001
Upper large intestine	0.0101 ± 0.0002	0.0124 ± 0.0002
Heart wall	0.0438 ± 0.0062	0.0456 ± 0.0034
Kidneys	0.0275 ± 0.0001	0.0303 ± 0.0001
Liver	0.0204 ± 0.0030	0.0263 ± 0.0031
Lungs	0.0180 ± 0.0017	0.0233 ± 0.0038
Muscle	0.0086 ± 0.0001	0.0104 ± 0.0002
Ovaries	0.0000 ± 0.0000	0.0136 ± 0.0003
Pancreas	0.0263 ± 0.0002	0.0297 ± 0.0002
Red marrow	0.0095 ± 0.0001	0.0118 ± 0.0001
Bone surfaces	0.0098 ± 0.0001	0.0122 ± 0.0002
Skin	0.0066 ± 0.0001	0.0081 ± 0.0001
Spleen	0.0151 ± 0.0001	0.0183 ± 0.0001
Testes	0.0088 ± 0.0002	0.0000 ± 0.0000
Thymus	0.0098 ± 0.0002	0.0119 ± 0.0001
Thyroid	0.0087 ± 0.0002	0.0096 ± 0.0002
Urinary bladder wall	0.0328 ± 0.0002	0.0472 ± 0.0002
Uterus	0.0000 ± 0.0000	0.0163 ± 0.0003
EDE[a]	0.0174 ± 0.0005	0.0220 ± 0.0005
ED[a]	0.0125 ± 0.0003	0.0165 ± 0.0005

[a] EDE and ED are given in units of mSv MBq^{-1}.

The various residence times used to create five different scenarios for absorbed dose calculations produced a range of results (Table 4.20). The doses calculated from the residence times quantified in the adult populations studied here show little variance (brain, heart wall, liver, and lungs). For the kidneys, pancreas, and urinary bladder wall, the residence times were diverse between the uniform distribution values and previously published values; the maximum doses varied between 1.6 and 4.3 times the minimum doses. For the remaining organs, the maximum dose was no greater than a factor of 1.5 higher than the minimum dose. Hence, a few individual organ doses estimated for this fairly healthy population varied significantly, beyond the factor of two that is estimated for absorbed doses (Roedler et al. 1972; Kaul et al. 1980; Loevinger 1990; Howell et al. 1999).

Table 4.20: The range of absorbed doses determined in the five cases.

Organ	Absorbed dose (mGy MBq^{-1})					
	Males			Females		
	Minimum	Maximum	Ratio	Minimum	Maximum	Ratio
Adrenals	0.0110	0.0146	1.33	0.0135	0.0180	1.33
Brain	0.0403	0.0411	1.02	0.0529	0.0539	1.02
Breasts	0.0073	0.0102	1.40	0.0090	0.0127	1.41
Gall bladder	0.0117	0.0153	1.31	0.0136	0.0178	1.31
Lower large intestine	0.0110	0.0144	1.31	0.0136	0.0178	1.31
Small intestine	0.0102	0.0136	1.33	0.0117	0.0153	1.31
Stomach	0.0097	0.0134	1.38	0.0118	0.0165	1.40
Upper large intestine	0.0100	0.0134	1.34	0.0124	0.0166	1.34
Heart wall	0.0437	0.0452	1.03	0.0456	0.0475	1.04
Kidneys	0.0139	0.0291	2.09	0.0173	0.0323	1.87
Liver	0.0203	0.0216	1.06	0.0262	0.0279	1.06
Lungs	0.0179	0.0195	1.09	0.0232	0.0252	1.09
Muscle	0.0086	0.0114	1.33	0.0104	0.0140	1.35
Ovaries	0.0000	0.0000	-----	0.0136	0.0178	1.31
Pancreas	0.0149	0.0282	1.89	0.0194	0.0321	1.65
Red marrow	0.0094	0.0126	1.34	0.0117	0.0158	1.35
Bone surfaces	0.0097	0.0134	1.38	0.0121	0.0166	1.37
Skin	0.0065	0.0091	1.40	0.0080	0.0113	1.41
Spleen	0.0141	0.0168	1.19	0.0172	0.0204	1.19
Testes	0.0088	0.0115	1.31	0.0000	0.0000	-----
Thymus	0.0097	0.0132	1.36	0.0116	0.0162	1.40
Thyroid	0.0085	0.0123	1.45	0.0094	0.0138	1.47
Urinary bladder wall	0.0130	0.0408	3.14	0.0135	0.0582	4.31
Uterus	0.0000	0.0000	-----	0.0160	0.0211	1.32
EDE[a]	0.0172	0.0197	1.15	0.0218	0.0252	1.16
ED[a]	0.0125	0.0148	1.18	0.0164	0.0193	1.18

[a] EDE and ED are given in units of mSv MBq^{-1}.

4.5.3 Discussion

4.5.3.1 Gender differences

The dose estimates calculated from varying the residence times for the kidneys, pancreas, spleen, urinary bladder contents, and the total body show interesting results. For all organs other than these and other than the organs with measured residence times (i.e. – brain, heart wall, liver, and lungs), there is little variance between the sexes amongst the five different cases.

Within each case, there is no significant gender difference in the absorbed doses to the kidneys, pancreas, or spleen. However, there is a difference amongst the five different cases. The previously published residence times for the kidneys and pancreas used in case 2 are higher than the residence times calculated according to the uniform distribution values used in case 1. Similarly, the urinary bladder contents residence time used in case 3 is much higher than the uniform distribution value used in case 2. Interestingly, increases in the residence times from one case to another did not directly correspond to equivalent increases in doses, as seen in Table 4.21.

Table 4.21: Comparison between the factor increases in residence time and the corresponding factor increases in total organ dose.

Organ	Factors between residence times and doses in different cases			
	Males		Females	
	Residence time	Total dose	Residence time	Total dose
Kidneys	3.2	2.1	2.7	1.9
Pancreas	3.3	1.9	2.5	1.7
Urinary bladder wall	23.5	3.2	26.9	4.1

This indicates that surrounding organs (e.g. - liver for the kidneys and pancreas; intestines and uterus for the urinary bladder wall) contribute a significant portion of the total dose to those organs. In addition, the contributions from surrounding organs are different for women than for men due to organ size and relative position and distance within the body. Conversely, the urinary bladder contents irradiate several important neighboring organs, including the lower large intestines, ovaries, testes, and uterus.

As with the separate patient populations, the combined patient populations show a significant gender difference in the absorbed dose to the brain ($p < 0.01$), the liver ($p < 0.01$) and the lungs ($p < 0.01$), but no statistical gender difference in the absorbed dose to the heart wall. By means of S-values alone, there is a significant gender difference in the absorbed doses to the urinary bladder wall, as seen in Table 4.19, cases 3 to 5. In these cases, the absorbed dose to the urinary bladder wall is approximately 44% higher in females than in males.

4.5.3.2 Comparison to previously published results

4.5.3.2.1 Organ dose estimates

As stated previously, the brain and heart wall doses for the adult males determined here are similar to previously published values for the North American adult male, while the liver and lung doses are slightly higher. With the exception of the heart wall, the absorbed doses for these organs for the adult females are approximately twice

any previously published values. The heart wall dose lies in the opposite direction; it is less than half any previously published estimate.

The kidney doses estimated in the five cases ranged from 0.0139 to 0.0291 mGy MBq^{-1} and 0.0173 to 0.0323 mGy MBq^{-1} for the adult males and females, respectively. These values encompass the average dose estimates of 0.0214 and 0.0250 mGy MBq^{-1} previously published for North American adults, respectively. Similarly, the pancreas dose estimated in the five cases ranged from 0.0149 to 0.0282 mGy MBq^{-1} for the adult males; these values encompass the average dose estimate of 0.0176 mGy MBq^{-1} previously published. Previously published pancreas doses for the adult female (0.0160 mGy MBq^{-1}) are lower than the lowest value calculated in the five cases (range: 0.0194 to 0.0321 mGy MBq^{-1}).

Despite the obvious lack of biokinetic data for the spleen, there have been 10 enormously different doses estimated for the adult North American male, ranging from 0.0110 to 0.0500 mGy MBq^{-1} (Table 4.3). The average value of 0.0280 mGy MBq^{-1} is approximately twice as large as the range of values calculated here (0.0141 to 0.0172 mGy MBq^{-1}). The average dose previously published for adult males is also twice as large as the previously published dose for adult females (0.014 mGy MBq^{-1}), which is smaller than but closer to the range calculated here (0.0172 to 0.0204 mGy MBq^{-1}).

Just as there is a vast difference in dose estimates for an organ with little biokinetic data, there is also a tremendous range of doses for an organ investigated over two decades by different authors. The urinary bladder contents residence time has been measured in a total of 332 individuals in five studies of North American and Japanese populations. The values published from these studies vary by an order of magnitude, from 0.040 h to 0.198 h. A value of 0.317 h has been published by ICRP (1988; 1999), but this value was based on the data measured by Jones and others (1982), an average value of 0.198 h, without explanation as to the difference. Despite the large number of subjects studied, the absorbed doses published in the 10 estimates for the North American adult male vary over an order of magnitude, from 0.0389 to 0.3100 mGy MBq^{-1}, leading to an average value of 0.1342 mGy MBq^{-1}. The average value published for the adult female is 0.2100 mGy MBq^{-1}. These are significantly higher than the any of the dose estimates calculated for the 15 male and 13 female subjects investigated here, despite the wide range of urinary bladder contents residence times used. The primary reason for this difference is the inclusion of the surface dose to the mean dose in all previously published dose estimates. However, even if the surface doses are added to the mean doses, the summed doses are still well below the average published doses, as seen in Table 4.22.

Table 4.22: The total urinary bladder wall dose, including the surface dose from non-penetrating radiations emitted from the urinary bladder contents.

Case	Absorbed dose (mGy MBq^{-1})			
	Males		Females	
	Surface dose	Total dose	Surface dose	Total dose
1	0.0026	0.0156	0.0030	0.0170
2	0.0026	0.0156	0.0030	0.0170
3	0.0620	0.1030	0.0817	0.1397
4	0.0620	0.1000	0.0817	0.1367
5	0.0511	0.0841	0.0674	0.1144

Finally, previously published dose estimates for the testes and ovaries are comparable to the values calculated for the males and females in these patient populations, respectively. The range of doses for the uterus (0.0160 to 0.0211 mGy MBq^{-1}), however, is much lower than previously published values for women (0.0260 mGy MBq^{-1}).

4.5.3.2.2 Effective dose equivalent and effective dose estimates

Although the MIRD Committee has not accepted calculations of EDE and ED for individuals, the values have persisted in the literature and are generally used as an overall indicator of the risk for a procedure. As a comparison, then, to other nuclear medicine procedures, it appears that the EDE for FDG is comparable to several other common radiopharmaceuticals, as seen in Table 4.23.

Table 4.23: Comparison of EDE estimates for common nuclear medicine radiopharmaceuticals.

Radiopharmaceutical	Imaging modality	EDE (mSv MBq^{-1})[a]
^{11}C-carbon monoxide	PET	0.65×10^{-2}
^{13}N-ammonia	PET	0.22×10^{-2}
^{15}O-water	PET	0.11×10^{-2}
^{15}O-oxygen	PET	0.11×10^{-2}
^{18}F-fluorodeoxyglucose (males)[b]	PET	1.80×10^{-2}
^{18}F-fluorodeoxyglucose (females)[b]	PET	2.30×10^{-2}
^{18}F-sodium fluoride	PET	2.70×10^{-2}
^{82}Rb	PET	0.12×10^{-2}
^{99m}Tc (oral administrations)	SPECT	2.50×10^{-2}
^{99m}Tc-DTPA	SPECT	0.82×10^{-2}
^{99m}Tc-Pertechnetate	SPECT	1.10×10^{-2}
^{99m}Tc-Sestamibi	SPECT	1.50×10^{-2}
^{111}In-DTPA	SPECT	4.10×10^{-2}
^{131}I-sodium iodide	SPECT[c]	1.10×10^{1}
^{201}Tl-chloride	SPECT	1.60×10^{-1}

[a] All dose estimates are taken from CDE, Inc. Dosimetry Services (2003), with the exception of the dose estimates for ^{18}F-fluorodeoxyglucose.
[b] Averaged from cases 1-5.
[c] Rectilinear scanning is also used.

4.5.3.3 Comparison to the MIRD Dose Estimate Report

The MIRD Committee recently published a Dose Estimate Report (DER) on the dosimetry of FDG (Hays et al. 2002). Due to a lack of biological data and the ever-increasing introduction of new radiopharmaceuticals, the MIRD Committee has relied on specific Task Groups to develop these DERs. The Task Group that produced the FDG DER was comprised of several prominent internal dosimetrists. Surprisingly, this publication does not meet the objectives of the MIRD Committee as stated in its first

meeting. The purpose of the Committee is to provide the best possible dose estimates by collecting and evaluating metabolic data on the distribution of radiopharmaceuticals at organ and sub-organ levels, taking into account variables such as age, clinical state, anatomical, and physiological data (Smith 1968).

Several contradictions between the standards of the MIRD Committee as stated in 1968 and the procedure used in this DER exist. For example, the residence times used in this DER were garnered from only four different studies: Hays and Segall (1999), Mejia and others (1991), Jones and others (1982), and Niven and others (2001). There is no mention of the comprehensive study of the bladder by Dowd and others (1991) while the combined MRI/PET multi-organ, multi-slice study by Deloar and others (1998) is not included; both offer valuable information with regards to the distribution of FDG. In addition, the data used in the DER are open to discussion; the values published are inconsistent with either the methods stated in the publication or with previously published results.

The residence times quoted in the DER for the study by Hays and Segall are revised values from their previously published paper (Hays and Segall 1999). In the DER they included two subjects whose data were previously omitted for not meeting the paired criteria between the fasting and glucose-loaded states. However, the inclusion of these two subjects consistently lowered the residence times for the brain, liver, lungs, and urinary bladder contents (Table 4.24).

Table 4.24: Comparison of residence times published by the same authors at different times.

Organ	Residence time (h)	
	Hays and Segall (1999)	Hays et al. (2002)
	5 subjects	7 subjects
Brain	0.245 ± 0.090	0.22 ± 0.09
Heart	0.133 ± 0.065	0.13 ± 0.06
Liver	0.161 ± 0.057	0.15 ± 0.05
Lungs	0.084 ± 0.028	0.07 ± 0.03
Urinary bladder contents[a]	0.101 ± 0.041	0.09 ± 0.02

[a] Value is based on a two hour voiding schedule.

In order for the residence times to change in this fashion with the inclusion of only two subjects, the values for these two subjects must have been fairly low compared to the previous five subjects, and yet the standard deviations are the same or lower than previously published. In addition, a total body residence time of 2.38 h for this patient population is published in the DER; this value is not included in the previous publication and its origin is not explained.

The second set of data utilized in the DER is the residence times originally published for a Japanese population by Mejia and others (1991) but scaled for the North American adult. The values published in the DER do not appear to correspond to this modification based on a replication for the heart wall, lungs, and urinary bladder contents, as seen in Table 4.25.

Table 4.25: Comparison of measured vs. calculated residence times in Japanese and North American adult males.

Organ	Residence times based on a Japanese population (h)		
	Mejia et al. (1991) Japanese (measured)	Hays et al. (2002) North American (calculated)	Niven (2003) North American (calculated[a])
Brain	0.178	0.18	0.179
Heart wall	0.085	0.09	0.067
Kidneys	0.034	0.03	0.032
Liver	0.112	0.11	0.133
Lungs	0.023	0.02	0.021
Pancreas	0.008	0.006	0.006
Spleen	0.010	0.01	0.013
Urinary bladder contents[b]	0.162	0.12	0.342[d]
Urinary bladder contents[c]	0.123		0.162[d]

[a] The North American mathematical model organ masses were obtained from Stabin (1996) and the Japanese mathematical model organ masses were obtained from Deloar and others (1998), with the exception of the urinary bladder contents.
[b] Value is based on a two hour voiding schedule.
[c] Value is the average of four subject on a one hour voiding schedule and four subjects on a two hour voiding schedule.
[d] A urinary bladder contents mass of 100 g for the Japanese adult male was obtained from Tanaka and Kawamura (2003).

Although Hays and others (2002) performed a calculation scaling the residence times, with the exception of the pancreas, it appears that the original data were used instead. The fact that the DER referenced a residence time for a two hour urinary void interval for the eight subjects reported in the study by Mejia and others (1991) when only four of those subjects had a two hour void interval supports this suggestion; the average urinary bladder contents residence time for the two hour voiding schedule was 0.162 h while the average for all subjects was 0.123 h. In either case, a scaled urinary bladder contents residence time for the North American adult would have to be higher than 0.12 h since

the urinary bladder contents mass for the Japanese adult is smaller than the North American adult.

Finally, the DER combined biological data obtained in adult females with data obtained in adult males in both the values measured by Hays and Segall (1999) and by Niven and others (2001). The data obtained by Niven and others in studies of adult males (8 subjects, 14 measurements) and adult females (6 subjects, 12 measurements) were averaged without regard to the fact that duplicate studies were performed on some of the subjects (data presented earlier) and that a biological difference had been proven. No weighting factors were applied or patient averages calculated to account for duplicate vs. single measurements. The duplicate studies in fact revealed that a single dose estimate could be expected to be a true dose estimate for that particular patient (Niven et al. 2001). Based on that knowledge, the Task Group could have utilized only the first measurement for a patient in which duplicate studies were performed. Analyzing the residence times for the adult male and female brains in this manner yields averages of 0.217 ± 0.037 h and 0.278 ± 0.038 h, respectively. Even if all the residence times for the males and the females were averaged, disregarding the duplicate studies, the average values would be 0.216 ± 0.039 h and 0.270 ± 0.035 h for the adult males and females, respectively. In either case, there is a significant difference between the genders; the residence times for women are at least 22% higher than those for men, although Hays and others claim only a 5% difference. It is therefore unclear as to how they have arrived at their conclusion that the difference between the male and female data could be ignored.

Finally, it is disappointing that the Task Group used the S-values from MIRD Pamphlet No. 11 (Snyder et al. 1975), which is based on an old phantom. Rather, they should have used the newer mathematical model (Cristy and Eckerman 1987), and in fact did use the organ masses from this model. It is also disappointing that the Task Group did not investigate the use of the adult female mathematical model (Stabin 1995) or the use of any child phantoms, despite some publications on the biokinetic distribution of FDG in infants (Ruotsalainen et al. 1992; Ruotsalainen et al. 1996).

4.6 Conclusion

There is a significant difference in the residence times of FDG in the brains and hearts of adult males as compared to females; the residence times in females are larger in the brain but smaller in the heart wall. There does not appear to be a difference in the residence times of the liver and lungs. With the limited biological distribution data obtained here, it appears in several cases that the organ dose estimates for females are similar, although generally higher, as compared to their male counterparts. However, in the primary organs of interest for FDG distribution, there are definite differences. The brain, liver, and lung doses are in all cases higher in women than in men. Similarly, the doses to the ovaries are higher than the doses to the testes. When the urinary bladder contents residence times are significantly higher than the uniform distribution concentrations, there is a large difference in the urinary bladder wall dose, with the dose to the females being approximately 44% higher than the males.

Previously published dose estimates for the males are, in most cases, either similar or are contained within the current dose estimate range. Previously published doses for females, however, are extremely different from the current dose estimates; in most cases they are lower than the current dose estimates, in some cases by a factor of two. In contrast, the previously published values for the dose to the heart wall are higher by a factor of two. It is apparent that the calculation of dose estimates for female subjects were previously not given much consideration, either in data collection or in the necessity of the calculation. The only two previously published dose estimates used the 15 year-old child/adult female hermaphrodite mathematical model (ICRP 1988; ICRP 1999). This is especially poignant as the MIRD DER published in 2002 masks previously published gender differences, does not attempt to suggest possible variations in FDG biokinetics, and lacks any mention of the distribution or dose of FDG in children and infants. Therefore, the residence times and dose estimates for FDG calculated here are currently the most comprehensive for female subjects.

Footnotes

† Personal communication, Michael Stabin 6 March 2001.

Chapter 5: Neonate Dosimetry of FDG

5.1 Introduction

Interest in pediatric dosimetry is twofold; first, the radiation absorbed dose to a child will be higher than that to an adult per unit administered activity, and second, the risk to a child will likely be higher than that to an adult for the same absorbed dose (ICRP 1993). Unfortunately, the lack of relevant biokinetic data in children and infants has permitted the process of applying data obtained from animals or adults to continue. The purpose of this study was to collect biodistribution data in very low birth weight infants in order to provide a more accurate dose estimate of FDG to newborns.

5.2 Literature review

As stated previously, several absorbed dose estimates to humans from FDG have been reported, though most of these have been for adults. The majority of the dose estimates reported are based on data obtained from animal biodistribution studies or on a combination of animal biodistribution studies and human biodistribution studies. These same biodistribution studies of FDG from female mongrel dogs (Gallagher et al. 1977) and adult humans (Jones et al. 1982) have been used in the determinations of the absorbed doses to newborns and to children, assuming that the distribution is the same (ICRP 1988; Stabin and Gelfand 1998; ICRP 1999). Fortunately, there are published

estimates of the absorbed doses to children from FDG where children were actually studied. Ruotsalainen and others (1992; 1996) acquired biodistribution data on the brain and bladder from newborn infants during their neurological studies.

Table 5.1 summarizes those studies that reported absorbed doses to children from FDG, Table 5.2 summarizes the significant biological data reported in those studies, and Table 5.3 displays the absorbed doses reported in those studies. Although biological data were measured and dose estimates were calculated by Niven and Nahmias (2003), the data are not included in Tables 5.2 and 5.3 because the data are included later in the text.

Table 5.1: Summary of studies reporting absorbed doses to children from FDG.

Authors	Subjects	Number	Age of humans	Sex of humans	Age for whom dose is reported
ICRP 1988	dogs	2			1, 5, 10, and 15 years
	humans	11	20-86 years	not reported	
Ruotsalainen et al. 1992	humans	20	infants	not reported	newborn
Ruotsalainen et al. 1996	humans	21	infants	not reported	newborn
Stabin and Gelfand 1998	dogs	2			newborn
	humans	11	20-86 years	not reported	
ICRP 1999	dogs	2			1, 5, 10, and 15 years
	humans	11	20-86 years	not reported	
Niven and Nahmias 2003	humans	10	newborns	4 male, 6 female	newborn

Table 5.2: Summary of studies reporting residence times for FDG.

Author	Residence times (h)				
	Brain	Heart wall	Kidneys	Bladder contents	Total body
ICRP 1988	0.148[a]	0.098[a]	0.024[a]	0.317[a]	2.134[a]
Ruotsalainen et al. 1992	0.730			not reported[b]	
Ruotsalainen et al. 1996	0.215[c]			0.038	2.134[a]
Stabin and Gelfand 1998	0.148[a]	0.098[a]	0.024[a]	0.317[a]	2.134[a]
ICRP 1999	0.148[a]	0.098[a]	0.024[a]	0.317[a]	2.134[a]

[a] Value was not measured by the authors.

[b] Biodistribution was measured but a value was not reported.

[c] Value published by the authors; a value of 0.230 h was calculated from the authors' published data.

Table 5.3: Summary of studies reporting absorbed doses for FDG (newborn unless otherwise noted).

Author	Absorbed doses (mGy MBq^{-1})									
	Adrenals	**Brain**	**Breasts**	**Gall-bladder**	**LLI wall**	**Small intestine**	**Stomach**	**ULI wall**	**Heart wall**	**Kidneys**
ICRP 1988 (1 year-old)	0.065	0.046	0.052		0.076	0.074	0.062	0.069	0.350	0.094
Ruotsalainen et al. 1992		0.501								
Ruotsalainen et al. 1996	0.210	0.240			0.200	0.210	0.210	0.210	0.890	0.510
Stabin and Gelfand 1998		0.078							0.651	0.217
ICRP 1999 (1 year-old)	0.072	0.048	0.056	0.066	0.076	0.077	0.068	0.072	0.350	0.096

Table 5.3 continued: Summary of studies reporting absorbed doses for FDG (newborn unless otherwise noted).

Author	Absorbed doses (mGy MBq^{-1})									
	Liver	Lungs	Muscle	Ovaries	Pancreas	Red marrow	Bone surfaces	Skin	Spleen	Testes
ICRP 1988 (1 year-old)	0.064	0.060		0.082	0.070	0.056	0.056		0.063	0.076
Ruotsalainen et al. 1992										
Ruotsalainen et al. 1996	0.410	0.200			0.780	0.290			0.220	0.290
Stabin and Gelfand 1998	0.193	0.265	0.157	0.205	0.590	0.145	0.157		0.590	0.004
ICRP 1999 (1 year-old)	0.070	0.065	0.065	0.082	0.076	0.061	0.066	0.052	0.069	0.073

Table 5.3 continued: Summary of studies reporting absorbed doses for FDG (newborn unless otherwise noted).

Author	Absorbed doses (mGy MBq^{-1})					
	Thymus	Thyroid	Bladder wall	Uterus	EDE	ED
ICRP 1988 (1 year-old)		0.062	0.890	0.110	0.130	
Ruotsalainen et al. 1992			1.406			
Ruotsalainen et al. 1996		0.200	1.030			
Stabin and Gelfand 1998		0.169	0.807		0.301	0.229
ICRP 1999 (1 year-old)	0.068	0.068	0.590	0.100		0.095

5.3 Brain, Heart, Lung, and Kidney Data

5.3.1 Materials and methods

5.3.1.1 Subjects

Ten very low birth weight (VLBW) infants born prematurely and undergoing clinical PET scans for suspected lung inflammation were included in this study. The lung inflammation study was approved by the ethics board of McMaster University Medical Centre, and informed consent from the parents was obtained before each infant was transported to the nuclear medicine department. Four male and six female newborns were studied in a sleeping state within three days of birth. No sedation was used. The infants were 28 wks (range: 26-30 wks) gestational age and weighed on average 1.07 kg (range: 0.61-1.50 kg). These infants were approximately one-third the weight of a full term newborn infant (Cristy and Eckerman 1987).

5.3.1.2 PET scanning protocol

All studies were performed on the ECAT 953/31 PET scanner (Siemens Medical Systems, Inc., Nuclear Medicine Group, 810 Innovation Drive, Knoxville Tennessee, USA 37932) in the Department of Nuclear Medicine at McMaster University Medical Centre. The description of this scanner may be found in Chapter 4, section 4.3.1.2.

A dynamic PET study for each infant was performed for approximately 90 min at five min per frame following intravenous injection of on average 3.5 MBq kg^{-1}

(95 μCi kg^{-1}) of FDG. The first 45 min scan was over the head, while the second 45 min scan was over the chest, allowing for ROIs to be drawn over the brain, heart wall, lungs, and in five infants, the kidneys. Images were reconstructed using a filtered backprojection algorithm and a Hann filter with a cutoff of 12 mm. Attenuation correction was calculated from a manually positioned ellipse in each of the axial planes for the brain (Huang et al. 1981). Measured attenuation correction was not performed for the organs in the chest because this would have required additional time and exposure of the infants from the transmission source. The data were not decay corrected.

5.3.1.3 Description of measurements

Regions of interest were drawn on all planes that included the organs. The activities and volumes determined from the ROIs were summed so that a time-activity curve was produced for each organ. In the case of the heart, ROIs were drawn over the whole heart, as heart wall was difficult to distinguish in such small infants. The radioactivity measured was then apportioned entirely to the heart wall; there would be little activity left in the blood during the second scan. The heart wall volume was calculated knowing the percent volume it occupies within the whole heart (Cristy and Eckerman 1987). The time-activity curve was integrated by numerical integration using the trapezoidal rule (Siegel et al. 1999). Because no data were obtained over the chest for the first 45 min, instantaneous uptake with no washout was assumed, so that the activity measured at the first time point was extrapolated back to the start of the scan. As well, it was assumed that the drug was fixed in the patient at completion of the scan and that it

decayed only by its physical half-life thereafter, according to the method given by Smith (1966). The exponential portion of this time activity curve was integrated analytically and summed with the numerical integration to yield the cumulated activity.

5.3.2 Results

5.3.2.1 Residence times

The organ volumes determined from the planar images were converted to masses using brain, heart muscle, and kidney densities from ICRP 23 (1975) and lung density from Cristy and Eckerman (1987). These densities are 1.030 g cm^{-3}, 1.0298 g cm^{-3}, 1.035 g cm^{-3}, and 0.296 g cm^{-3}, respectively. The average organ masses for the VLBW infants are compared to the newborn mathematical model in Table 5.4.

Table 5.4: Organ masses determined in very low birth weight infants.

Subject	Organ masses (g)				
	Brain	**Heart wall**	**Kidney[a]**	**Lungs**	**Total body**
1	260.4	2.5	10.8	50.1	1395
2	212.2	4.8	0.0	12.7	1142
3	197.8	2.1	0.0	5.1	608
4	341.9	7.0	16.7	27.2	1260
5	264.6	2.3	13.3	10.4	1060
6	266.5	3.6	9.3	11.3	960
7	239.8	5.2	0.0	19.5	1501
8	256.1	6.0	0.0	38.2	900
9	219.6	4.3	0.0	10.3	850
10	226.3	6.3	4.7	22.5	1000
Mean	248.5	4.4	10.9	20.7	1070
SD	40.5	1.8	4.5	14.3	27.0
Newborn model[b]	352.0	25.4	22.9	50.6	3600.0

[a] The mean and standard deviations correspond only to those values that were measured in the five infants.
[b] All organ masses were taken from Stabin (1996).

The average residence times calculated for these infants were 0.282 ± 0.067 h, 0.018 ± 0.010 h, 0.012 ± 0.005 h, and 0.048 ± 0.032 h for the brain, heart wall, kidneys, and lungs, respectively; the data acquired are displayed in Table 5.5. It should be noted that the average residence time for the kidneys is that determined in those VLBW infants in whom the kidneys were visible. The residence times for the lungs range from 0.009-0.122 h; the largest residence time was determined to be an outlier (Milton and Arnold 1995). If this outlier is removed, the average residence time becomes 0.040 ± 0.018 h.

Table 5.5: Biological and biokinetic data obtained in VLBW infants.

Subject (#)	Sex	Weight (kg)	Age (weeks)[a]	Injected activity (MBq)	Residence time (h)			
					Brain	Heart wall	Kidneys[b]	Lungs
1	female	1.40	30	3.6	0.277	0.007	0.009	0.122
2	male	1.14	28	3.3	0.257	0.018	0.000	0.024
3	female	0.61	26	2.7	0.199	0.005	0.000	0.009
4	female	1.26	29	4.7	0.364	0.030	0.018	0.062
5	male	1.06	28	3.1	0.359	0.008	0.013	0.028
6	male	0.96	26	3.6	0.287	0.022	0.015	0.038
7	female	1.50	30	4.7	0.306	0.022	0.000	0.040
8	male	0.90	28	3.2	0.156	0.010	0.000	0.053
9	female	0.85	26	3.7	0.269	0.024	0.000	0.037
10	female	1.00	28	2.7	0.341	0.036	0.005	0.071
Mean		1.07	28	3.5	0.282	0.018	0.012	0.048
SD		0.27	2	0.7	0.067	0.010	0.005	0.031

[a] This is the gestational age; all subject were studied within three days of birth.

[b] The mean and standard deviation correspond only to those values, which were measured in the five infants.

Assuming no elimination of FDG from the body, the average residence time for the remainder of the body is 2.284 ± 0.090 h.

The typical rapid incorporation of FDG in the brain was seen in these infants (Figure 5.1), where the dashed portions of the curves represent exponential extrapolation. The uptake in the heart wall, kidneys, and lungs is much lower, and appears to be relatively constant at later time points. The activities measured in these organs, normalized to the administered activity, represent not a single slice but the entire volume as summed from all the PET images for the study.

Figure 5.1: Time-activity curves normalized to the administered activity for one of the VLBW infants.

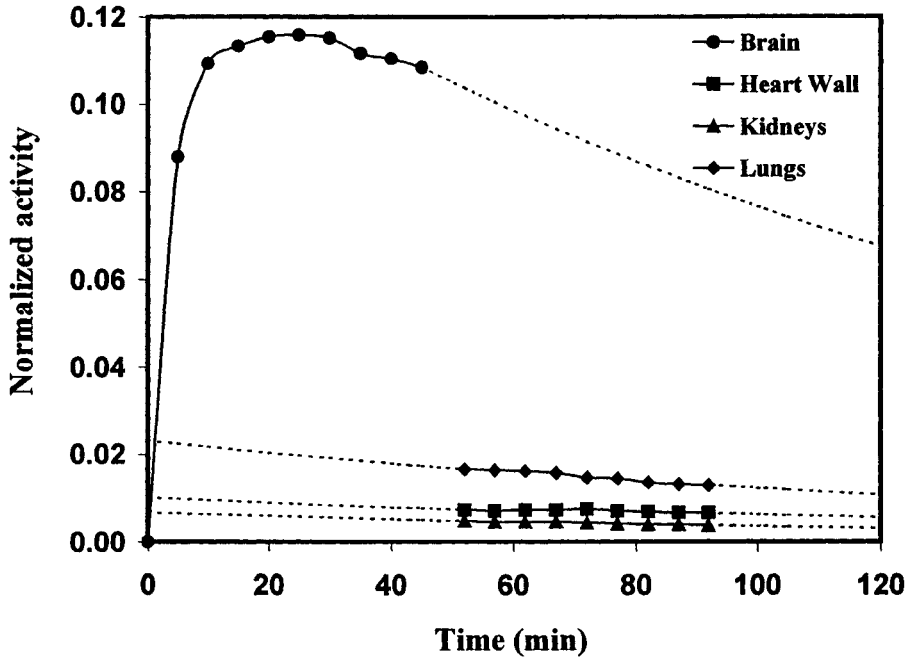

5.3.2.2 Dose estimates

The dose estimates were calculated according to Equations (3.21) and (3.23). The differences in organ masses between this patient population and the MIRDOSE phantoms were corrected for by adjusting the S-values as given in Equation (3.22). The self-doses and the total absorbed doses of the newborn mathematical model are compared to the patient-specific doses of the VLBW infants in Tables 5.6 to 5.9.

Table 5.6: Comparison of mathematical model and patient-specific doses calculated for the brain of the VLBW infants.

Subject (#)	Brain (mGy MBq^{-1})			
	Mathematical model		Patient-specific VLBW	
	Self-dose	Total dose	Self-dose	Total dose
1	0.163	0.186	0.213	0.236
2	0.150	0.174	0.237	0.260
3	0.117	0.141	0.196	0.220
4	0.213	0.235	0.219	0.241
5	0.211	0.233	0.272	0.294
6	0.168	0.192	0.216	0.239
7	0.180	0.203	0.254	0.277
8	0.092	0.116	0.122	0.146
9	0.158	0.181	0.241	0.264
10	0.200	0.222	0.298	0.320
Mean	0.165	0.188	0.227	0.250
SD	0.039	0.038	0.048	0.047

Table 5.7: Comparison of mathematical model and patient-specific doses calculated for the heart wall of the VLBW infants.

Subject (#)	Heart wall (mGy MBq^{-1})			
	Mathematical model		Patient-specific VLBW	
	Self-dose	Total dose	Self-dose	Total dose
1	0.046	0.125	0.437	0.516
2	0.111	0.185	0.561	0.635
3	0.032	0.108	0.363	0.438
4	0.191	0.264	0.663	0.736
5	0.047	0.119	0.482	0.554
6	0.140	0.214	0.928	1.002
7	0.137	0.210	0.634	0.707
8	0.065	0.143	0.260	0.338
9	0.153	0.228	0.852	0.926
10	0.224	0.298	0.855	0.929
Mean	0.115	0.189	0.603	0.678
SD	0.066	0.065	0.225	0.224

Table 5.8: Comparison of mathematical model and patient-specific doses calculated for the kidneys of the VLBW infants.

Subject (#)	Kidneys (mGy MBq^{-1})			
	Mathematical model		Patient-specific VLBW	
	Self-dose	Total dose	Self-dose[a]	Total dose[a]
1	0.064	0.134	0.132	0.201
2	0.000	0.192	0.000	0.192
3	0.000	0.198	0.000	0.198
4	0.129	0.195	0.174	0.240
5	0.097	0.164	0.163	0.230
6	0.107	0.176	0.253	0.322
7	0.000	0.187	0.000	0.187
8	0.000	0.199	0.000	0.199
9	0.000	0.190	0.000	0.190
10	0.035	0.103	0.162	0.229
Mean	0.087	0.154	0.177	0.244
SD	0.037	0.036	0.046	0.046

[a] The mean and standard deviations correspond only to those values that were measured in the five infants. The total doses for all 10 subjects are 0.174 ± 0.032 mGy MBq^{-1} and 0.219 ± 0.041 mGy MBq^{-1} for the mathematical model and the patient-specific dose estimates, respectively.

Table 5.9: Comparison of mathematical model and patient-specific doses calculated for the lungs of the VLBW infants.

Subject (#)	Lungs (mGy MBq^{-1})			
	Mathematical model		Patient-specific VLBW	
	Self-dose	Total dose	Self-dose	Total dose
1	0.374	0.437	0.378	0.440
2	0.074	0.140	0.284	0.350
3	0.029	0.096	0.274	0.341
4	0.190	0.253	0.346	0.409
5	0.087	0.150	0.402	0.465
6	0.117	0.182	0.500	0.565
7	0.122	0.186	0.306	0.371
8	0.163	0.230	0.214	0.281
9	0.115	0.181	0.541	0.606
10	0.217	0.281	0.478	0.541
Mean	0.149	0.214	0.372	0.437
SD	0.097	0.096	0.108	0.107

5.3.3 Discussion

It is difficult to compare the residence times measured in this patient population with previously published results. The residence time determined in the VLBW infants for the brain is higher than the most recently published value by Ruotsalainen and others (1996). When comparing the residence times for the brain, there is a statistical difference ($p < 0.02$) between the data obtained in this study, 0.282 ± 0.067 h and the value published by Ruotsalainen and others (1996), 0.215 ± 0.068 h. However, when comparing the actual value calculated from the data published by Ruotsalainen and others (1996), 0.230 ± 0.083 h, there is no statistical difference. The inconsistency in reported and calculated values by these authors may be explained if the largest residence time had

been removed when calculating the mean and standard deviation. The residence times reported by Ruotsalainen and others (1996) for the brain ranged from 0.061-0.476 h; the largest residence time was determined to be an outlier (Milton and Arnold 1995). If this outlier is removed, the average residence time becomes 0.218 ± 0.063 h, yielding again a statistical difference between these data and the VLBW infant data ($p < 0.02$).

The difference in masses between the patient population examined in this study and the newborn mathematical model employed in MIRDOSE 3.1 is reflected in the dose estimates shown in Tables 5.6 to 5.9. The non-patient-specific (i.e., newborn mathematical model) total doses are lower, although the brain doses are within the uncertainty of the data. For all organs, however, there is a significant difference between the mathematical model and patient-specific dose estimates ($p < 0.01$).

The largest difference between newborn mathematical model and patient-specific self-dose is to the heart wall. The difference between the model and patient-specific dose to the heart wall can be explained by the difference in target organ masses. The patient-specific S-value in the dose equation is a mass-adjusted model S-value; a smaller patient target organ mass yields a larger patient-specific S-value, producing a larger dose. The organ masses of the infants measured from PET scan data are considerably smaller than those of the newborn mathematical model, as seen in Table 5.4. It is apparent that the VLBW infants examined in this study are approximately one-third the size of the newborn model. To ascertain that these organ masses are appropriate for infants of this

age, the organ masses of an average 28 wk old fetus are compared to the masses obtained for these VLBW infants.

Table 5.10: Comparison of 28 week-old fetus to VLBW infant organ masses

Subject	Organ masses (g)				
	Brain	**Heart wall**	**Kidney**	**Lungs**	**Total body**
VLBW infants	248.5 ± 40.5	4.4 ± 1.8	10.9 ± 4.5	20.7 ± 14.3	1070.0 ± 27.0
28 week old fetus[a,b]	164.5 ± 69.7	7.5 ± 1.4[c]	13.0 ± 6.4	27.0 ± 14.1[c]	1000.0 ± 200.0

[a] All organ masses were taken from ICRP (1975).
[b] Values for males and females are averaged together.
[c] Values estimated from graphs.

The organ masses are similar, despite the fact that these infants were imaged when ill and that the majority of data compared with ICRP 23 (1975) are based on a selective group in which conditions possibly leading to significant changes in body or organ masses were eliminated (Schulz et al. 1962).

The average doses to the VLBW infant brain and lungs obtained in this study are comparable to recently published data by Ruotsalainen and others (1996); the average doses to the heart wall and kidneys are comparable to results published by Stabin and Gelfand (1998), as seen in Table 5.3.

5.4 Comprehensive dosimetry calculations

5.4.1 Additional residence times

As with the dose calculations for the adults, several approaches have been taken for calculating a range of dose estimates for these VLBW infants. The residence times measured in this study have been combined with previously published residence times that were either measured or calculated.

5.4.1.1 Organs

Again, the key organs identified with the uptake of FDG in adults are the brain, heart wall, kidneys, liver, lungs, pancreas, spleen, and urinary bladder contents. With the lack of biokinetic data of FDG in infants and children, only brain and urinary bladder contents residence times have been published in previous studies. Therefore, some trends observed in the adult populations have been applied to this patient population. This procedure is not meant to indicate that the actual biodistribution in infants is similar, only to provide a general sense of the possible magnitude of variation in infants.

The brain, heart wall, kidney, and liver data collected in the VLBW infants were applied in these dose calculations. The average residence time for the kidneys determined in the five infants was applied to the remaining five infants in whom the kidneys were not visible.

Additional residence times used in calculating the range of doses are culled from previously published results. The only data used in these calculations that were measured in infants are the urinary bladder contents residence times provided by Ruotsalainen and others (1996). However, their values were measured in 21 newborns and ranged from 0.001-0.569 h (0.038 ± 0.120 h). The two highest data points were determined to be outliers (Milton and Arnold 1995); once removed, the average residence time drops by more than a factor of three to 0.008 ± 0.006 h. Considering that the range of urinary bladder contents residence times reported for adults is much higher, a value of 0.101 h (Hays and Segall 1999) was also used. This value was obtained assuming a bladder voiding interval of 120 min, which is the voiding interval given for newborns in ICRP 80 (1999).

The average residence times for the heart contents and liver measured by Niven and others in adult populations are on average 1.9 times higher than their expected uniform distribution residence times. Therefore, residence times of 0.050 h and 0.169 h were used for the heart contents and liver, respectively. Similarly, the average residence times for the pancreas and the spleen measured by Mejia and others (1991) and Deloar and others (1998) are on average 2.8 and 1.4 times higher than their expected uniform distribution residence times, respectively. Therefore, a value of 0.006 h was used for the pancreas and a value of 0.009 h was used for the spleen. Five scenarios were developed:

case1: calculated assuming uniform distribution but using brain, heart wall, kidney, and lung data measured by Niven and others.

case 2: same as case 1, but using the heart contents, liver, pancreas, and spleen residence times scaled from previously published results as discussed.

cases 3 and 4: same as case 2, but using the urinary bladder contents residence time of 0.038 h previously measured in infants (Ruotsalainen et al. 1996). This value is used for comparison rather than the calculated value of 0.008 h as it is too similar to the uniform distribution value of 0.009 h.

case 5: same as case 2, but using the urinary bladder contents residence time of 0.101 as calculated for the voiding period of 120 min (Hays and Segall 1999).

5.4.1.2 Total body and remainder of the body

As with adults, assuming instantaneous and complete uptake without loss is most likely an overestimate. Although FDG urinary concentration has been reported to be lower in infants than in adults (Ruotsalainen et al. 1992; Ruotsalainen et al. 1996), FDG excretion would reduce the activity in the total body. Therefore, the residence time of 2.639 h was used in cases 1 to 3, while the previously reported value of 2.134 h was used for the total body residence time in cases 4 and 5. Summaries of these residence times are presented in Tables 5.11 to 5.15.

Table 5.11: Summary of residence times for case 1.

Subject (#)	Sex	Residence times (h)									
		Brain	Heart wall	Heart contents	Kidneys	Liver	Lungs	Pancreas	Spleen	Bladder contents	Total body
1	male	0.277	0.007	0.027	0.009	0.089	0.122	0.002	0.007	0.009	2.639
2	male	0.257	0.018	0.027	0.012	0.089	0.024	0.002	0.007	0.009	2.639
3	male	0.199	0.005	0.027	0.012	0.089	0.009	0.002	0.007	0.009	2.639
4	male	0.364	0.030	0.027	0.018	0.089	0.062	0.002	0.007	0.009	2.639
5	male	0.359	0.008	0.027	0.013	0.089	0.028	0.002	0.007	0.009	2.639
6	male	0.287	0.022	0.027	0.015	0.089	0.038	0.002	0.007	0.009	2.639
7	male	0.306	0.022	0.027	0.012	0.089	0.040	0.002	0.007	0.009	2.639
8	male	0.156	0.010	0.027	0.012	0.089	0.053	0.002	0.007	0.009	2.639
9	female	0.269	0.024	0.027	0.012	0.089	0.037	0.002	0.007	0.009	2.639
10	female	0.341	0.036	0.027	0.005	0.089	0.071	0.002	0.007	0.009	2.639

Table 5.12: Summary of residence times for case 2.

Subject (#)	Sex	Residence times (h)									
		Brain	Heart wall	Heart contents	Kidneys	Liver	Lungs	Pancreas	Spleen	Bladder contents	Total body
1	male	0.277	0.007	0.050	0.009	0.169	0.122	0.006	0.009	0.009	2.639
2	male	0.257	0.018	0.050	0.012	0.169	0.024	0.006	0.009	0.009	2.639
3	male	0.199	0.005	0.050	0.012	0.169	0.009	0.006	0.009	0.009	2.639
4	male	0.364	0.030	0.050	0.018	0.169	0.062	0.006	0.009	0.009	2.639
5	male	0.359	0.008	0.050	0.013	0.169	0.028	0.006	0.009	0.009	2.639
6	male	0.287	0.022	0.050	0.015	0.169	0.038	0.006	0.009	0.009	2.639
7	male	0.306	0.022	0.050	0.012	0.169	0.040	0.006	0.009	0.009	2.639
8	male	0.156	0.010	0.050	0.012	0.169	0.053	0.006	0.009	0.009	2.639
9	female	0.269	0.024	0.050	0.012	0.169	0.037	0.006	0.009	0.009	2.639
10	female	0.341	0.036	0.050	0.005	0.169	0.071	0.006	0.009	0.009	2.639

Table 5.13: Summary of residence times for case 3.

Subject (#)	Sex	Residence times (h)									
		Brain	Heart wall	Heart contents	Kidneys	Liver	Lungs	Pancreas	Spleen	Bladder contents	Total body
1	male	0.277	0.007	0.050	0.009	0.169	0.122	0.006	0.009	0.038	2.639
2	male	0.257	0.018	0.050	0.012	0.169	0.024	0.006	0.009	0.038	2.639
3	male	0.199	0.005	0.050	0.012	0.169	0.009	0.006	0.009	0.038	2.639
4	male	0.364	0.030	0.050	0.018	0.169	0.062	0.006	0.009	0.038	2.639
5	male	0.359	0.008	0.050	0.013	0.169	0.028	0.006	0.009	0.038	2.639
6	male	0.287	0.022	0.050	0.015	0.169	0.038	0.006	0.009	0.038	2.639
7	male	0.306	0.022	0.050	0.012	0.169	0.040	0.006	0.009	0.038	2.639
8	male	0.156	0.010	0.050	0.012	0.169	0.053	0.006	0.009	0.038	2.639
9	female	0.269	0.024	0.050	0.012	0.169	0.037	0.006	0.009	0.038	2.639
10	female	0.341	0.036	0.050	0.005	0.169	0.071	0.006	0.009	0.038	2.639

Table 5.14: Summary of residence times for case 4.

Subject (#)	Sex	Residence times (h)									
		Brain	Heart wall	Heart contents	Kidneys	Liver	Lungs	Pancreas	Spleen	Bladder contents	Total body
1	male	0.277	0.007	0.050	0.009	0.169	0.122	0.006	0.009	0.038	2.134
2	male	0.257	0.018	0.050	0.012	0.169	0.024	0.006	0.009	0.038	2.134
3	male	0.199	0.005	0.050	0.012	0.169	0.009	0.006	0.009	0.038	2.134
4	male	0.364	0.030	0.050	0.018	0.169	0.062	0.006	0.009	0.038	2.134
5	male	0.359	0.008	0.050	0.013	0.169	0.028	0.006	0.009	0.038	2.134
6	male	0.287	0.022	0.050	0.015	0.169	0.038	0.006	0.009	0.038	2.134
7	male	0.306	0.022	0.050	0.012	0.169	0.040	0.006	0.009	0.038	2.134
8	male	0.156	0.010	0.050	0.012	0.169	0.053	0.006	0.009	0.038	2.134
9	female	0.269	0.024	0.050	0.012	0.169	0.037	0.006	0.009	0.038	2.134
10	female	0.341	0.036	0.050	0.005	0.169	0.071	0.006	0.009	0.038	2.134

Table 5.15: Summary of residence times for case 5.

Subject (#)	Sex	Residence times (h)									
		Brain	Heart wall	Heart contents	Kidneys	Liver	Lungs	Pancreas	Spleen	Bladder contents	Total body
1	male	0.277	0.007	0.050	0.009	0.169	0.122	0.006	0.009	0.101	2.134
2	male	0.257	0.018	0.050	0.012	0.169	0.024	0.006	0.009	0.101	2.134
3	male	0.199	0.005	0.050	0.012	0.169	0.009	0.006	0.009	0.101	2.134
4	male	0.364	0.030	0.050	0.018	0.169	0.062	0.006	0.009	0.101	2.134
5	male	0.359	0.008	0.050	0.013	0.169	0.028	0.006	0.009	0.101	2.134
6	male	0.287	0.022	0.050	0.015	0.169	0.038	0.006	0.009	0.101	2.134
7	male	0.306	0.022	0.050	0.012	0.169	0.040	0.006	0.009	0.101	2.134
8	male	0.156	0.010	0.050	0.012	0.169	0.053	0.006	0.009	0.101	2.134
9	female	0.269	0.024	0.050	0.012	0.169	0.037	0.006	0.009	0.101	2.134
10	female	0.341	0.036	0.050	0.005	0.169	0.071	0.006	0.009	0.101	2.134

5.4.2 Dose estimates

Again, Equations (3.21) to (3.23) were used in calculating the absorbed dose estimates. For these subjects, patient-specific dose calculations were performed for the brain, heart wall, kidneys, and liver. Otherwise, the doses calculated are related to the reference newborn mathematical model. The weighting factors for the EDE and the ED were obtained from ICRP 26 (1977) and ICRP 67 (1994), respectively. The doses calculated for the organs of these patient populations are given in Table 5.16.

Table 5.16: Summary of the average absorbed doses corresponding to the residence times stated in five different cases.

Organ	Absorbed dose (mGy MBq^{-1})		
	Case 1	Case 2	Case 3
Adrenals	0.190 ± 0.006	0.189 ± 0.006	0.187 ± 0.006
Brain	0.250 ± 0.047	0.249 ± 0.047	0.249 ± 0.047
Breasts	0.157 ± 0.004	0.154 ± 0.004	0.152 ± 0.004
Gall bladder	0.201 ± 0.006	0.209 ± 0.006	0.207 ± 0.006
Lower large intestine	0.194 ± 0.007	0.186 ± 0.007	0.187 ± 0.007
Small intestine	0.198 ± 0.007	0.193 ± 0.007	0.192 ± 0.007
Stomach	0.191 ± 0.006	0.189 ± 0.006	0.187 ± 0.006
Upper large intestine	0.198 ± 0.007	0.195 ± 0.007	0.194 ± 0.007
Heart wall	0.678 ± 0.224	0.692 ± 0.224	0.692 ± 0.224
Kidneys	0.201 ± 0.055	0.204 ± 0.055	0.203 ± 0.055
Liver	0.210 ± 0.005	0.331 ± 0.005	0.331 ± 0.005
Lungs	0.437 ± 0.107	0.441 ± 0.107	0.440 ± 0.107
Muscle	0.176 ± 0.006	0.170 ± 0.006	0.169 ± 0.006
Ovaries	0.197 ± 0.008	0.189 ± 0.008	0.190 ± 0.008
Pancreas	0.200 ± 0.002	0.426 ± 0.002	0.425 ± 0.002
Red marrow	0.170 ± 0.004	0.164 ± 0.004	0.162 ± 0.004
Bone surfaces	0.186 ± 0.005	0.180 ± 0.005	0.178 ± 0.005
Skin	0.153 ± 0.005	0.147 ± 0.005	0.146 ± 0.005
Spleen	0.196 ± 0.002	0.233 ± 0.002	0.232 ± 0.002
Testes	0.175 ± 0.006	0.167 ± 0.006	0.169 ± 0.006
Thymus	0.183 ± 0.005	0.178 ± 0.005	0.175 ± 0.005
Thyroid	0.192 ± 0.006	0.184 ± 0.006	0.181 ± 0.006
Urinary bladder wall	0.189 ± 0.007	0.182 ± 0.007	0.212 ± 0.007
Uterus	0.200 ± 0.008	0.193 ± 0.008	0.198 ± 0.008
EDE[a]	0.249 ± 0.026	0.269 ± 0.026	0.268 ± 0.026
ED[a]	0.208 ± 0.012	0.214 ± 0.010	0.215 ± 0.010

[a] EDE and ED are given in units of mSv MBq^{-1}.

Table 5.16 continued: Summary of the average absorbed doses corresponding to the residence times stated in five different cases.

Organ	Absorbed dose (mGy MBq^{-1})	
	Case 4	Case 5
Adrenals	0.146 ± 0.006	0.142 ± 0.006
Brain	0.243 ± 0.047	0.243 ± 0.047
Breasts	0.118 ± 0.004	0.114 ± 0.004
Gall bladder	0.165 ± 0.006	0.161 ± 0.006
Lower large intestine	0.142 ± 0.007	0.144 ± 0.007
Small intestine	0.147 ± 0.007	0.146 ± 0.007
Stomach	0.145 ± 0.006	0.140 ± 0.006
Upper large intestine	0.149 ± 0.007	0.147 ± 0.007
Heart wall	0.680 ± 0.224	0.679 ± 0.224
Kidneys	0.189 ± 0.055	0.188 ± 0.055
Liver	0.319 ± 0.005	0.319 ± 0.005
Lungs	0.427 ± 0.107	0.426 ± 0.107
Muscle	0.129 ± 0.006	0.127 ± 0.006
Ovaries	0.144 ± 0.008	0.146 ± 0.008
Pancreas	0.408 ± 0.002	0.407 ± 0.002
Red marrow	0.125 ± 0.004	0.121 ± 0.004
Bone surfaces	0.137 ± 0.005	0.133 ± 0.005
Skin	0.111 ± 0.005	0.108 ± 0.005
Spleen	0.218 ± 0.002	0.216 ± 0.002
Testes	0.129 ± 0.006	0.134 ± 0.006
Thymus	0.135 ± 0.005	0.130 ± 0.005
Thyroid	0.138 ± 0.006	0.133 ± 0.006
Urinary bladder wall	0.170 ± 0.007	0.236 ± 0.007
Uterus	0.152 ± 0.008	0.163 ± 0.008
EDE[a]	0.240 ± 0.026	0.240 ± 0.025
ED[a]	0.181 ± 0.010	0.184 ± 0.010

[a] EDE and ED are given in units of mSv MBq^{-1}.

The various residence times used to produce five different scenarios for absorbed dose calculations produced a range of results (Table 5.17). As with the adults, the doses calculated from the residence times quantified in the very low birth weight infant population studied here show little variance (brain, heart wall, kidneys, and lungs). For the liver and pancreas, the residence times taken from previously published values were much greater than the uniform distribution values; the maximum doses varied between 1.6 and 2.1 times the minimum doses, respectively. For the remaining organs, the maximum dose was less than a factor of 1.5 higher than the minimum dose. This is true even for the urinary bladder wall dose, although the maximum urinary bladder contents residence time was not as large in the newborns. Hence, there appears to be less variation in the organ doses estimated for this patient population as compared to the adult patient populations. But as with the adults, the lack of biokinetic measurements in patients hinders accurate quantification of doses, making these broad estimates of residence times necessary.

Table 5.17: The range of absorbed doses determined in the five cases.

Organ	Absorbed dose (mGy MBq^{-1})		
	Minimum	Maximum	Ratio
Adrenals	0.142	0.190	1.34
Brain	0.243	0.250	1.03
Breasts	0.114	0.157	1.38
Gall bladder	0.161	0.209	1.30
Lower large intestine	0.142	0.194	1.37
Small intestine	0.146	0.198	1.36
Stomach	0.140	0.191	1.36
Upper large intestine	0.147	0.198	1.34
Heart wall	0.678	0.692	1.02
Kidneys	0.188	0.204	1.08
Liver	0.210	0.331	1.58
Lungs	0.426	0.441	1.03
Muscle	0.127	0.176	1.39
Ovaries	0.144	0.197	1.37
Pancreas	0.200	0.426	2.13
Red marrow	0.121	0.170	1.41
Bone surfaces	0.133	0.186	1.40
Skin	0.108	0.153	1.42
Spleen	0.196	0.233	1.19
Testes	0.129	0.175	1.35
Thymus	0.130	0.183	1.40
Thyroid	0.133	0.192	1.44
Urinary bladder wall	0.170	0.236	1.39
Uterus	0.152	0.200	1.32
EDE[a]	0.240	0.269	1.12
ED[a]	0.181	0.215	1.19

[a] EDE and ED are given in units of mSv MBq^{-1}.

5.4.3 Discussion

5.4.3.1 Case differences

The variation in residence times for the primary organs with respect to FDG uptake provides insight into the possible range of doses expected in these VLBW infants. The organs for which data were collected by Niven and Nahmias (2003) and for which patient-specific dose estimates were calculated did not vary, despite the variations in the residence times used in the five cases (brain, heart wall, kidneys, and lungs). This is true even when the residence time for the heart contents increased by a factor of 1.9 between case 1 and case 2; the penetrating dose from its nearest neighbor cannot compete with the self-dose. In contrast, however, increases in the residence times for the liver, pancreas, and spleen yielded increases in the respective organ doses, although not in a one-to-one ratio. Increasing the residence times by factors of 1.9, 3.0, and 1.3 resulted in increased dose factors of 1.6, 2.1, and 1.2 for the liver, pancreas, and spleen, respectively. It is apparent that the spleen self-dose contributes more to the spleen total dose than the pancreas self-dose to its total dose, because the ratio of the dose increase to the residence time increase is 93% for the spleen but only 71% for the pancreas.

Similarly, a factor of 4.2 increase in the urinary bladder contents residence time between case 2 and case 3 only yields a factor of 1.2 increase in the organ dose. Like the heart wall, the majority of the total organ dose to the urinary bladder wall is derived from other sources, including the wall self-dose. In fact, for most organs, the remainder of the body is a major contributing factor, as evidenced by the virtually one-to-one ratio

decrease in remainder of the body residence time and total organ dose, as seen in the comparison between case 3 and case 4. With the exception of the brain, heart wall, kidneys, liver, lungs, pancreas, and spleen, where the self-dose is the primary contributing factor, a factor of 0.8 decrease in remainder of the body residence time produced on average a factor of 0.8 decrease in the total organ dose.

As with the adults, an increase in the urinary bladder contents residence time manifests itself not only in the urinary bladder dose but also in vital neighboring organs. This is seen is cases 3 and 5, where several of the important organs, (i.e. - lower large intestine, ovaries, testes, and uterus) all show slight increases in dose while the remaining organs either do not change or show a slight decrease in total dose (the reduction is due to the decrease in the remainder of the body residence time).

5.4.3.2 Comparison to previously published results

5.4.3.2.1 Organ dose estimates

Prior to the works of Ruotsalainen and others (1992; 1996) there were no published estimates of doses to newborns or infants from FDG. These studies were of a Finnish newborn population with serious neurological symptoms. The first study examined 20 newborns at about 36 weeks gestational age, weighing on average 3.1 ± 0.7 kg. The second study examined 21 newborns from the same population at about 40 weeks gestational age and weighing on average 3.6 ± 1.3 kg. For both studies, ROIs were drawn on 3-6 slices at the thalamus level in the brain and on 1-3 slices at the level

of highest accumulation in the bladder. The brain volume was calculated according to a formula based on the weight of the infant, while the bladder content volume was estimated from PET images. Ruotsalainen and others (1996) estimated other organ masses for their patient population assuming linear proportionality between their patient masses and the newborn model masses, having first subtracted the mass of the brain from the whole body mass. Furthermore, they scaled the cumulated activity measurements for other organs from the cumulated activities measured in an adult Japanese population (Mejia et al. 1991), but did not report these values. This correction factor was based on an assumed proportionality between the organ mass and the body mass (sans brain) between their calculated patient masses and the adult model masses.

The most recently published estimate of the dose to newborns is by Stabin and Gelfand (1998). As seen in Table 5.1, this estimate was derived mainly from biokinetic data obtained in dogs (Gallagher et al. 1977). Brain and bladder biokinetic data were obtained from an adult North American population (Jones et al. 1982).

The average absorbed doses to VLBW infants are compared to previously published results in Table 5.18. The dose estimates used for comparison are those found using the residence times from case 1, because these yielded the highest doses for most organs. The doses calculated in this study are generally comparable as they are on the same order of magnitude, with the exceptions of the dose to the brain by Stabin and Gelfand (1998) and the decreasing trend in the dose to the bladder wall.

Table 5.18: Summary of reported absorbed doses to newborns from FDG.

Organs	Absorbed dose (mGy MBq^{-1})			
	Ruotsalainen et al. (1992)	**Ruotsalainen et al. (1996)[a]**	**Stabin and Gelfand (1998)[b]**	**Niven (2003)[c]**
Brain	0.50	0.24	0.08	0.25
Heart wall		0.89	0.65	0.68
Kidneys		0.51	0.22	0.20[d]
Lungs		0.20	0.27	0.44
Urinary bladder wall	1.41	1.03	0.81	0.19
ED[e]		0.43	0.23	0.21

[a] Only the brain and bladder contents were measured in newborns. The remaining data were approximated from an adult Japanese population.

[b] Only the brain and bladder contents were measured in adult humans. The remaining data were obtained from dogs.

[c] The residence times described in case 1 were used to obtain these estimates.

[d] The urinary bladder contents was not a measured source organ.

[e] ED is given in units of mSv MBq^{-1}.

The brain dose estimate by Stabin and Gelfand (1998) is likely an underestimate due to the fact that the biokinetic data were extrapolated from adults. The brain comprises approximately 2% of the adult body mass, whereas it is about 12% in the full term newborn and 16% in the 28 wk old fetus (ICRP 1975). The absorbed doses to the heart wall, kidneys, and lungs calculated in this study are closer to those calculated by Stabin and Gelfand (1998) than to those calculated by Ruotsalainen and others (1996). It is difficult, however, to compare the doses more quantitatively due to the extrapolation of data obtained from dogs and adult populations.

It is interesting to note the order of magnitude decrease over time in the dose to the bladder wall. This trend can be broken, however, if the bladder contents residence times provided by Ruotsalainen and others (1996) are examined. As stated earlier, the two highest data points were determined to be outliers; when they are removed, the average residence time drops by more than a factor of three, from 0.038 h to 0.008 h. This brings the average urinary bladder contents residence time closer to the uniform distribution residence time of 0.009 h calculated in case 1. Exclusion of the doses corresponding to these residence times in turn yields a dose of 0.39 mGy MBq^{-1} to the bladder wall, which is more in line with the doses calculated in this study. Another reason for this difference is the inclusion of the surface dose to the mean dose in all previously published dose estimates. In all but the last case, however, even if the surface doses are added to the mean doses, the summed urinary bladder wall doses are still well below the average doses, as seen in Table 5.19.

Table 5.19: The total urinary bladder wall dose, including the surface dose from non-penetrating radiations emitted from the urinary bladder contents.

Case	Absorbed dose (mGy MBq^{-1})	
	Surface dose	Total dose
1	0.050	0.239
2	0.050	0.232
3	0.213	0.425
4	0.213	0.383
5	0.566	0.803

Although the infants in this study are less than one-third the size of the newborn model, those organ doses for which patient-specific adjustments were made correspond to those previously published for infants approximately the size of the newborn model. It is expected that if the masses of the remaining organs in these VLBW infants were known, patient-specific adjustments for those organs would in fact lead to higher organ doses than those presently calculated for these infants.

This is the first time several measurements of residence times for FDG have been acquired in infants. Because attenuation correction was not performed for the chest organs, the cumulated activities measured for the heart wall and kidneys are thought to be an underestimate of the true cumulated activities (attenuation through the lungs would be minimal, most likely less than 5%). This is most likely offset somewhat by the assumption of instantaneous uptake with no washout for the initial part of the chest scan. Extrapolating to the beginning of the acquisition probably causes an overestimation of the

residence time because the most natural uptake is a gradual accumulation; this gradual uptake, however, is not always seen in adults.

5.4.3.2.2 Effective dose equivalent and effective dose estimates

As a first approximation, the ED estimated for the VLBW infants in this study is similar to that found for newborns from various ^{99m}Tc labeled diagnostic agents commonly used in pediatric nuclear medicine procedures. These estimates range from 0.03 mGy MBq^{-1} for ^{99m}Tc DTPA to 0.16 mGy MBq^{-1} for ^{99m}Tc HMPAO (Stabin and Gelfand 1998).

5.4.3.3 Comparison to adults

The organ doses and the ED estimated in this study are an order of magnitude higher than those reported for adults by Niven and others and in the most recently published estimate to adults by ICRP (1999). As stated previously, it is known that the doses to children and infants are higher per unit administered activity simply due to a difference in the organ masses, given the same biodistribution. It is also known that the biokinetics for children, and certainly newborns, will likely differ from adults. The magnitude of this variation, however, is still largely to be determined. A comparison of the residence times for the adults to those of the VLBW infants determined by Niven and others may be found in Table 5.20.

Table 5.20: Comparison of residence times measured in adults to VLBW infants.

Organ	Residence times (h)		
	Adult male	**Adult female**	**VLBW infant**
Brain	0.222 ± 0.033	0.270 ± 0.027	0.282 ± 0.067
Heart wall	0.061 ± 0.012	0.048 ± 0.006	0.018 ± 0.010
Lungs	0.073 ± 0.014	0.076 ± 0.024	0.048 ± 0.031

The values in the VLBW infant study are higher in the brain but lower in the heart wall and lungs; these values are statistically different from the adult males ($p < 0.05$), but not with the adult females. This suggests that there is a biological difference in the biodistribution of FDG compared to adults.

5.5 Conclusion

Patient-specific dosimetry methods yielded radiation absorbed dose estimates to VLBW infants from FDG that are not entirely different from previously published results, although there are few studies for comparison. With the exception of the brain, the comparisons are made primarily based on results obtained from animals and adults. Fortunately, varying key organ residence times produced organ dose ranges that were tolerable; the maximum dose estimate for each organ was within a factor of 1.6 of the minimum dose estimate, except for the pancreas at a factor 2.1.

The limited biokinetic data available for infants makes dose estimates difficult to quantify with reasonable certainty. The biokinetic data determined in the infants in this study are the most extensive to date, with only four organs investigated. The fact that the

organ doses are an order of magnitude higher than that for adults emphasizes the need for more accurate distribution data.

Chapter 6: Conclusions and Future Work

6.1 Summary of the current MIRD Committee situation

6.1.1 Dose equations

The need for patient-specific dosimetry has been determined (Wessels and Siegel 1997; Mattsson and Johansson 1999; Stabin et al. 1999; Howell et al. 1999; Zanzonico 2000)), but its method has not been well established nor has it been routinely required for dose estimates. This problem has become more prevalent with the need for patient-specific dose estimates in therapeutic situations. This issue has been addressed in this paper in much detail; a comprehensive review of internal dosimetry equations has been provided. A revised set of MIRD dose equations has been developed, Equations (3.21) to (3.23), which is applicable whether mathematical model or patient-specific doses are desired. These equations also solve the problem of the incorrect reduction of total-body SAFs or S-values when considering the contents of a walled organ as a source (Stabin and Sparks 1999).

6.1.2 Dose estimates

The MIRD Committee expressed the intent to collect and evaluate metabolic data of new and routinely used radiopharmaceuticals under normal and abnormal conditions (Smith 1968; Smith 1970). It included the proposal to provide anatomical and

physiological data for patients of *various* ages and body types. Yet to this day biological data are scarcely collected and reported, the majority of data relied upon for internal dosimetry calculations are derived from animals, and the compendia of anatomical and physiological data generally represent healthy, young individuals. These are unfulfilled objectives.

What is further discouraging is that the MIRD Committee itself silently enables these behaviors. This is no clearer than in the latest MIRD Dose Estimate Report, No. 19 (Hays et al. 2002). This publication should provide the defining dose estimate for FDG, yet a comprehensive review of FDG residence times and dose estimates was not performed, gender-specific data were combined and applied to an adult male mathematical model, and there is no mention of biokinetic data or dose estimates for infants or children.

6.2 Summary of new FDG dose estimates

6.2.1 Adult and infant data

There is a definite difference in the uptake of FDG between adult males and females for the brain and heart wall, the primary organs of interest in diagnostic studies with FDG. The radiation absorbed doses estimated for the adult male populations are similar to previously published dose estimates, but the doses for the adult female populations are much higher in most cases. This difference is most likely due to the fact that the residence times calculated in the adult female populations studied here are the

first data published exclusively for women; previous dose estimates relied on data obtained in animals and adult males.

In addition, the set of VLBW infant data is the most comprehensive yet published for newborns and it indicates there is a biokinetic difference in the uptake of FDG between adults and infants. The only organs previously studied were the brain and urinary bladder contents, with only minimal data obtained from a few PET images. The brain dose estimated from the VLBW patient population is comparable to the previously published brain dose where data were obtained in infants; the remaining organ doses are somewhat similar to previously published values even though they were obtained from extrapolating animal and adult biokinetic data.

Overall, the individual organ dose estimates ranged from 0.9×10^{-2} to 4.5×10^{-2} mSv MBq^{-1} for the adult males and from 0.9×10^{-2} to 5.8×10^{-2} mSv MBq^{-1} for the adult females; the brain, heart wall, and urinary bladder wall received the highest doses. The individual organ dose estimates for the VLBW infants ranged from 1.1×10^{-1} to 6.9×10^{-1} mSv MBq^{-1}; the heart wall, lungs, and pancreas received the highest doses.

The dose estimates per unit administered activity to newborns are an order of magnitude higher than those for adults, simply due to their overall smaller body size. Fortunately, the nominal activity given to children and infants is lower than that given to adults, yielding similar total doses.

6.2.2 Risk estimates

It is the position of the MIRD Committee that there will be "no judgment as to the medical significance of the estimated absorbed dose" (Smith 1968). In addition, the Health Physics Society recommends against making any quantitative estimation of health risks for an individual effective dose below 50 mSv (HPS 2003). These positions are in line with several members of the internal dosimetry community who believe that individual organ doses are the fundamentally important quantity that should be evaluated for the effects of exposure of the patient (Poston 1993; Stabin et al. 1993; Poston 1994; Toohey and Stabin 1999).

The results obtained from the adult and infant population investigated here show that the use of effective dose can be misleading, especially when the radiopharmaceutical concentration in an individual organ can be so diverse. Fortunately, in the clinical and research studies performed with FDG-PET, the usual activity injected is between 185 and 370 MBq for all adults. Assuming an average concentration of 3.7 MBq kg^{-1}, a full-term newborn would be injected with approximately 13 MBq. These injected activities lead to maximum individual organ doses of 16.6 mGy, 21.5 mGy, and 9.0 mGy for the adult male heart wall, the adult female urinary bladder wall, and the newborn heart wall, respectively. The maximum effective doses would be 5.5 mSv, 7.1 mSv, and 2.8 mSv for the adult male, adult female, and newborn, respectively. These doses are far below the recommended low-dose limit of 50 mSv as determined by the Health Physics Society.

6.3 Future work

6.3.1 Organ distribution data

Knowledge of the biodistribution of FDG throughout the body is still lacking, especially for women, infants, and children. Further investigations into the uptake of FDG in the kidneys, liver, and pancreas would allow for a more accurate quantification of the doses to these organs. In addition, data pertaining to the uptake and excretion of FDG in the urine is paramount for an accurate dose estimate; individual voiding times must be observed over a longer period of time, possibly up to 24 hours. All these data must be collected for a variety of ages, nationalities, and pathological conditions for both sexes in order to determine the likely range of doses received by the general public in a routine FDG-PET scan.

The procedures used to obtain biokinetic data and estimate radiation absorbed dose are the same regardless of whether the radiopharmaceutical is for diagnostic or therapeutic studies. Therefore, despite the generally low doses received from FDG-PET, an accurate quantification of the dose should be considered important, especially considering that FDG is an analog of sugar, one of the basic energy molecules of the body. Yet if the dosimetry community does not strive to gather and analyze data on such a prevalent radiopharmaceutical, how conscientious is it about applying the same techniques on therapeutic radiopharmaceuticals? Low dose metabolic studies are used to predict therapeutic effects at high doses. Better dose estimates for low dose studies means the doses calculated for a mathematical model will correlate better with the dose

effects observed in patients (Stabin 1999). An accurate quantification of the biokinetic behavior of radiopharmaceuticals is therefore of paramount importance in reducing dose errors; there is limited tolerance for organ damage at high doses. Information with regards to the age, sex, weight, organ mass, etc. of the patient population in clinical and research studies must be gathered and patient-specific dose estimates must be calculated.

6.3.2 Database for international collaboration

In order to meet the standards set by the MIRD Committee in 1968, collaborative work must be done internationally in the internal dosimetry community. The MIRD Committee should coordinate and support efforts to investigate, collect, and evaluate data regarding the anatomical and physiological changes in the disease state. The intent of diagnostic imaging, and hence the driving force behind so many new radiopharmaceuticals, is to determine the existence or lack of a pathological condition in the human body. A diagnosis is generally made based on a difference from the norm; the patient population is therefore varied.

A database of diagnostic and therapeutic centers should be initiated and records concerning the use of radiopharmaceuticals and dosimetry-relevant patient statistics should be recorded. The patient population would then be international. Retrospective studies of these patients would provide useful information with regards to the dose distributions according to age, sex, pathological condition, and nationality, thereby achieving the goals of the MIRD Committee and the internal dosimetry community.

References

Anonymous. MIRDOSE 3 distribution suspended. Journal of Nuclear Medicine 41:13N-14N, 19N; 2000.

Atkins HL, Cloutier RJ, Lathrop KA, Freeman LM, McAfee JG, Nelp WB, Patton DD, Smith EM. Summary of current radiation dose estimates to humans with various liver conditions from 99mTc-sulfur colloid. MIRD Dose Estimate Report No. 3. Journal of Nuclear Medicine 16:108A-108B; 1975.

Atkins HL, Robertson JS, Croft BY, Tsui B, Susskind H, Ellis KJ, Loken MK, Treves S. Estimates of radiation absorbed doses from radioxenons in lung imaging. MIRD Dose Estimate Report No. 9. Journal of Nuclear Medicine 21:459-465; 1980.

Atkins HL, Thomas SR, Buddemeyer U, Chervu LR. Radiation absorbed dose from technetium-99m-labeled red blood cells. MIRD Dose Estimate Report No. 14. Journal of Nuclear Medicine 31:378-380; 1990.

Atkins HL, Weber DA, Susskind H, Thomas SR. Radiation absorbed dose from technetium-99m-diethylenetriaminepentaacetic acid aerosol. MIRD Dose Estimate Report No. 16. Journal of Nuclear Medicine 33:1717-1719; 1992.

Atkins HL, Robertson JS, Akabani G. Radiation absorbed dose estimates from inhaled krypton-81m gas in lung imaging. MIRD Dose Estimate Report No. 17. Journal of Nuclear Medicine 34:1382-1384; 1993.

Bellina CR, Guzzardi R. CAMIRD/III: a revised version of the CAMIRD/II and MIRD-S packages for internal dose calculation: concise communication. Journal of Nuclear Medicine 21:379-383; 1980.

Berger MJ. Energy deposition in water by photons from point isotropic sources. MIRD Pamphlet No. 2. Journal of Nuclear Medicine 9(Supp. 1):15-25; 1968.

Berger MJ. Distribution of absorbed dose around point sources of electrons and beta particles in water and other media. MIRD Pamphlet No. 7. Journal of Nuclear Medicine 12(Supp. 5):5-23; 1971.

Berman M. Kinetic models for absorbed dose calculations. MIRD Pamphlet No. 12. New York: Society of Nuclear Medicine; 1977.

Beyer T, Townsend DW, Brun T, Kinahan PE, Charron M, Roddy R, Jerin J, Young J, Byars L, Nutt R. A combined PET/CT scanner for clinical oncology. Journal of Nuclear Medicine 4:1369-1379; 2000.

Blau M, McAfee JG, Rohrer RH, Snyder WS, Smith EM. Summary of current radiation dose estimates to human from 197Hg- and 203Hg-labeled chlormerodrin. MIRD Dose Estimate Report No. 6. Journal of Nuclear Medicine 16:1095-1098; 1975.

Blau M, Wicks R, Thomas SR, Lathrop KA. Radiation absorbed dose from albumin microspheres labeled with technetium-99m. MIRD Dose Estimate Report No 10. Journal of Nuclear Medicine 23:915-917; 1982.

Bolch WE, Bouchet LG, Robertson JS, Wessels BW, Siegel JA, Howell RW, Erdi AK, Aydogan B, Costes S, Watson EE, Brill AB, Charkes ND, Fisher DR, Hays MT, Thomas SR. The dosimetry of nonuniform activity distributions--radionuclide S values at the voxel level. MIRD Pamphlet No. 17. Journal of Nuclear Medicine 40:11S-36S; 1999.

Bolch WE, Patton PW, Rajon DA, Shah AP, Jokisch DW, Inglis BA. Considerations of marrow cellularity in 3-dimensional dosimetric models of the trabecular skeleton. Journal of Nuclear Medicine 43:97-108; 2002.

Bouchet LG, Bolch WE, Weber DA, Atkins HL, Poston JW Sr. Radionuclide S values in a revised dosimetric model of the adult head and brain. MIRD Pamphlet No. 15. Journal of Nuclear Medicine 40:62S-101S; 1999a.

Bouchet LG, Bolch WE, Wessels BW, Weber D. MIRD head and brain dosimetry: absorbed fractions of energy and absorbed dose per unit cumulated activity within pediatric and adult head and brain models for use in nuclear medicine internal dosimetry. New York: Society of Nuclear Medicine; 1999b.

Bouchet LG, Bolch WE, Howell RW, Rao DV. S values for radionuclides localized within the skeleton. Journal of Nuclear Medicine 41:189-212; 2000.

Brooks RS, Di Chiro G. Principles of computer assisted tomography (CAT) in radiographic and radioisotopic imaging. Physics in Medicine and Biology 21:689-732; 1976.

Brownell GL, Sweet WH. Localization of brain tumors with positron emitters. Nucleonics 11:40-45; 1953.

Brownell GL, Ellett WH, Reddy R. Absorbed fractions for photon dosimetry. MIRD Pamphlet No. 3. Journal of Nuclear Medicine 27(Supp. 1):29-39; 1968.

Brownell GL, Ackerman RH, Strauss HW, Elmaleh DR, Cochavi S, Alpert N, Correia JA, Kearfott KJ, Taveras J. Preliminary imaging results with 18F-2-fluoro-2-deoxy-D-glucose. Journal of Computer Assisted Tomography 4:473-477; 1980.

Brownell GL, Budinger TF, Lauterbur PC, McGeer PL. Positron tomography and nuclear magnetic resonance imaging. Science 215:619- 626; 1982.

Butler PF, Fitzgerald LT, Vanek KN, Brookemen VA. A computer program to determine cumulated activity and absorbed radiation dose. In: Cloutier RJ, Coffey JL, Snyder WS, Watson EE, eds. Radiopharmaceutical dosimetry symposium. Rockville: U.S. Department of Health, Education, and Welfare; (FDA) 76-8044; 1976: 127-139.

Butler PF, Fitzgerald LT, Brookeman VA, Vanek KN. Determination of internal radiation absorbed dose: a computer method. Health Physics 33:459-463; 1977.

CDE, Inc. Dosimetry Services. Dose estimates: adult [online]. Available at: http://www.internaldosimetry.com/freedosestimates/adult/. Accessed on 1 February 2003.

Chugani HT, Phelps ME. Maturational changes in cerebral function in infants determined by 18FDG positron emission tomography. Science 231:840-843; 1986.

Clarke SEM. Application of the effective dose equivalent to nuclear medicine patients. Journal of Nuclear Medicine 35:187; 1994.

Cloutier RJ, Smith SA, Watson EE, Snyder WS, Warner GG. Dose to the fetus from radionuclides in the bladder. Health Physics 25:147-161; 1973a.

Cloutier RJ, Watson EE, Hayes RL, Nelson B, Smith EM. Summary of current radiation dose estimates to humans from 66Ga-, 68Ga-, and 72Ga-citrate. MIRD Dose Estimate Report No. 2. Journal of Nuclear Medicine 14:755-756; 1973b.

Cloutier RJ, Watson EE, Rohrer RH, Smith EM. Calculating the radiation dose to an organ. Journal of Nuclear Medicine 14:53-55; 1973c.

Cloutier RJ, Freeman RM, McAfee JG, McCormack KR, Patton DD, Rosenthall L, Smith EM. Summary of current radiation dose estimates to humans with various liver conditions from 198Au-colloidal gold. MIRD Dose Estimate Report No. 4. Journal of Nuclear Medicine 16:173-74; 1975.

Cloutier RJ, Watson EE. Internal dosimetry – an introduction to the ICRP technique. In: Williams LE, ed. Nuclear medical physics. Boca Raton: CRC Press, Inc.; 1987: 143-162.

Coffey JL, Watson EE. Calculating dose from remaining body activity: a comparison of two methods. Medical Physics 6:307-308; 1979.

Coffey JL, Cristy M, Warner GG. Specific absorbed fractions for photon sources uniformly distributed in the heart chambers and heart wall of a heterogeneous phantom. MIRD Pamphlet No. 13. Journal of Nuclear Medicine 22:65-71; 1981.

Coleman RE. FDG imaging. Nuclear Medicine and Biology 27:689-690; 2000.

Cristy M. Mathematical phantoms representing children of various ages for use in estimates of internal dose. Oak Ridge: Oak Ridge National Laboratory; ORNL/NUREG/TM-367; 1980.

Cristy M, Eckerman KF. Specific absorbed fractions of energy at various ages from internal photon sources. Oak Ridge: Oak Ridge National Laboratory; ORNL/TM-8381/V1; 1987.

Deloar HM, Fujiwara T, Shidahara M, Nakamura T, Watabe H, Narita Y, Itoh M, Miyake M, Watanuki S. Estimation of absorbed dose for 2-[F-18]fluoro-2-deoxy-D-glucose using whole-body positron emission tomography and magnetic resonance imaging. European Journal of Nuclear Medicine 25:565-574; 1998.

Dillman LT. Radionuclide decay schemes and nuclear parameters for use in radiation-dose estimation. MIRD Pamphlet No. 4. Journal of Nuclear Medicine 10(Supp. 2):5-32; 1969.

Dillman LT. Radionuclide decay schemes and nuclear parameters for use in radiation-dose estimation, Part 2. MIRD Pamphlet No. 6. Journal of Nuclear Medicine 11(Supp. 4):5-32; 1970.

Dillman LT, Von der Lage FC. Radionuclide decay schemes and nuclear parameters for use in radiation-dose estimation. MIRD Pamphlet No. 10. New York: Society of Nuclear Medicine; 1975.

Dowd MT, Chen CT, Wendel MJ, Faulhaber PJ, Cooper MD. Radiation dose to the bladder wall from 2-[18F]fluoro-2-deoxy-D-glucose in humans. Journal of Nuclear Medicine 32:707-712; 1991.

Doyle LW, Nahmias C, Firnau G, Kenyon DB, Garnett ES, Sinclair JC. Regional cerebral glucose metabolism of newborn infants measured by positron emission tomography. Developmental Medicine and Child Neurology 25:143-151; 1983.

Early PJ. Use of diagnostic radionuclides in medicine. Health Physics 69:649-661; 1995.

Eary JF, Press OW, Badger CC, Durack LD, Richter KY, Addison SJ, Krohn KA, Fisher DR, Porter BA, Williams DL. Summary of current radiation dose estimates to humans from 123I, 124I, 126I, 130I, and 131I as sodium rose bengal. MIRD Dose Estimate Report No. 7. Journal of Nuclear Medicine 16:1214-1217; 1975.

Eckerman KF, Cristy M. The reference individual of radiation protection. Proceedings of the conference: Workshop on voxel phantoms. Oak Ridge: Oak Ridge National Laboratory; OSTI ID 219488/CONF-9507235-1; 1995.

Eckerman KF, Stabin MG. Electron absorbed fractions and dose conversion factors for marrow and bone by skeletal regions. Health Physics 78:199-214; 2000.

Ellett WH, Callahan AB, Brownell GL. Gamma-ray dosimetry of internal emitters: Monte Carlo calculations of absorbed dose from point sources. British Journal of Radiology 38:45-52; 1964.

Ellett WH, Callahan AB, Brownell GL. Gamma-ray dosimetry of internal emitters II: Monte Carlo calculations of absorbed dose from uniform sources. British Journal of Radiology 38:541-544; 1965.

Ellett WH, Humes RM. Absorbed fractions for small volumes containing photon-emitting radioactivity. MIRD Pamphlet No. 8. Journal of Nuclear Medicine 12(Supp. 5):25-32; 1971.

Feller PA. CAMIRD/II – computer software to facilitate absorbed-dose calculations. In: Cloutier RJ, Coffey JL, Snyder WS, Watson EE, eds. Radiopharmaceutical dosimetry symposium. Rockville: U.S. Department of Health, Education, and Welfare; (FDA) 76-8044; 1976: 119-126.

Furhang EE, Chui CS, Sgouros G. A Monte Carlo approach to patient-specific dosimetry. Medical Physics 23:1523-1529; 1996.

Gallagher BM, Ansari A, Atkins H, Casella V, Christman DR, Fowler JS, Ido T, MacGregor RR, Som P, Wan CN, Wolf AP, Kuhl DE, Reivich M. 18F-labeled 2-deoxy-2-fluoro-D-glucose as a radiopharmaceutical for measuring regional myocardial glucose metabolism in vivo: tissue distribution and imaging studies in animals. Journal of Nuclear Medicine 18:990-996; 1977.

Gallagher BM, Fowler JS, Gutterson NI, MacGregor RR, Wan C, Wolf AP. Metabolic trapping as a principle of radiopharmaceutical design: some factors responsible for the biodistribution of [18F] 2-deoxy-2-fluoro-D-glucose. Journal of Nuclear Medicine 19:1154-1161; 1978.

Graham MC, Bigler RE. Principles of positron emission tomography (PET). In: Rao DV, Chandra R, Graham MC, eds. Principles of nuclear medicine: recent advances. New York: American Institute of Physics, Inc.; 1984: 284-409.

Harding LK, Elliott AT, Shields RA. Application of the effective dose equivalent to nuclear medicine patients. Journal of Nuclear Medicine 35:185-186; 1994.

Hawkins RA, Hoh C, Dahlbom M, Choi Y, Glaspy J, Tse N, Slamon D, Chen B, Messa C, Maddahi J, Phelps ME. PET cancer evaluations with FDG. Journal of Nuclear Medicine 32:1555-1558; 1991.

Hays MT, Segall GM. A mathematical model for the distribution of fluorodeoxyglucose in humans. Journal of Nuclear Medicine 40:1358-1366; 1999.

Hays MT, Watson EE, Thomas SR, Stabin M. Radiation absorbed dose estimates from 18F-FDG. MIRD Dose Estimate Report No. 19. Journal of Nuclear Medicine 43:210-214; 2002.

Health Physics Society. Radiation risk in perspective: position statement of the Health Physics Society [online]. Available at: http://hps.org/hpspublications/papers.html. Accessed 1 February 2003.

Hine GJ, Brownell GL. Radiation dosimetry. New York: Academic Press, Inc.; 1956.

Hoffman EJ, Phelps ME, Mullani NA, Higgins CS, Ter-Pogossian MM. Design and performance characteristics of a whole-body positron transaxial tomograph. Journal of Nuclear Medicine 17:493-502; 1976.

Hounsfield GN. Computed medical imaging. Science 210:22-28; 1980.

Howell RW, Rao DV, Bouchet LG, Bolch WE, Goddu SM. MIRD cellular S values: self-absorbed dose per unit cumulated activity for selected radionuclides and monoenergetic electron and alpha particle emitters incorporated into different cell compartments. Reston: Society of Nuclear Medicine; 1997.

Howell RW, Wessels BW, Loevinger R, Watson EE, Bolch WE, Brill AB, Charkes ND, Fisher DR, Hays MT, Robertson JS, Siegel JA, Thomas SR. The MIRD perspective 1999. Journal of Nuclear Medicine 40:3S-10S; 1999.

Huang S, Phelps ME, Hoffman EJ, Sideris K, Selin CJ, Kuhl DE. Noninvasive determination of local cerebral metabolic rate of glucose in man. American Journal of Physiology: Endocrinology and Metabolism 238:E69-E82; 1980.

Huang SC, Carson RE, Phelps ME, Hoffman EJ, Schelbert HR, Kuhl DE. A boundary method for attenuation correction in positron computed tomography. Journal of Nuclear Medicine 22:627-637; 1981.

International Commission on Radiological Protection. Report of the task group on reference man. Oxford: Pergamon Press; ICRP Publication 23; 1975.

International Commission on Radiological Protection. Recommendations of the International Commission on Radiological Protection. Oxford: Pergamon Press; ICRP Publication 26; Annals of the ICRP 1(3); 1977.

International Commission on Radiological Protection. Limits for the intake of radionuclides by workers. Oxford: Pergamon Press; ICRP Publication 30, Part 1; Annals of the ICRP 2(3/4); 1979.

International Commission on Radiological Protection. Protection of the patient in nuclear medicine. Oxford: Pergamon Press; ICRP Publication 52; Annals of the ICRP 17(4); 1987.

International Commission on Radiological Protection. Radiation dose to patients from radiopharmaceuticals. Oxford: Pergamon Press; ICRP Publication 53; Annals of the ICRP 18(1/4); 1988.

International Commission on Radiological Protection. 1990 recommendations of the International Commission on Radiological Protection. Oxford: Pergamon Press; ICRP Publication 60; Annals of the ICRP 21(1-3); 1991.

International Commission on Radiological Protection. Radiological protection in biomedical research. New York: Elsevier Science Inc.; ICRP Publication 62; Annals of the ICRP 22(3); 1993.

International Commission on Radiological Protection. Age-dependent doses to members of the public from intake of radionuclides. New York: Elsevier Science Inc.; ICRP Publication 67, Part 2; Annals of the ICRP 23(3/4); 1994.

International Commission on Radiological Protection. Basic anatomical and physiological data for use in radiological protection: the skeleton. Oxford: Elsevier Science, Ltd., 1995; ICRP Publication 70; Annals of the ICRP 25(2); 1995.

International Commission on Radiological Protection. Radiation dose to patients from radiopharmaceuticals. New York: Elsevier Science Inc.; ICRP Publication 80, Addendum 2; Annals of the ICRP 28(3); 1999.

International Commission on Radiological Protection. Draft ICRP report: Basic anatomical and physiological data for use in radiological protection: reference

values. Available at: http://www.icrp.org/download_anatomical.htm. Accessed on 22 June 2002.

International Commission on Radiation Units and Measurements. Tissue substitutes in radiation dosimetry and measurement. Bethesda; International Commission on Radiation Units and Measurements; 1989.

Johansson L, Mattsson S, Nosslin B, Leide-Svegborn S. Reply. European Journal of Nuclear Medicine 20:448-449; 1993.

Johnson TK. MABDOS: a generalized program for internal radionuclide dosimetry. Computer Methods and Programs in Biomedicine 27:159-167; 1988.

Johnson TK, McClure D, McCourt S. MABDOSE I: characterization of a general purpose dose estimation code. Medical Physics 26:1389-1395; 1999a.

Johnson TK, McClure D, McCourt S. MABDOSE II: validation of a general purpose dose estimation code. Medical Physics 26:1396-1403; 1999b.

Jones SC, Alavi A, Christman D, Montanez I, Wolf AP, Reivich M. The radiation dosimetry of 2-[F-18]fluoro-2-deoxy-D-glucose in man. Journal of Nuclear Medicine 23:613-617; 1982.

Jones SC, Alavi A, Christman D, Reivich M. Reply. Journal of Nuclear Medicine 24:447-448; 1983.

Jones T. The imaging science of positron emission tomography. European Journal of Nuclear Medicine 23:807-813; 1996.

Kassis A.I. The MIRD approach: remembering the limitations. Journal of Nuclear Medicine 33:781-781; 1992.

Kaul A, Henrichs K, Roedler HD. Radionuclide biokinetics and internal dosimetry in nuclear medicine. La Ricerca in Clinica e in Laboratorio 10:629-660; 1980.

Kereiakes JG, Wellman HN, Simmons G, Saenger EL. Radiopharmaceutical dosimetry in pediatrics. Seminars in Nuclear Medicine 2:316-327; 1972.

Kereiakes JG, Feller PA, Ascoli FA, Thomas SR, Gelfand MJ, Saenger EL. Pediatric radiopharmaceutical dosimetry. In: Cloutier RJ, Coffey JL, Snyder WS, Watson EE, eds. Radiopharmaceutical dosimetry symposium. Rockville: U.S. Department of Health, Education, and Welfare; (FDA) 76-8044; 1976: 77-90.

Kiefer H, Maushart R, Mejdahl V. Radiation protection dosimetry. In: Attix FH, Roesch WC, Tochilin E, eds. Radiation dosimetry. 2nd edition. New York: Academic Press; 1969: 557-616.

Kilbourn MR. Radiopharmaceuticals. In: Schwaiger M, ed. Cardiac positron emission tomography. Boston: Kluwer Academic Publishers; 1996: 65-78.

Kinnala A, Suhonen-Polvi H, Aarimaa T, Kero P, Korvenranta H, Ruotsalainen U, Bergman J, Haaparanta M, Solin O, Nuutila P, Wegelius U. Cerebral metabolic rate for glucose during the first six months of life: an FDG positron emission tomography study. Archives of Diseases in Childhood 74:F153-F157; 1996.

Kinnala A, Nuutila P, Ruotsalainen U, Teras M, Bergman J, Haaparanta M, Solin O, Korvenranta H, Aarimaa T, Wegelius U, Kero P, Suhonen-Polvi H. Cerebral metabolic rate for glucose after neonatal hypoglycemia. Early Human Development 49:63-72; 1997.

Kirpalani H, Abubakar K, Nahmias C, deSa D, Coates G, Schmidt B. [18F]fluorodeoxyglucose uptake in neonatal acute lung injury measured by positron emission tomography. Pediatric Research 41:892-896; 1997.

Kolbert KS, Sgourous G, Scott AM, Bronstein JE, Malane RA, Zhang J, Kalaigian H, McNamara S, Schwartz L, Larson SM. Implementation and evaluation of patient-specific three-dimensional internal dosimetry. Journal of Nuclear Medicine 38:301-308; 1997.

Lathrop KA, Johnston RE, Blau M, Rothschild EO. Radiation dose to humans from Se-75-L-selenomethionine. MIRD Pamphlet No. 9. Journal of Nuclear Medicine 13(Supp. 6):7-30; 1972.

Lathrop KA, Johnston RE, Blau M, Rothschild EO, Smith EM. Selenium-75-L-selenomethionine. MIRD Dose Estimate Report No. 1. Journal of Nuclear Medicine 14:49-50; 1973.

Lathrop KA, Atkins HL, Berman M, Hays MT, Smith EM. Summary of current radiation dose estimates to normal humans from 99mTc as sodium pertechnetate. MIRD Dose Estimate Report No. 8. Journal of Nuclear Medicine 17:74-77; 1976.

Leenders KL, Gibbs JM, Trackowiak RSJ, Lammerstma AA, Jones T. Positron emission tomography of the brain: new possibilities for the investigation of human cerebral pathophysiology. Progress in Neurobiology 23:1-38; 1984.

Loevinger R, Holt JG, Hine GJ. Internally administered radioisotopes. In: Hine GJ, Brownell GL, eds. Radiation dosimetry. New York: Academic Press, Inc.; 1956: 801-872.

Loevinger R, Berman M. A formalism for calculation of absorbed dose from radionuclides. Physics in Medicine and Biology 13:205-217; 1968a.

Loevinger R, Berman M. A schema for absorbed-dose calculations for biologically-distributed radionuclides. MIRD Pamphlet No. 1. Journal of Nuclear Medicine 9(Supp. 1):7-14; 1968b.

Loevinger R. Distributed radionuclide sources. In: Attix FH, Roesch WC, Tochilin E, eds. Radiation dosimetry. 2nd edition. New York: Academic Press; 1969: 51-90.

Loevinger R. Some remarks on the MIRD schema for absorbed-dose calculations for biologically-distributed radionuclides. In: Cloutier RJ, Edwards CL, Snyder WS, eds. Medical radionuclides: radiation dose and effects. Proceedings of a symposium held at the Oak Ridge Associated Universities. Oak Ridge: United States Atomic Energy Commission; AEC Symposium Series 20; 1970: 481-488.

Loevinger R, Berman M. A revised schema for calculating the absorbed dose from biologically distributed radionuclides. MIRD Pamphlet No. 1, Revised. New York: Society of Nuclear Medicine; 1976.

Loevinger R, Budinger T, Watson E. MIRD primer for absorbed dose calculations. New York: Society of Nuclear Medicine; 1988.

Loevinger R. The MIRD perspective. In: Adelstein JS, Kassis AI, Burt RW, eds. Dosimetry of Administered Radionuclides. Washington D.C.: The College; 1990: 29-43.

Loevinger R, Budinger T, Watson E. MIRD primer for absorbed dose calculations. Revised edition. New York: Society of Nuclear Medicine; 1991.

Mardirossian G, Brill AB, Harwood SJ, Olsen J, Dwyer KA, Siegel JA. Radiation absorbed dose estimates for indium-111-labeled B72.3, an IgG antibody to ovarian and colorectal cancer. MIRD Dose Estimate Report No. 18. Journal of Nuclear Medicine 39:671-676; 1998.

Marinelli LD. Dosage determinations with radioactive isotopes. American Journal of Roentgenology and Radium Therapy 47:210-216; 1942.

Mattsson S, Johansson L. Medical internal dosimetry: where are we going? In: Schlafke-Stelson AT, Stabin MG, Sparks RB, Smith FB, eds. Proceedings of the sixth international radiopharmaceutical dosimetry symposium. Oak Ridge: Oak Ridge Institute for Science and Education; ORISE 99-0164; 1999: 1-11.

Mejia AA, Nakamura T, Masatoshi I, Hatazawa J, Masaki M, Watanuki S. Estimation of absorbed doses in humans due to intravenous administration of fluorine-18-fluorodeoxyglucose in PET studies. Journal of Nuclear Medicine 32:699-706; 1991.

Melcher CL. Scintillation crystals for PET. Journal of Nuclear Medicine 41:1051-1055; 2000.

Milton JS, Arnold JC. Introduction to probability and statistics: principles and applications for engineering and the computer sciences. New York: McGraw-Hill, Inc.; 1995.

Miraldi FD. Historical highlights in the development of positron emission tomography. Proceedings of the Society of Nuclear Medicine Central Chapter, Spring Meeting. Available at: http://www.ccsnm.org/Spring%201999%20Proceedings.pdf. Accessed on 30 June 2002.

Mitchell J. Applications of recent advances in nuclear physics to medicine. British Journal of Radiology 19:481-487; 1946.

National Nuclear Data Center. Databases: MIRD [online]. Available at: http://www.nndc.bnl.gov/nndc/formmird.html. Accessed on 30 January 2001.

National Nuclear Data Center. Databases: MIRD [online]. Available at: http://www.nndc.bnl.gov/nndc/formmird.html. Accessed on 14 April 2002.

Niven E, Thompson M, Nahmias C. Absorbed dose to the adult male and female brain from 18F-Fluorodeoxyglucose. Health Physics 80:62-66; 2001.

Niven E, Nahmias C. Absorbed dose to very low birth weight infants from 18F-fluorodeoxyglucose. Health Physics 84:????; 2003.

Nosslin B. The need for more metabolic data for the updating of ICRP 17. Proceedings of the British Institute of Radiology: dosimetry and risks to patients in radiopharmaceutical investigations. British Journal of Radiology 54:431; 1981.

Phelps ME, Hoffman EJ, Huang SC, Kuhl DE. ECAT: a new computerized tomographic imaging system for positron-emitting radio-pharmaceuticals. Journal of Nuclear Medicine 19:635-647; 1978a.

Phelps ME, Hoffman EJ, Selin C, Huang SC, Robinson G, MacDonald N, Schelbert H, Kuhl DE. Investigation of [18F] 2-fluoro-2-deoxyglucose for the measure of myocardial glucose metabolism. Journal of Nuclear Medicine 19:1311-1319; 1978b.

Phelps ME, Huang SC, Hoffman EJ, Selin C, Sokoloff, L, Kuhl DE. Tomographic measurement of local cerebral glucose metabolic rate in humans with (F-18) 2-fluoro-2-deoxy-D-glucose: validation of method. Annals of Neurology 6:371-388; 1979.

Phelps ME. PET: the merging of biology and imaging into molecular imaging. Journal of Nuclear Medicine 41:661-681; 2000.

Poston JW. Application of the effective dose equivalent to nuclear medicine patients. Journal of Nuclear Medicine 34:714-716; 1993.

Poston JW. Reply. Journal of Nuclear Medicine 35:188-189; 1994.

Raabe OG. Introduction to internal radiation dosimetry. In: Raabe O, ed. Internal radiation dosimetry: Health Physics Society, 1994 summer school. Madison: Medical Physics Publishing; 1994: 1-26.

Radiation Internal Dose Information Center. About RIDIC [online]. Available at: http://www.orau.gov/ehsd/ridicint.htm. Accessed on 9 April 2002.

Raichle ME. Developing a functional anatomy of the human brain with positron emission tomography. Current Neurology 9:61-178; 1989.

Reddy AR, Ellett WH, Brownell GL. Gamma-ray dosimetry of internal emitters III: Monte Carlo calculations of absorbed dose for low-energy gamma-rays. British Journal of Radiology 45:512-515; 1967.

Reivich M, Kuhl D, Wolf A, Greenberg J, Phelps M, Ido T, Casella V, Fowler J, Gallagher B, Hoffman E, Alavi A, Sokoloff L. Measurement of local cerebral glucose metabolism in man with 18F-2-fluoro-2-deoxy-D-glucose. Acta Neurologica Scandinavia 56(Supp.64):190-191; 1977.

Reivich M, Kuhl D, Wolf A, Greenberg J, Phelps M, Ido T, Casella V, Fowler J, Hoffman E, Alavi A, Som P, Sokoloff L. The [18F]fluorodeoxyglucose method for the measurement of local cerebral glucose utilization in man. Circulation Research 44:127-137; 1979.

Reivich M, Alavi A, Greenberg J, Farkas T, Wolf A. 18F-fluorodeoxyglucose method for measuring local cerebral glucose metabolism in man: technique and results. Progress in Nuclear Medicine 7:138-148; 1981.

Reivich M, Alavi A, Wolf A, Greenberg JH, Fowler J, Christman D, MacGregor R, Jones SC, London J, Shiue C, Yonekura Y. Use of 2-deoxy-D[1-^{11}C]glucose for the determination of local cerebral glucose metabolism in humans: variation within and between subjects. Journal of Cerebral Blood Flow and Metabolism 2:307-319; 1982.

Robertson JS, Marr RB, Rosenblum M, Radeka V, Yamamoto YL. 32-crystal positron transverse section detector. In: Freedman GS, ed. Tomographic imaging in nuclear medicine. New York: Society of Nuclear Medicine; 1973: 142-153.

Robertson JS, Price RR, Budinger TF, Fairbanks VF, Pollycove M. Radiation absorbed doses from iron-52, iron-55, and iron-59 used to study ferrokinetics. MIRD Dose Estimate Report No. 11. Journal of Nuclear Medicine 24:339-348; 1983.

Robertson JS, Ezekowitz MD, Dewanjee MK, Lotter MG, Watson EE. Radiation absorbed dose estimates for radioindium-labeled autologous platelets. MIRD Dose Estimate No. 15. Journal of Nuclear Medicine 33:777-780; 1992.

Roedler HD, Kaul A, Berner W, Koeppe P, Glaubitt D. Development of an extended formalism for internal dose calculation and for practical application to several biologically distributed radioelements. In: Assessment of radioactive contamination in man. Proceedings of a symposium on assessment of radioactive organ and body burdens. Vienna: International Atomic Energy Agency; 1972: 515-540.

Ruddy TD, deKemp RA, Beanlands RS. Taking PET to heart. Canadian Medical Association Journal 161:1131; 1999.

Ruotsalainen U, Eronen E, Suhonen-Polvi H, Kinnala A, Teras M, Wegelius U. Dosimetric measurements in [18F]FDG brain studies of newborn infants. In: Voipio-Pulkki LM, Wegelius U, eds. Medical applications of cyclotrons VI. Proceedings of the sixth symposium on the medical applications of cyclotrons. Turku: Turun Yliopisto; 1992: A75-A76.

Ruotsalainen U, Suhonen-Polvi H, Eronen E, Kinnala A, Bergman J, Haaparanta M, Teras M, Solin O, Wegelius U. Estimated radiation dose to the newborn in FDG-PET studies. Journal of Nuclear Medicine 37:387-393; 1996.

Russell JR, Stabin MG, Sparks RB, Watson E. Radiation absorbed dose to the embryo/fetus from radiopharmaceuticals. Health Physics 73:756-769; 1997.

Schlafke-Stelson AT, Watson EE, Cloutier RJ. A History of internal dosimetry. Health Physics 69:766-782; 1995.

Schlesinger T. Dosimetry of internal emitters - a guide to the MIRD technique. In: Brodsky A, ed. CRC handbook of radiation measurement and protection. West Palm Beach: CRC Press, Inc.; 1978: 511-526.

Schulz DM, Giordano DA, Schulz DH. Weights of organs of fetuses and infants. Archives of Pathology 74:244-250; 1962.

Scott AM. Current status of positron emission tomography in oncology. Internal Medicine Journal 31:27-36; 2001.

Seltzer RA, Kereiakes JG, Saenger EL. Radiation exposure from radioisotopes in pediatrics. New England Journal of Medicine 271:84-90; 1964.

Seventh International Radiopharmaceutical Dosimetry Symposium. Previous meetings [online]. Available at: http://www.doseinfo-radar.com/previous.html. Accessed 9 April 2002.

Shields RA, Lawson RS. Use of the effective dose equivalent. Journal of Nuclear Medicine 35:186-187; 1994.

Siegel JA, Thomas SR, Stubbs JB, Stabin MG, Hays MT, Koral KF, Robertson JS, Howell RW, Wessels BW, Fisher DR, Weber DA, Brill AB. Techniques for quantitative radiopharmaceutical biodistribution data acquisition and analysis for use in human radiation dose estimates. MIRD pamphlet No. 16. Journal of Nuclear Medicine 40:37S-61S; 1999.

Skehan SJ, Issenman R, Mernagh J, Nahmias C, Jacobson K. 18F-fluorodeoxyglucose positron tomography in diagnosis of paediatric inflammatory bowel disease. The Lancet 354:836-837; 1999.

Smith EM, Harris CC, Rohrer RH. Calculation of local energy deposition due to electron capture and internal conversion. Journal of Nuclear Medicine 7:23-31; 1965.

Smith EM. Calculating absorbed doses from radiopharmaceuticals. Nucleonics 24:33-39, 68; 1966.

Smith EM. Introduction: activities of the Medical Internal Radiation Dose Committee. Journal of Nuclear Medicine 9(Supp.1):5-6; 1968.

Smith EM. General considerations in calculation of the absorbed dose of radiopharmaceuticals used in nuclear medicine. In: Cloutier RJ, Edwards CL, Snyder WS, eds. Medical radionuclides: radiation dose and effects. Proceedings of a symposium held at the Oak Ridge Associated Universities. Oak Ridge: United States Atomic Energy Commission; AEC Symposium Series 20; 1970: 17-27.

Snyder WS, Ford MR, Warner GG, Fisher HL Jr. Estimates of absorbed fractions for monoenergetic photon sources uniformly distributed in various organs of a heterogeneous phantom. MIRD Pamphlet No. 5. Journal of Nuclear Medicine 10(Supp. 3):5-52; 1969.

Snyder WS. Estimation of absorbed fraction of energy from photon sources in body organs. In: Cloutier RJ, Edwards CL, Snyder WS, eds. Medical radionuclides: radiation dose and effects. Proceedings of a symposium held at the Oak Ridge Associated Universities. Oak Ridge: United States Atomic Energy Commission; AEC Symposium Series 20; 1970: 33-49.

Snyder WS, Ford MR, Warner GG, Watson SB. A tabulation of dose equivalent per microcurie-day for source and target organs of an adult for various radionuclides. Oak Ridge: Oak Ridge National Laboratory Report; ORNL 5000; 1974.

Snyder WS, Ford MR, Warner GG, Watson SB. "S," absorbed dose per unit cumulated activity for selected radionuclides and organs. MIRD Pamphlet No. 11. New York: Society of Nuclear Medicine; 1975.

Snyder WS, Ford MR, Warner GG. Estimates of specific absorbed fractions for photon sources uniformly distributed in various organs of a heterogeneous phantom. MIRD Pamphlet No. 5, Revised. New York: Society of Nuclear Medicine; 1978.

Sokoloff L, Reivich M, Kennedy C, Des Rosiers MH, Patlak CS, Pettigrew KD, Sakurada O, Shinohara M. The [14C]deoxyglucose method for the measurement of local cerebral glucose utilization: theory, procedure, and normal values in the conscious and anesthetized albino rat. Journal of Neurochemistry 28:897-916; 1977.

Spiers FW. Radioisotopes in the human body – physical and biological aspects. New York: Academic Press; 1968.

Spiers FW. Determination of absorbed dose to bone and red bone marrow. In: Cloutier RJ, Edwards CL, Snyder WS, eds. Medical radionuclides: radiation dose and effects. Proceedings of a symposium held at the Oak Ridge Associated Universities. Oak Ridge: United States Atomic Energy Commission; AEC Symposium Series 20; 1970: 347-367.

Stabin MG, Stubbs J, Watson E. Recent controversy in radiation dosimetry. European Journal of Nuclear Medicine. 20:371-372; 1993.

Stabin MG. A model of the prostate gland for use in internal dosimetry. Journal of Nuclear Medicine 35:516-520; 1994a.

Stabin MG. Patient dose from diagnostic and therapeutic radiopharmaceuticals. In: Raabe O, ed. Internal radiation dosimetry: Health Physics Society, 1994 summer school. Madison: Medical Physics Publishing; 1994b: 375-392.

Stabin MG, Watson EE, Cristy M, Ryman JC, Eckerman KF, Davis JL, Marshal D, Gehlen MK. Mathematical models and specific absorbed fractions of photon energy in the nonpregnant adult female and at the end of each trimester of pregnancy. Oak Ridge: Oak Ridge National Laboratory Report; ORNL/TM-12907; 1995.

Stabin MG. MIRDOSE: personal computer software for internal dose assessment in nuclear medicine. Journal of Nuclear Medicine 37:538-546; 1996.

Stabin MG, Stubbs JB, Toohey RE. Radiation dose estimates for radiopharmaceuticals. Oak Ridge, TN: Radiation Internal Dose Information Center, Oak Ridge Institute for Science and Education; NUREG/CR-6345; 1996.

Stabin MG. Health concerns related to radiation exposure of the female nuclear medicine patient. Environmental Health Perspectives 105(Supp.6):1403-1409; 1997.

Stabin MG, Gelfand MJ. Dosimetry of pediatric nuclear medicine procedures. Quarterly Journal of Nuclear Medicine 42:93-112; 1998.

Stabin MG. Internal dosimetry in the use of radiopharmaceuticals in therapy – science at a crossroads? Cancer Biotherapy and Radiopharmaceuticals 14:81-89; 1999.

Stabin MG, Sparks RB. Some issues in the use of the remainder of the body S-value correction. In: Schlafke-Stelson AT, Stabin MG, Sparks RB, Smith FB, eds. Proceedings of the sixth international radiopharmaceutical dosimetry symposium. Oak Ridge: Oak Ridge Institute for Science and Education; ORISE 99-0164; 1999: 440-445.

Stabin MG, Tagesson M, Thomas SR, Ljungberg M, Strand SE. Radiation dosimetry in nuclear medicine. Applied Radiation and Isotopes 50:73-87; 1999.

Stocklin GL. Is there a future for clinical fluorine-18 radiopharmaceuticals (excluding FDG)? European Journal of Nuclear Medicine 25:1612-1616; 1998.

Suhonen-Polvi H, Kero P, Korvenranta H, Ruotsalainen U, Haaparanta M, Bergman J, Simell O, Wegelius U. Repeated fluorodeoxyglucose positron emission tomography of the brain in infants with suspected hypoxic-ischaemic brain injury. European Journal of Nuclear Medicine 20:759-765; 1993.

Suhonen-Polvi H. FDG positron emission tomography of the brain in early infancy: methodology, dosimetry and clinical studies. Turku: Turun Yliopisto; 1995.

Suhonen-Polvi H, Ruotsalainen U, Kinnala A, Bergman J, Haaparanta M, Teras m, Makela P, Solin O, Wegelius U. FDG-PET in early infancy: simplified quantitation methods to measure cerebral glucose utilization. Journal of Nuclear Medicine 36:1249-1254; 1995.

Tanaka G, Kawamura H. Reference man models based on normal data from human populations [online]. Available at: http://www.oita-nhs.ac.jp/~irpa10/CD-ROM/Full/00602_03a_195sr13h00563.pdf. Accessed on 2 February 2003.

Ter-Pogossian MM, Phelps ME, Hoffman EJ, Mullani NA. A positron-emission transaxial tomograph for nuclear imaging (PETT). Radiology 114:89-98; 1975.

Ter-Pogossian MM. The origins of positron emission tomography. Seminars in Nuclear Medicine 22:140-149; 1992.

Thomas SR, Stabin MG, Chen CT, Samaratunga RC. Summary of current radiation dose estimates to humans from 123I, 124I, 125I, 126I, 130I, 131I, and 132I as sodium iodide. MIRD Dose Estimate Report No. 5. Journal of Nuclear Medicine 16:857-860; 1975.

Thomas SR, Atkins HL, McAfee JG, Blaufox MD, Fernandez M, Kirchner PT, Reba RC. Radiation absorbed dose from Tc-99m diethylenetriaminepentaacetic acid (DTPA). MIRD Dose Estimate Report No. 12. Journal of Nuclear Medicine 25:503-505; 1984.

Thomas SR, Stabin MG, Chen CT, Samaratunga RC. A dynamic urinary bladder model for radiation dose calculations. MIRD Pamphlet No. 14. Journal of Nuclear Medicine 33:783-802; 1992.

Thomas SR, Stabin MG, Chen CT, Samaratunga RC. A dynamic urinary bladder model for radiation dose calculations. MIRD Pamphlet No. 14, Revised. Journal of Nuclear Medicine 40:102S-123S; 1999.

Thomas SR. Administered cumulated activity for ventilation studies. MIRD Pamphlet No. 18. Journal of Nuclear Medicine 42:520-526; 2001.

Thomson WH, Chandler ST, Griffiths C. Limitations of the effective dose equivalent. Journal of Nuclear Medicine 35:188; 1994.

Thorp PS, Levin SD, Garnett ES, Nahmias C, Firnau G, Toi A, Upton ARM, Nobbs PT, Sinclair JC. Patterns of cerebral glucose metabolism using 18FDG and positron tomography in the neurologic investigation of the full term newborn infant. Neuropediatrics 19:146-153; 1988.

Toohey RE, Stabin MG. Comparative analysis of dosimetry parameters for nuclear medicine. In: Schlafke-Stelson AT, Stabin MG, Sparks RB, Smith FB, eds. Proceedings of the sixth international radiopharmaceutical dosimetry symposium. Oak Ridge: Oak Ridge Institute for Science and Education; ORISE 99-0164; 1999: 532-550.

Townsend DW, Cherry SR. Combining anatomy and function: the path to true image fusion. European Radiology 11:1968-1974; 2001.

Trott NG. Dosimetry of radionuclides. In: Baarli J, ed. Health and Medical Physics. Proceedings of the international school of physics "Enrico Fermi". Amsterdam: North-Holland Publishing Co.; Course 66; 1977: 54-66.

Turner JE. Atoms, radiation, and radiation protection. 2nd edition. New York: John Wiley and Sons, Inc.; 1995.

United Nations Scientific Committee on the Effects of Atomic Radiation. Sources and effects of ionizing radiation: UNSCEAR 2000 report to the General Assembly, with scientific annexes. New York: United Nations; 2000.

Wagner HN. Probing the chemistry of the mind. New England Journal of Medicine 312:44-46; 1985.

Watson EE, Stabin MG, Davis JL, Eckerman KF. A model of the peritoneal cavity for use in internal dosimetry. Journal of Nuclear Medicine 30:2002-2011; 1989.

Watson EE, Stabin MG, Siegel JA. MIRD formulation. Medical Physics 20:511-514; 1993.

Watson EE. The MIRD internal dose methodology. In: Raabe O, ed. Internal radiation dosimetry: Health Physics Society, 1994 summer school. Madison: Medical Physics Publishing; 1994: 355-374.

Watson EE. Foreword. Journal of Nuclear Medicine 40:1S-2S; 1999.

Weber DA, Eckerman KF, Dillman LT, Ryman JC. MIRD: radionuclide data and decay schemes. New York: Society of Nuclear Medicine; 1989a.

Weber DA, Makler PT Jr, Watson EE, Coffey JL, Thomas SR, London J. Radiation absorbed dose from Tc-99m labeled bone imaging agents. MIRD Dose Estimate Report No. 13. Journal of Nuclear Medicine 30:1117-1122; 1989b.

Weber DA. Biologic data, models, and dosimetric methods for internal emitters. In: Adelstein JS, Kassis AI, Burt RW, eds. Dosimetry of administered radionuclides. Proceedings of a symposium. Washington D.C.: The College; Frontiers in Nuclear Medicine; 1990: 58-73.

Wessels BW, Siegel JA. Dosimetry overview: keeping score on the scorekeepers. Cancer 80(Supp.):2501-2504; 1997.

Wilder RB, Shen S, DeNardo, GL. Dosimetry for radioimmunotherapy: a rapidly evolving field. Cancer Biotherapy and Radiopharmaceuticals 14:67-70; 1999.

Wooten WW. Radionuclide kinetics in MIRD dose calculations. Journal of Nuclear Medicine 24:621-624; 1983.

Wrenn F, Good M, Handler P. The use of positron emitting radioisotopes for the localization of brain tumours. Science 113:525-527; 1951.

Yamaguchi H, Kato Y, Shiragai A. The transformation method for the MIRD absorbed fraction as applied to various physiques. Physics in Medicine and Biology 20:593-601; 1975.

Yamaguchi H. Estimation of internal radiation dose for various physiques using MIRD adult absorbed fractions. Acta Radiologica: Oncology, Radiation, Physics, Biology 17:429-439; 1978.

Yoriyaz H, Stabin MG, dos Santos A. Monte Carlo MCNP-4B-based absorbed dose distribution estimates for patient-specific dosimetry. Journal of Nuclear Medicine 42:662-669; 2001.

Zanzonico PB. Internal radionuclide radiation dosimetry: a review of basic concepts and recent developments. Journal of Nuclear Medicine 41:297-308; 2000.

Zubal IG, Harrell CR, Smith EO, Rattner Z, Gindi G, Hoffer PB. Computerized three-dimensional segmented human anatomy. Medical Physics 21:299-302; 1994.